UNIVERSITÀ
DEGLI STUDI
FIRENZE

DOTTORATO DI RICERCA IN
INGEGNERIA INDUSTRIALE

CICLO XXIX

COORDINATORE
Prof. Maurizio DE LUCIA

Development of Innovative Modelling, Real Time and Hardware In the Loop Techniques for Industrial Systems

Settore Scientifico Disciplinare ING-IND/13

Dottorando
Dott. Galardi Emanuele

Tutore
Prof. Allotta Benedetto

Coordinatore
Prof. De Lucia Maurizio

Anni 2014/2016

ISBN XXX-XX-XXXX-XXX-X
D/XXXX/XXXX/XX

Abstract

Hardware In the Loop (HIL) simulations are testing tools that have been widely applied in recent years for the design and testing of components and systems. In particular, a part of the real environment is inserted in the simulation loop. The HIL architecture, whose nature results partly physical and partly simulated, is employed to test a component or system in Real Time (RT). The continuous development of technologies for the fast prototyping of RT code has contributed to speed up the diffusion of complex HIL testing techniques. However, this approach still appears to be poorly followed in the energy field where, concerning the study of complex plants, the accurate modelling of these systems results in high computation times that are not acceptable for RT simulations. Therefore, the thesis focused on the development of innovative techniques for the modelling, RT and HIL testing of industrial systems, which aimed at obtaining the best compromise between accuracy and efficiency. In particular, the proposed strategies have been applied in two distinct test cases. The first one concerns with the development of both an efficient model of a turbo-machinery auxiliary plant and of a suitable RT control system for the execution of functional tests procedure on a real plants. The second one aimed at developing an innovative control system for Turbine Bypass Valves (TBVs) through HIL tests performed on a dedicated test rig. The research work has been executed by the Section of Applied Mechanics from the Department of Industrial Engineering of the University of Florence in collaboration with General Electric S.p.A and Velan ABV S.p.A, which provided the required tools and experimental data.

Acknowledgments

Always the same, acknowledgments are the toughest part to be written: I barely can find these few words, which I would like to express with extreme synthesis; so, forgive me.

I would like to express my sincere gratitude to professors Benedetto Allotta and Andrea Rindi, for their helpful support during this years and who allowed me to join the MDM Lab, which is more than a simple research laboratory. For this reason, I wish to thank all the people of MDM Lab, as engg. Enrico Meli, Luca Pugi, Susanna Papini, Alessandro Ridolfi, Lorenzo Marini, Daniele Nocciolini, Pierluca D'Adamio, Giovanni Pallini and all the other people that, more or less recently, joined and left the laboratory. You haven't been simply colleagues, but also I would say friends to me.

I also would like to thanks all the people of Ge Nuovo Pignone S.p.A. and Velan ABV S.p.A., who contributed to help the development of the research activity described in this thesis.

Then, I really wish to thank my family. Without them, I wouldn't be who I am now: my mom Rosalba and dad Riccardo who gave me life, than my grandparents Silvana and Orlando. Of course, I would thank Bruno and Anna, and my great-grandparent Amelia: I can still feel them beside me. In addition, I would thank my sister Eleonora, my aunt Angela and all my (old and new) friends.

Finally I especially wish to thank Claudia, whose love supported me all these years. This work wouldn't have been possible without her.

Contents

List of Figures

List of Tables

Introduction

The growing of computing performances of modern computers determined an increase in the use of numerical simulations and, in parallel, of Hardware In the Loop (HIL) simulations for the design and testing of complex mechatronics and embedded systems. In particular, HIL applications are simulation tools that have been widely applied in recent years [1, 2]. The basic idea is that of including a part of the real environment in the simulation loop during the system development, without actually installing it on hardware. Rather than testing the control algorithm on a purely mathematical model of the system, real hardware in the simulation loop can be used. Furthermore, the evaluation of tested system is carried out in Real Time (RT), ensuring that the embedded control system can deliver the control input within the desired sampled period of time. This is important as the lack of control signal at the end of the sample period can affect stability of both the simulated and psychical systems.

The success of HIL methods is mainly due to the increase in computing power of modern computers that made RT simulations accessible to the industrial companies and no longer relegated only to the academic field. Moreover, the development of Real Time Operating systems (RTOs) [3, 4, 5], with increasingly complex and versatile interfaces, made the development of RT applications extremely user-friendly, reducing the computer and programming skills for their realization.

The typical industrial applications are historically focused on the automotive technology, where HIL technologies contributed to the design and verification of smart (active or semi-active) suspensions for the suppression of vibrations, control instrumentation, ABS systems, control of airbags and safety systems [6, 7, 8, 9, 10, 11, 12].

Other industrial fields of application usually regard the power electronics (e.g. for the desing of inverters and electric motors drives) [13, 14, 15, 16, 17, 18], railways engineering [19, 20, 21], aerospace [22], military [23, 24] and biomedical implants [25] industries; while traditional applications in the academic field usually regard the robotics (e.g. for the validation of impedance and force control strategies) [26, 27, 28]. Also, HIL simulations technology is applied in other industries which produce consumer goods (e.g. household appliances, televisions and video recorders, home security systems, telephones), telecommunications systems (e.g telephone stations, stations for mobile telephony), land and environment protection systems [29, 30].

The continuous development of technologies for the fast prototyping of RT code has contributed to speed up the diffusion of complex HIL testing techniques also to the fluid systems technology, which covers different applications: pneumatic brake systems in the railway sector; in the automation area, control strategies for fluid components and plants; also, in the industrial field, hydraulic and pneumatic distributed systems (e.g. lube oil units or steam plants). In particular, HIL applications can be found in the energy industry as well, for instance in [31].

Moreover, an increasing interest in the application of HIL techniques can be noticed, for instance to large energy production facilities, including thermal plant controllers [32], electrical power management systems [33], or even large hydro-power plants [34]. However, even in many recent works related to thermal engineering [35], the application of HIL techniques is often confined to the testing of electronic control units (ECU) [6].

However, this approach still appears to be poorly followed in the energy field while, concerning the study of complex plants, the accurate modelling of these systems results in high computation times that are not acceptable for RT simulations.

In addition, a limit for this type of applications is often represented by the development of sufficiently efficient mathematical model of the simulated part. The experiences documented in literature usually refer to models that are mainly devoted to a specific application or that use expensive software packages, which are more versatile but developed for specific applications too.

Therefore, the research activity aimed at developing an innovative approach to the HIL testing of components and systems in the energy industry. In particular, this thesis focuses on the description of an efficient modelling approach for the dynamic simulation of thermal-fluid plants, considering both the incompressible and

compressible fluids, which have been employed to develop respectively auxiliary lubrication systems and steam-power plants, which will be analyzed in the present thesis.

The modelling and RT implementation strategies of the developed model on dedicated RT platforms are described in order to realize accurate and optimized models to obtain the best compromise between accuracy and efficiency, which is mandatory to meet the typical constraints introduced by the RT implementation. During the research activity, a library of components for the modelling of fluid plants was developed, considering also elements characterized by a high degree of complexity. Another important feature of the proposed modelling strategy involves the possibility to develop large plants models, characterized by lots of components. In addition, it is interesting to notice that the models are designed with a modular approach and therefore the library elements may directly be inserted and customized to produce a heavily customized code for both virtual HazOp analyses and RT simulations.

The research activity has been performed via numerical simulations, thorough the Matlab-Simulink software, of plant dynamics taking into consideration a few real contexts of practical interest and by executing experimental tests in collaboration with the project partners. In facts, the proposed modelling, RT and HIL techniques have been applied in two distinct test cases that are introduced to determine the effectiveness and reliability of the proposed approach:

The first test-case regards the development of both an efficient model of a turbo-machinery auxiliary plant and of a suitable RT control system for the execution of functional tests procedure on a real auxiliary plant.

The second one aimed at developing an innovative control system for Turbine Bypass Valves (TBVs) through HIL tests performed on a dedicated test rig. The second project belongs to the project *High Efficiency Valves* (CUP:D55C12009530007) which is financed by the program POR CREO FESR of Regione Toscana (European Funds for Regional Industrial R&D projects).

UNIONE EUROPEA
Fondo europeo di sviluppo regionale
PON Ricerca e Competitività 2007-2013
Ministero dell'Istruzione, dell'Università e della Ricerca
Ministero dello Sviluppo Economico
investiamo nel vostro futuro

Regione Toscana
Diritti Valori Innovazione Sostenibilità
POR CReO 2007-13
PROGRAMMA OPERATIVO REGIONALE OBIETTIVO COMPETITIVITÀ REGIONALE e OCCUPAZIONE
Fondo Europeo di Sviluppo Regionale
REPUBBLICA ITALIANA
UNIONE EUROPEA

The research work has been executed by the Section of Applied Mechanics from the Department of Industrial Engineering of the University of Florence in collaboration with General Electric S.p.A and Velan ABV S.p.A (respectively the industrial partners of the project concerning the first and the second test-cases), which provided the required tools and experimental data to validate the techniques proposed in this thesis.

UNIVERSITÀ DEGLI STUDI FIRENZE
DIPARTIMENTO DI INGEGNERIA INDUSTRIALE
GE Oil & Gas
VELAN ABV
Università degli Studi di Firenze
MDM LAB

Structure of the thesis

This thesis starts with an initial chapter presenting the state-of-the-art on the topic of the Real-Time (RT) simulations. In particular, the main working principles of Real-Time Operating Systems and scheduling paradigms are explained. Moreover, the concept of Hardware In the Loop (HIL) test is introduced.

The second chapter deals with a survey of the modelling approaches commonly used to study the dynamics of fluid systems. Then, according to Bond-graph modelling theory, an innovative modelling method is introduced to describe both the fluid dynamic and thermal transients of both compressible and incompressible fluids to achieve the required compromise between accuracy and efficiency.

The third chapter presents a practical application of Real-Time technologies. First, the modelling of an auxiliary lubrication system for turbo-machinery is presented, than the RT control is realized and performed through a Real-Time Operating system (RTOs). The model based-approach for the development of the controller will be validated according to the experimental data obtained during a functional test procedure.

Finally, the fourth chapter concerns with the development of an innovative control system for Turbine Bypass Valves (TBVs) through Hardware In the Loop (HIL) tests performed on a dedicated test rig. First, both the RT modelling and control aspects of a two-stages steam power plant are treated. Subsequently, the HIL architecture is described and the developed controller is validated according to tests carried out through the built rig.

Chapter 1

Real Time and HIL technologies: State-of-the-art

The growing of computing power of modern computers caused an increase in the use of numerical simulations and, in parallel, of HIL simulations in both the design phase and validation of components and complex systems. In particular, Hardware in the loop (HIL) simulations are techniques employed to the develop and test complex mechatronic systems [1, 2]. This kind of simulations are being widely used in the field of embedded systems, which indicate very complex electronic systems, devoted to a particular application and implemented in heterogeneous architectures. Through the development of mechatronics technology the HIL testing methods are being employed in many areas and, first of all, in the automotive one.

As said before, this thesis describes an efficient modelling approach for the dynamic simulation of thermal-fluid plants devoted to the development of innovative HIL architectures for the design and testing of industrial systems. However, a preliminary description of HIL architectures is useful to understand the procedures employed to develop the HIL applications proposed in the next chapters.

Therefore, this chapter provides an overview of the HIL systems. First, the aim is to explain how the Real Time Operating systems (RTOs) work, then the main features of HIL simulations will be described, showing the general architecture and compositional elements in these kind of applications.

1.1 Real Time Operating systems

A Real Time Operating system (RTOs) is an operating system devoted to support RT software applications [3, 4]. These kind of systems are used whenever a system response within a determined time is mandatory. Therefore, a RTOs must ensure that a task is processed within a specific time interval (deadline). An appropriate process scheduling is required to ensure this goal. Moreover, the provided answers and results must be those which are predicted (this feature is common to all processing systems). Generally, time scheduled tasks are iteratively repeated with an assigned frequency. The time scheduling of tasks, which is managed by the scheduler (see section 1.1.1), is affected by small errors and fluctuations (gitter).

RTOs can be classified according to the kind of events that have to be managed:

- *Event-driven*: in this case the system react to external events occurring in casual time instants. This kind of events are generally called *aperiodic events*.
- *Time-driven*: these RTOs work periodically, according to events occurring in predetermined periods of time. This kind of events are generally called *periodic events*.

Moreover, another classification is possible according to the kind of reaction to events:

- *Hard Real Time* systems: the temporal deadlines must be strictly respected to avoid catastrophic effects (often used in safety critical applications, e.g. air traffic control systems, nuclear reactors, the industrial plants, defense systems).
- *Firm Real Time*: occasionally, the temporal deadlines could not be respected as their violations do not imply catastrophic effects, but the usefulness of results decreases ad the delay with respect to the deadline grows (e.g. data-base transactions or on-line applications).
- *Soft Real Time* systems: occasionally, the temporal deadlines could not be respected as the correct system operation is not affected (e.g inputs of keyboard characters, telecommunications systems, video and audio transmission systems, automated manufacturing...).

In particular, the two applications that will be presented in the following chapters of this thesis belong to the casuistry of *Hard Real Time* systems.

Concerning the hardware implementation, two possible architectures can be exploited:

- The first one involves the use of two distinct calculators communicating through two boards. On the target PC is booted a simplified operating system (e.g. with no graphical interface, limited access to devices) with a RT kernel 1.1.3 while the host PC provides a HMI (for the process management, to display the controlled and measured variables and data storage) of the RT system. The communication between the two calculators is implemented via Ethernet boards or a wireless LAN connection. The communication between hardware and software is performed through one or more I/O cards installed on the target PC. For instance, both National Instrument (LabVIEW) and Mathworks (Matlab) use this type of architecture for their RT tools (respectively LabVIEW Real-Time and xPC Target).
- The second one is based on a single calculator on which an open-source operating system (e.g. Linux) is patched with a RT plug-in.

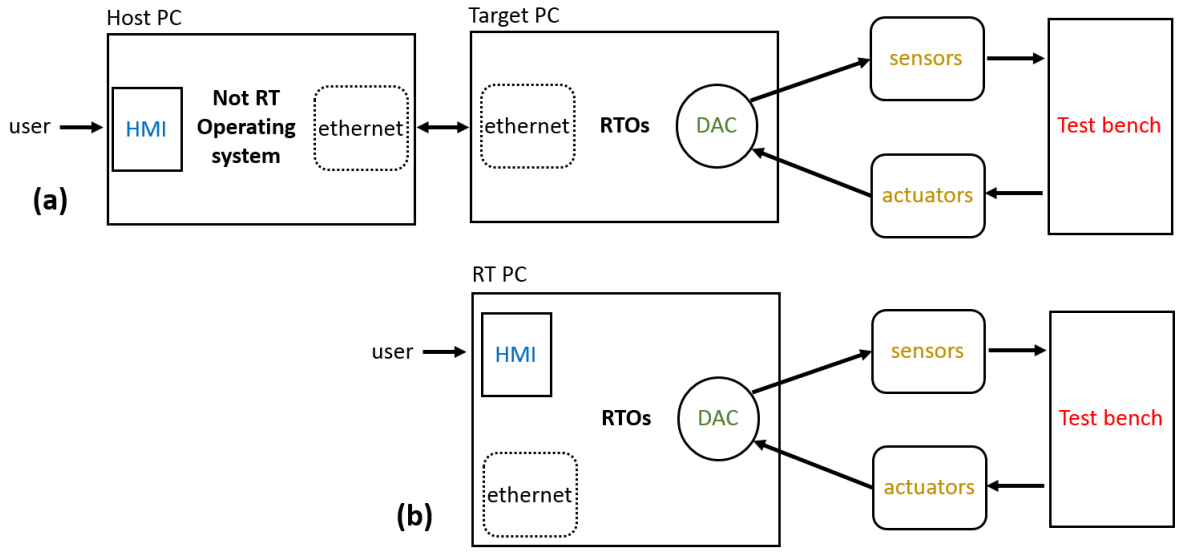

Figure 1.1: Architectures of RT systems with two calculators (a) and a single calculator (b).

1.1.1 Scheduling

The main difference between a not-RT system and an RTOs is mainly due to the scheduler. The scheduler is an algorithm that controls the access to the CPU from

the various calculator processes. The scheduling is critical to ensure the computational efficiency of the calculator, ensuring an optimized use of the CPU among processes that work in parallel considering the interrupts, i.e. operations which are asynchronously activated by an external event such an hardware generated signal. Typical examples of interrupts are emergency procedures, execution of operations which are triggered by a particular value of a simulated or acquired signal or generated by I/O units, memories and hard-disk.

Therefore, the scheduling problem aims at a feasible scheduling in the whole set of the tasks. In particular, the following conditions have to be guaranteed:

- Each task should be terminated within its deadline.
- Each priority constraint has to be respected.
- All shared resources (mutually exclusive) have to be properly used.

A process (or task) can be defined as a sequence of instructions that (in absence of other activities) is executed from the CPU in a continuative way till to its completion. In particular, the possible states of a task are the following:

- *Ready*: ready for execution, waiting for the CPU.
- *Pended*: waiting for a resource which is required by the task to proceed in the execution.
- *Delayed*: waiting for the end of a predetermined timeout.
- *Suspended*: it is the initial state of a just created task.

The tasks in *ready* state are ready to be executed. The way in which tasks access to the CPU is a function of the algorithm implemented on the scheduler. In particular, the most important aspects are priority and preemption:

-*Priority*: this attribute defines the importance of a task with respect to the others. It defines a criterion for an optimized execution in a context characterized by limited resources: tasks with higher priority can start before or even pause (if preemption is admitted) the execution of another task with lower priority to be completed. Background or idle tasks have the lowest priority. In particular, the priority can be distinguished in internal priority (defined according to several criteria as memory,

I/O requests, execution time) and external priority (user defined). Moreover, it can be defined a dynamic priority (aging): Processes in low priority are bypassed by processes in higher priority. However, it might happen that a process could never be executed (it is starved to death: starvation). Thence, when a process has been ready to run for a long time, his priority is dynamically increased by the scheduler.

-*Preemption*: if a ready process with higher priority than the one running on the CPU is in the queue, the scheduler forces up the CPU to be releases and to run the process with the highest priority. For instance, this is what often happens for the I/O. If a high-priority process is interrupted for the management of an I/O operation, the scheduler passes the CPU to the next process. If preemption is absent, the high-priority process should wait for the low-priority one to run. Conversely, the use of preemption allows the CPU to be releases from low-priority processes when high-priority processes return ready (e.g. when a I/O operation is over).

The tasks execution involves a certain time consumption. If the time needed for the execution of a task (turnaround time) exceeds the deadline (usually the sample time, which corresponds to the reciprocal of task frequency) it may be scheduled to execute before its previous instance has completed. The result is a task overrun. Therefore, when a task overrun occurs, the task execution causes a delay which exceeds the maximum allowed one. if the scheduler is non preemptive it cannot interrupt the execution of the task with potentially dangerous consequences. Consequently, preemptive schedulers are the most diffused in RT contexts and, in safety related applications, additional hardware and software protections are usually implemented (e.g. watchdog or redundant safe layouts).

More generally, the scheduler algorithm can be distinguished according to the following characteristics:

- *Preemptive*: preemption is allowed.
- *Non preemptive*: preemption is not allowed.
- *Static*: decisions referred to fixed parameters assigned to the tasks before their activation.
- *Dynamic*: decisions referred to parameters variable during the tasks execution.
- *Off-line*: decisions are taken before tasks activation according to prior known data and stored on a schedlunig table that in run-time is executed by a dispatcher.

- *On-line*: decisions are taken during the execution.
- *Best-Effort*: the schedule is decided according to a cost function globally defined on tasks set. Mean performances are privileged rather than timing constraints.
- *Guaranteed*: time constraints of each task is guaranteed. A guarantee test runs every time that a new task enters the system.

1.1.2 Classification of RT task scheduling algorithms

Several schemes of classification of RT task scheduling algorithms exist. A popular scheme classifies the RT task scheduling algorithms based on how the scheduling points, i.e. the points on time line at which the scheduler makes decisions regarding which task is to be run next, are defined. The main types of schedulers according to this classification scheme are: clock-driven, event-driven, and hybrid.

The clock-driven schedulers are those in which the scheduling points are determined by the interrupts received from a clock. In the event-driven ones, the scheduling points are defined by certain events which precludes clock interrupts. The hybrid ones use both clock interrupts as well as event occurrences to define their scheduling points.

A few important members of each of these three broad classes of scheduling algorithms are the following:

- Clock Driven: Table-driven, Cyclic.
- Event Driven: Simple priority-based, Rate Monotonic Analysis (RMA), Earliest Deadline First (EDF).
- Hybrid: Round-robin (RR).

Typical examples of clock-driven schedulers are table-driven and cyclic schedulers. Clock-driven schedulers are simple and efficient. Therefore, these are frequently used in embedded applications.

Important examples of event-driven schedulers are Earliest Deadline First (EDF) and Rate Monotonic Analysis (RMA). Event-driven schedulers are more sophisticated than clock-driven schedulers and usually are more proficient and flexible than clock-driven schedulers. These are more proficient because they can feasibly schedule

some task sets which clock-driven schedulers cannot. These are more flexible because they can feasibly schedule sporadic and aperiodic tasks in addition to periodic tasks, whereas clock-driven schedulers can satisfactorily handle only periodic tasks. The most known event-driven algorithms are the Earliest Deadline First (EDF) and the Rate Monotonic Analysis (RMA). It is worth to note that several variations to these two basic algorithms exist.

Another classification of RT task scheduling algorithms can be made based upon the type of task acceptance test that a scheduler carries out before it takes up a task for scheduling. The acceptance test is employed to decide whether a newly arrived task would at all be taken up for scheduling or be rejected. Based on the task acceptance test used, there are two broad categories of task schedulers:

- Planning-based.
- Best effort.

In planning-based schedulers, when a task arrives the scheduler first determines whether the task can meet its dead-lines, if it is taken up for execution. If not, it is rejected. If the task can meet its deadline and does not cause other already scheduled tasks to miss their respective deadlines, then the task is accepted for scheduling. Otherwise, it is rejected. In best effort schedulers, no acceptance test is applied. All tasks that arrive are taken up for scheduling and best effort is made to meet its deadlines. But, no guarantee is given as to whether a task deadline would be met.

Another type of classification of RT tasks is based on the target platform on which the tasks are to be run. The different classes of scheduling algorithms according to this scheme are:

- Uniprocessor.
- Multiprocessor.
- Distributed.

Uniprocessor scheduling algorithms are possibly the simplest of the three classes of algorithms. In contrast to uniprocessor algorithms, in multiprocessor and distributed scheduling algorithms first a decision has to be made regarding which task needs

to run on which processor and then these tasks are scheduled. In contrast to multiprocessors, the processors in a distributed system do not possess shared memory. Also in contrast to multiprocessors, there is no global up-to-date state information available in distributed systems. This makes uniprocessor scheduling algorithms that assume central state information of all tasks and processors to exist unsuitable for use in distributed systems. Further in distributed systems, the communication among tasks is through message passing. Communication through message passing is costly. This means that a scheduling algorithm should not incur too much communication over- head. So carefully designed distributed algorithms are normally considered suitable for use in a distributed system.

According to priority and preemption many schedulers have been developed. The most common scheduler algorithms are:

-*FCFS (First Come First Served)*: based on a First In First Out logic (tasks are executed in the order that they arrived), a preemption logic is not considered. Therefore, it is difficult to forecast its results (it depends on the arrival order of the tasks) causing a minor efficiency. Since it is non preemptive, short-time tasks are non favored (because of the long waiting times).

-*SJF (Shortest Job First)*: in this case the tasks which require a minor use of the CPU in terms of execution time are privileged. However, it is difficult to forecast CPU times that can be given by the user but, usually, are estimated by the algorithm itself (e.g. computing the weighted average of previous execution times). It can be both preemptive (in this case is also called SRTF-Shortest Remaining Time first) and non preemptive.

-*Time-Sharing Scheduling*: These algorithms are preemptive and characterized by a timer. A quantum of time is assigned to each task. The bigger is the quantum, the minor will be the interactivity degree among the tasks. Round Robin (RR) is one of the most employed of Hybrid and Time-Sharing Scheduling algorithms, which is an FCFS preemptive algorithm which uses the quantum of time. One of the advantages of this kind of algorithm with respect to FCFS is the possibility of ration among tasks. In addition, it is less efficient than a preemptive SRTF but the processes end up in the nearest time.

-*Multiple Queue Scheduling*: it represents a combination of multiple scheduling strategies as different tasks are managed with separate queues characterized by different schedulers. For example, in Unix background tasks are considered batch

(without preemption), while the foreground ones are interactive.

Concerning the most diffused operating systems (Linux and Windows) the implemented scheduling logics are the following:

- Linux Scheduling: there are two separate tasks queues, one relative to soft RT tasks (RR or FCFS scheduler with static priority) and user tasks (RR scheduler, which is not in real time and is characterized by dynamic priorities) that are managed through ticks (time units for the CPU usage). Each task is characterized by a certain number of ticks and when a task is ready the number of used ticks is decreased. When a task is dispatched (removed from the CPU and substituted) the task with the larger number of ticks is then executed. Finally, when all of the ready tasks have no more ticks, they are reassigned. It should be noticed that ticks depend on priority and, obviously, RT tasks have a very high priority. All the ready tasks have to use up all the credits, thus avoiding starvation unless lots of RT tasks are present.

- Windows Scheduling: as in Linux, there are soft RT tasks and user tasks. In user tasks, priority is reduced if is used the whole time quantum, but never decreases below a certain value (while in Linux it can reach zero). Consequently, starvation may occur, although an aging mechanism is present. In particular, Windows is characterized by mechanisms that privilege tasks with both the windows on the foreground and tasks using several devices (e.g monitor and keyboard). Generally, Windows operating system are not RTOs since the task execution time is unpredictable. Furthermore, hard disk drives introduce strong execution latencies, preventing to evaluate the time needed to retrieve the information. Finally, several implemented systems (direct memory access, cache, interrupts, power management systems) reduce predictability as well.

1.1.3 RT kernel

The kernel is a computer program that defines fundamental part of a modern operating system. Its purpose is to management and control over everything that occurs in the system (e.g. I/O requests from software, memory management, communication with peripherals).

A RT kernel assigns an execution time limit to each user level process and, once this time is expired, the resources are assigned to the next task. However it might happen that, while acquiring data with an I/O board, this approach does not guarantee that

all signals are correctly acquired and that the encoding and decoding algorithms are solved by the CPU.

For instance, the Linux RT kernel (see Figure 1.2 (b)) could be situated between the operating system kernel and the computer hardware.

The RT kernel modifies the task scheduling by replacing it with another with fixed priority and assigning the minimum priorities to the operating system kernel which is an independent task. The RT PlugIn receives all the hardware interrupts while the interrupts directed to the Linux kernel become low priority (software) interrupts. Obviously, the priority defines the execution order of RT tasks.

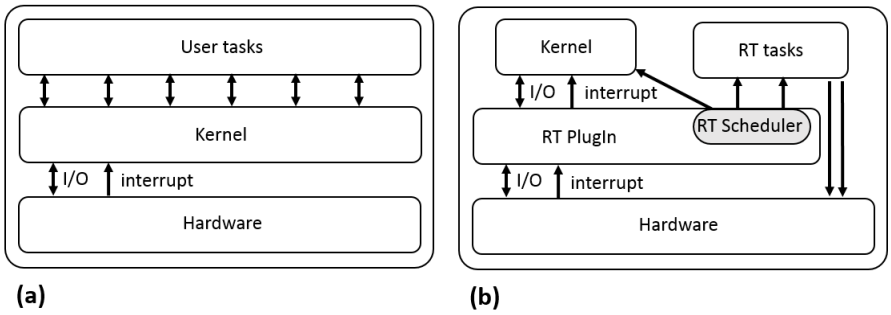

Figure 1.2: Architectures of non RT (a) and RT kernels (b).

1.2 Hardware In the Loop testing

In a HIL simulation, the test object (e.g. the ABS controller of a vehicle) is tested on a test rig that reproduces the system that this object must control (e.g. brakes). The overall system in which this is integrated (e.g. car) is simulated with a suitable mathematical model and runs on a RT platform. The communication between the real and virtual systems is obtained through sensors (brake system pressure measurement) and actuators (e.g. simulating the braking action on the pedal).

The main advantages of a HIL simulation in the design of a mechatronic product can be expressed in terms of:

- Reduction of the design time.
- Reduction of the testing cost.
- Improvement of tests safety.
- Inclusion of the human interaction.
- Enhancement of results faithfulness and quality.

The design time is reduced as the testing of a component is clearly more fast: the realization of a complete prototype to test the it is no longer necessary as it can be performed in the design stage, reducing the durance of the testing phase on the final prototype and consequently its costs, in terms of both running costs and costs due to safety precautions. Moreover, it should be considered that machines and control systems are usually developed in parallel, which means errors in the control system can only be found during commissioning. With HIL simulation, errors can be found early-on and solved early-on.

The safety of the testing phase is improved as a great part of the plant to which the component under test belongs is virtual. Therefore, since dangerous processes are non longer real but only simulated the safety of the tests can be considerably increased. For instance, it could be very useful in systems where heavy lift cranes are present and where personnel safety is of the utmost importance and therefore extensive safety procedures are required. Finally, the results of HIL simulations are more are more indicative of the real behavior of the system under test with respect to results obtained with purely virtual simulations.

In addition, in most testing procedures the human interaction is not included. However, HIL simulation can be employed to test the human interaction on machines, allowing to test if machines can be operated easily and comfortably. If the HIL simulation is extended with visualization screens they can be used to train operators.

Concerning the quality of design, if HIL simulation is embedded in a model based design process of a plant or component, it can be used already during its early stages. The HIL simulator will grow with the design of the real plant and can be used to continuously test their control systems. These tests may reveal problems that would otherwise have been found at the final phases of a design where the control system and plant are integrated, leading to a significant increase in the quality of machines and systems.

The realization of a HIL architecture is subjected to several development conditions. First, the virtual part must be implemented in a mathematical model which should be consistent with the physics of the process. Consequently, interdisciplinary skills for the modeling of complex systems are required (e.g. mechanics, electronics, industrial automation) as well as computer science knowledge. In addition, a RT hardware on which is implemented a suitable RTOs is required to execute RT simulations. As the model has to be compiled and uploaded on the RT hardware, a high efficiency level is required to meet the RT constraints described in the previous sections. Consequently, the development of RT model for the virtual part should aim at reaching the best compromise between accuracy and efficiency. Finally, the hardware architecture has to manage the I/O for the management of the signals between virtual simulation and test rig.

Therefore, the general architecture of a HIL system, as shown in Figure 1.3, is composed by the following parts:

- Software:

- The HMI (Human Machine Interface) allows the user to perform the on-line management of the testing conditions and the storage of the testing data.
- The RT model defines the virtual part of the complete plant physics, which is only simulated. Eventually, a RT control system is present.
- The DAC acquisition board performs the communication between the virtual model and both sensors and actuators respectively through the A/D and D/A

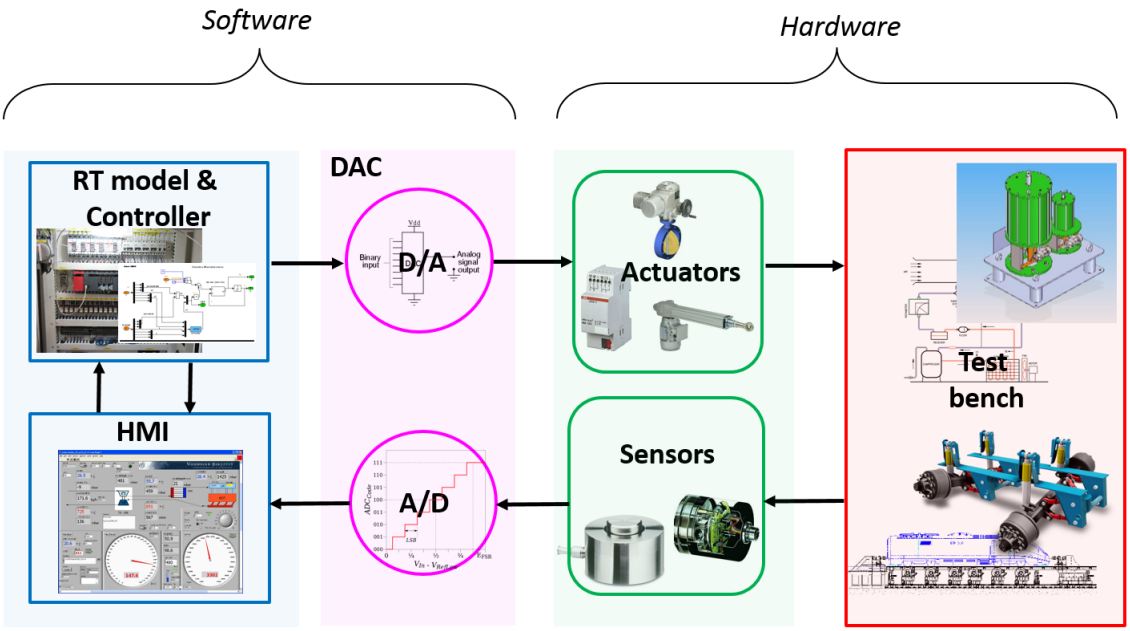

Figure 1.3: General architecture of a HIL simulation.

modules which are designed to convert an analogical signal to a digital one and vice versa.

- Hardware:

- The sensors are employed to monitor the state of the test rig.
- The actuators are used to interact with the rig.
- The test rig is the element of the HIL architecture on which the physical component under test is present.

Chapter 2

Modelling of fluid-thermal systems

This chapter introduces general modelling concepts to build fast and efficient lumped models of industrial plants which are characterized by the presence of compressible and/or incompressible fluids. In peculiar, the developed modelling method is optimized for RT simulation and consequently HIL testing of mechatronic components. For this reason, the proposed strategy is focused at obtaining the best trade-off between accuracy of the obtained results and execution efficiency.

Bond-graph modelling techniques are introduced to describe a mono dimensional flow, in order to approximate the distributed fluid models in high efficiency lumped ones. In particular, the proposed approach is followed to support fixed step solvers which are necessary for the further implementation on RT target. In facts, the execution on RT targets are constrained by the need of a limited execution time to respect assigned scheduling and timing of tasks (see chapter 1).

Some modelling applications examples are also introduced: the hydraulic and pneumatic components that are employed in industrial and mechatronics units (for instance valves, pumps, accumulators).

2.1 Modelling approach

2.1.1 State-of-the-art in fluid dynamics modelling

For RT applications, an efficient and integrated design of thermal-fluid plants should involve both the prototyping of the models [36], including all the integrated mechatronic components (e.g. electric and fluid actuators, pumps, valves, sensors) and the control algorithms [37]. However, this process appears to be poorly followed, especially in RT applications, in particular for all those components described by complex mathematical models, such as the Pressure Control Valve (PCV), Temperature Control Valve (TCV), Main Pressure Control Valve Actuator, Extraction Control Valve Actuator, Current-to-Pressure Converter (CPC), etc. [38].

Modern lubrication studies (based on Computational Fluid Dynamics techniques, CFD) assess with a high accuracy level the main components performances. For example, in bearing performances analyses, 3D CFD simulations are required to achieve reliable results for highly loaded Thrust Bearings [39], Journal Bearings [40], TPJBs [41] and dynamically loaded supports [42] (i.e., bearings of connecting rods for automotive engines). In addition, CFD studies, about particular valves commonly present in industrial plants [43], can be found. Pneumatic plants are studied with a high accuracy degree: as well, for instance, boilers [44] or steam plants dynamics [45] are considered. However, in complex plants the accurate modelling of these systems results in an high computation times, that is not acceptable for RT simulations.

Conversely, the typical plants components (e.g. valves or hydraulic bearings) and lubricant supply plants are based on simplified lumped parameter models [46]. At the same time, in the rotor-dynamic field, bearings are generally regarded as lumped parameters spring-damper systems [47, 48, 49]. This approach is very efficient but, usually, not very accurate.

Therefore, the research activity carried out in these years aimed at developing an accurate lumped parameter model, especially in transient operation, characterized by an high accuracy level, however with a greater efficiency. In particular, the modelling technique followed in literature [50, 51, 52, 53, 54, 55, 56, 57, 58] to describe mono-dimensional, isotropic, incompressible and compressible, viscous and laminar flows is the so-called Bond-graph approach, which will be briefly described in the following section 2.1.2. This method, which can be used to better approximate the distributed

models in terms of high efficiency lumped ones, is optimized for RT simulation and consequently HIL testing of complex plants.

2.1.2 Bond-graph modelling

The Bond-graph method is a graphical approach to modeling, which provides a way to understand and mathematically model basic as well as complex fluid systems that is consistent with other energetic domains (electric, electromechanical, thermal, mechanical, chemical, etc.).

According to this method, component energy ports are connected by bonds that specify the transfer of energy among system components belonging to various energetic domains. Power, the rate of energy transport between components, is the universal currency of physical systems. The concept of power can be described by the product between two power variables, *effort* and *flow*, that illustrates the energy transfer in a generic system using power bonds. In particular, a power bond is symbolized by a half-arrow, whose orientation indicates the direction of power transfer (Figure 2.1) between two subsystems (the power transfer is positive in the direction of the arrow).

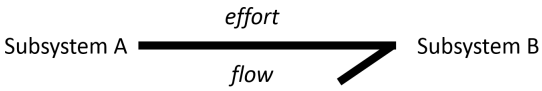

Figure 2.1: Bond-graph power system.

The Bond-graph representation is similar to the well known block diagrams and signal-flow graphs, however the arcs in bond-graphs represent bidirectional exchange of physical energy, while those in block diagrams and signal-flow graphs represent unidirectional flow of information.

Therefore, one way to consistently partition and connect subsystem models is by using effort and flow variables to quantify the system interactions. These power-conjugate variables (i.e., those whose product yields power) can be identified for each energy domains of interest, as summarized in Table 2.1.

The sections where the subsystems can be interconnected are those through which the power can flow among the subsystems. These parts are defined as *ports* and the physical subsystems realized with one or more doors are called *multiport*. A system

Table 2.1: Effort and flow variables in different physical domains.

Domain	Effort	Flow
Mechanical (translation)	Force $[N]$	Velocity $[m/s]$
Mechanical (rotation)	Torque $[Nm]$	Angular velocity $[rad/s]$
Electrical	Voltage $[V]$	Current $[A]$
Hydraulic	Pressure $[Pa]$	Volume flow rate $[m^3/s]$
Thermal	Temperature $[K]$	Entropy flow rate $[W/K]$
Chemical	Chemical potential $[kJ/mol]$	Mole flow rate $[mol/s]$
Magnetic	Magnetomotive force $[AT]$	Magnetic flux $[Wb]$

with a single port is called *1-port*, a system with two ports is called *2-ports* and so on. In particular, a 1-port element is connected to the network through a single energy port and a unique pair of effort and flow variables exists, while a 2-port element is connected through two energy ports to which correspond two pairs of effort and flow variables.

This basis assures energetically correct models, and provides a consistent way to connect system elements together. The graphical nature of bond graphs separates the system structure from the equations, making bond graphs ideal for visualizing the essential characteristics of a system. Therefore, the lumped parameter elements of resistance, capacitance and inertance are interconnected in an energy conserving way by bonds and junctions resulting in a network structure. Considering the Bond-graph representation, the derivation of system equations is so systematic that it can be implemented in algorithms. In facts, the modelling and simulation of physical multi-domain systems can be carried out through existing software (e.g., Matlab-Simscape, ENPORT, Modelica [59], Camp-G, SYMBOLS, LMS Amesim, COSMO, LorSim) that are based on the proposed approach. In particular, considering the activities carried out during these years, the research focused on the development of efficient thermal fluid models in Matlab, starting from the Bond-Graph approach.

2.2 Fluid models description

According to the Bond-graph modelling method described in the previous section 2.1.2, the fluid is described in terms of mass balance (continuity/mass conservation, Equation 2.1), momentum balance (Equation 2.2) and and energy balance (enthalpy balances and more generally expressions derived from the first principle of thermodynamics, Equation 2.3) based on the 1-D Navier-Stokes equations:

$$\frac{d\rho}{dt} = \frac{\frac{dm}{dt} - \rho\frac{dV}{dt}}{V(t)}; \tag{2.1}$$

$$\rho\left(\frac{\partial v_x}{\partial t} + v_x\frac{\partial v_x}{\partial x}\right) = -\frac{\partial p}{\partial x} - f_x + \rho g_x; \tag{2.2}$$

$$\frac{dh}{dt} = c_p\frac{dT}{dt} - T\left(\frac{\partial \nu_s}{\partial T}\right)_p\frac{dp}{dt}. \tag{2.3}$$

where the employed variables are the following: t defines the time $[s]$, V is the fluid volume $[m^3]$, ρ is the fluid density $[kg/m^3]$, m is the fluid mass $[kg]$, x represents the longitudinal direction in space $[m]$, v_x defines the longitudinal velocity $[m/s]$, p is the fluid pressure $[Pa]$, f_x defines the axial tangential effort $[kg/(m^2 \cdot s^2)]$, h is the specific enthalpy $[J/kg]$, c_p is the specific heat at constant pressure $[kJ/kg \cdot K]$, T represents the temperature $[K]$ and v_s defines the specific volume $[m^3/kg]$.

In order to reproduce the dynamical behaviour of thermal hydraulic systems, PDEs (Partial Differential Equations), Equations 2.1,2.2,2.3 are solved. Following the above-mentioned bond-graph approach [53, 54, 55], the plant model is discretized in lumped elements where the PDEs (Equations 2.1, 2.2, 2.3) are rewritten in terms of control volume balances. Therefore, the system can be described by an ODE (Ordinary Differential Equation) system.

To realize a lumped parameters model of the real plant, different elements have to be described. This way, the model is characterized by good accuracy, similar to the one of 3D models, obtaining a high numerical efficiency. Thus, the main elements are:

- Resistive-Inertial (RI) or just Resistive (R): RI-element is a lumped component where only the momentum balance is implemented, in order to calculate the mass flow rate $\dot{m}$ and the enthalpy flow rate H. The control sections, considering inlet and outlet conditions (temperature T, pressure p and enthalpy h), are calculated

by an adjacent capacitive element or imposed by an external source (boundary conditions). If transient terms (time derivative) in Equation 2.2 are neglected, only dissipative effects are modelled and the corresponding element is called R or pure resistive element, which is represented in Figure 2.2. Typical resistive elements are orifices, valves and almost every component in which drag or inertial effects are dominant while energy and mass exchanges are absent or negligible.

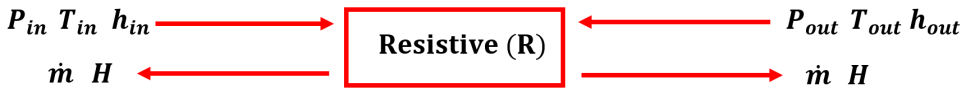

Figure 2.2: Resistive element.

- Capacitive (C): for the C elements, a lumped volume (or capacity) is described by energy and mass balances to calculate a local value of temperature T, pressure p and enthalpy h (assuming inlet and outlet mass flow rates $\dot{m}$, and enthalpy flow rates H as imposed). Moreover, both the thermal and the work exchanges can be considered introducing in Eq. 2.1, 2.3 the corresponding effects. The input / outputs of a typical capacitive element are illustrated in Figure 2.3. Typical components which can be represented as Capacitive elements are tanks, heat exchangers, junctions in which is modeled the mixing of different inlet flows and more general components associated to energy or mass exchanges.

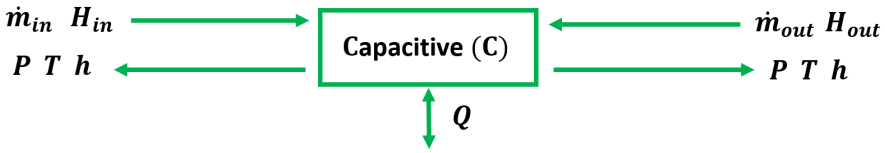

Figure 2.3: Capacitive element.

- Mixed Elements (ME): ME elements are composition of the RI and C elements to describe different components with particular physical behavior, e.g. boundary elements, T-connections, etc.

An important feature of this approach consists in the bidirectional variables exchange among the various blocks in which the network is discretized (see Figure 2.4).

Considering the aforementioned approach a large library of components (e.g. orifices, valves, actuators, etc..) commonly employed in industrial plants was

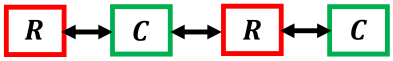

Figure 2.4: Discretized network of R-C elements

developed. Since many elements have been modeled and validated over time, even complex plants can be assembled. In addition, the high customization of the components allows to build and simulate the transient dynamics of different plants according to the specific requirements needed by industrial partners (see Figure 2.5).

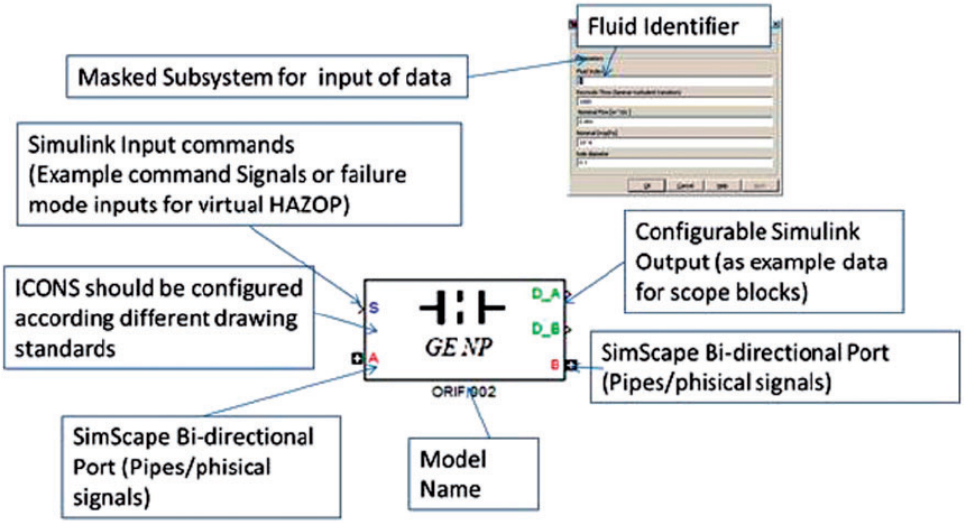

Figure 2.5: Example of simulation block, representing a flanged orifice, with corresponding conventions adopted for data-exchange ports.

Opposed to other known commercial products, the realized models have been customized in order to ease simulation of complex interactions with digital logic components and plant controllers including their sensors and measurement systems. In particular, the proposed approach is optimized for fixed step execution and fast prototyping of Real Time code both for RT-HIL testing and production purposes as well.

An additional characteristic of the developed models is robustness, making them suitable for virtual (simulated) Haz-Op analyses (component failures or off-design conditions) during the design process [60, 61, 62]. In facts, simulation of failures often correspond to ill conditioned models, that should be difficult to be treated from a numerical point of view. Consequently, robustness and stability of the simulation code represents a mandatory specification.

Finally, the proposed modelling strategy allows automatic model generation: in order to reduce errors and delays due to model transcription and data transcription from technical documentation, the developed Simulink model can be automatically generated by P&Id schemes, e.g. taken from GE PidXP configuration tool (an engineering tool/database for the definition and sketch of hydraulic systems). Using a simple tool internally developed by GE, the user is able to automatically extract a network topology from a P&Id scheme of the industrial system, where each component is associated to the corresponding database of properties and technical information and allows the automatic generation of the developed model simply using remote construction instructions. The topology of the automatically generated model is very similar to the P&Id scheme since there is 1:1 correspondence among P&Id symbols and library models. The relative positions of components are also reproduced to define an intuitive approach. It is important to notice that since the model is built in Matlab-Simulink, further customization and modifications are still possible, considering that most of the parameters are masked, and the blocks are accessible as standard masked subsystem. If a failure analysis is required, the failure list is automatically created starting from the elements present in the plant topology, where each component has several failure modes depending on the element characteristics (e.g. the three-way valve (TCV) can failure remaining open both in the hot side and in the cold one). The work-flow corresponding to the automatic model generation from PidXP is schematized in Figure 2.6.

It is interesting to notice that the software is designed with a modular approach, and so an expert user may directly drop, block to produce its own heavily customized code for simulation; on the other hand, standard analysis can be eventually performed by intermediate and entry level users following the automated-guided process, which strongly reduces the risk of human errors and can assure safety and repeatability of both failure analyses and RT simulations.

To summarize, the main modelling characteristics of the proposed approach are resumed in Figure 2.7.

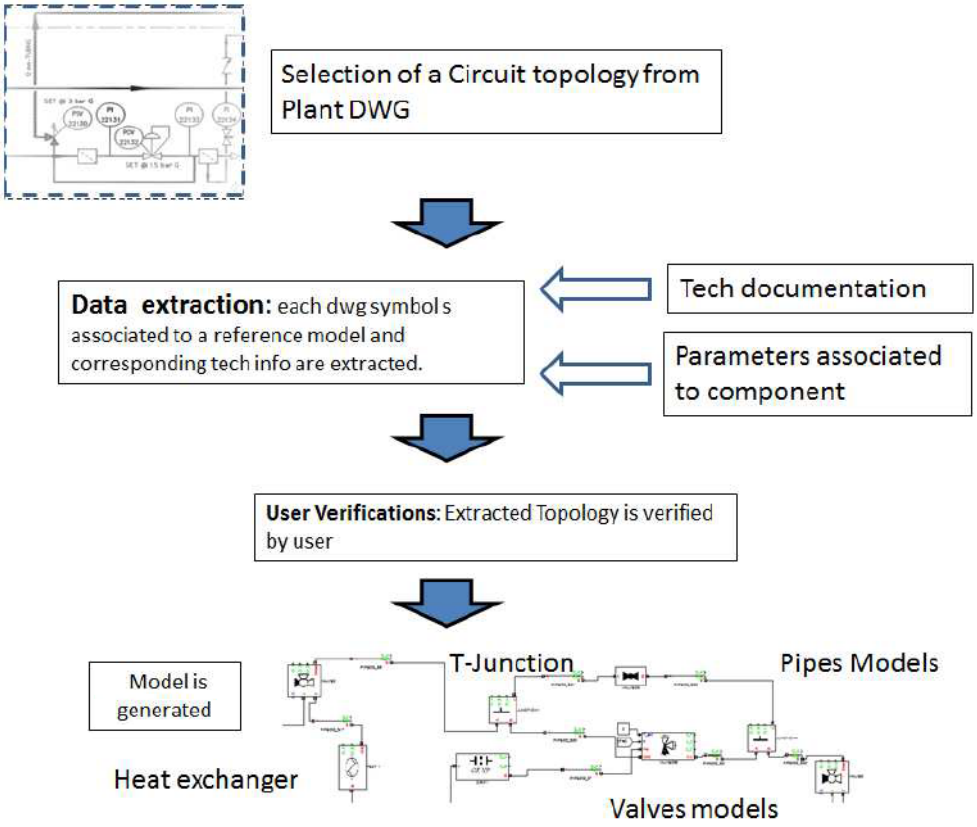

Figure 2.6: Typical workflow from P&Id scheme to the corresponding Matlab model.

2.2.1 Resistive components modelling

The resistive element is modelled starting from the equation of motion (momentum conservation) 2.4 generalized for the three-dimensional case:

$$\rho\left(\frac{\partial v_x}{\partial t}+v_x\frac{\partial v_x}{\partial x}+v_x\frac{\partial v_x}{\partial y}+v_x\frac{\partial v_x}{\partial z}\right)=-\frac{\partial p}{\partial x}\left(\frac{\partial \tau_{xx}}{\partial x}+\frac{\partial \tau_{yx}}{\partial y}+\frac{\partial \tau_{zx}}{\partial z}\right)+\rho g_x. \tag{2.4}$$

In the mono-dimensional case the Equation 2.4 can be simplified in the form shown in Equation 2.2.

Moreover, as visible in Figure 2.8, considering an uniform flow rate in a pipe with a constant section A, length l, inclined of an angle θ with respect to the ground, the momentum balance, shown in Equation 2.2, should be written as in Equation 2.5,

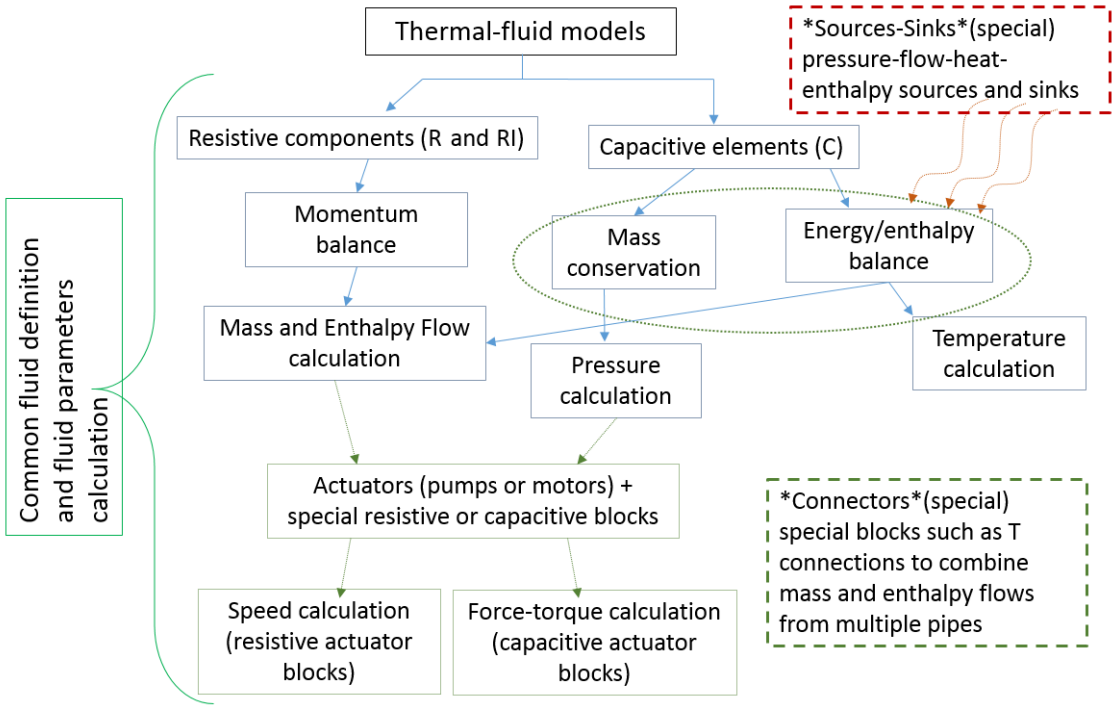

Figure 2.7: Main characteristics of the proposed modelling approach.

where $\dot{V}$ is the volumetric flow rate $[m3/s]$ assumed to be homogenous along the pipe

$$\rho l \frac{d\dot{V}}{dt} = (p_{in} - p_{out})\, A - \xi\,(Re)\, \frac{\rho \left|\dot{V}\right| \dot{V}}{2A} - \rho g sin\,(\theta)\, Al; \tag{2.5}$$

The ξ term represents the viscous friction factor which is calculated as a function of Reynolds number Re. In the form described by Equation 2.5, the volumetric flow rate can be calculated by means of the integration layout schematized in Figure 2.8.

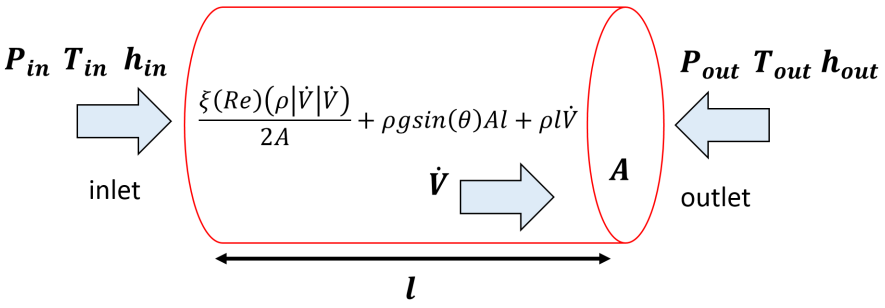

Figure 2.8: Sketch of a general RI element.

However, in several examples, the contribution of the time derivative terms are

negligible, then, the Equation 2.5 can be written in a simpler form (shown in Equation 2.6), that can be solved without any additional integrator block. That case the element is simply called R (or pure resistive) and corresponds to a simpler implementation.

$$\left(p_{in}-p_{out}\right)A-\xi\left(Re\right)\frac{\rho\left|\dot{V}\right|\dot{V}}{2A}-\rho gsin\left(\theta\right)Al-\rho l\frac{d\dot{V}}{dt}=0\Rightarrow\dot{V}=f\left(p_{in}-p_{out}\right); \quad (2.6)$$

The mass flow rate $\dot{m}$ is directly calculated from the volumetric flow rate $\dot{V}$ and the density value ρ in the inlet section. In addition, considering the iso-enthalpy hypothesis of the flow, the enthalpy flow rate H is computed starting from the specific enthalpy h

$$\begin{aligned}\dot{m}&=\rho\dot{V},\\ H&=h\dot{m}.\end{aligned} \quad (2.7)$$

The use of the R and the RI components allows the simulation of different components such as distributed or lumped pipe losses, orifices and valves, which can be defined through a variable area (flow coefficient). The controlled R components consist in a R systems which have the controller algorithm implemented using the Matlab blocks.

It is worth to note the possibility to model hydraulic actuators (such as pumps and motors) using a customized version of Equation 2.6, where $\dot{V}$ is directly calculated to model actuator behaviour: i.e. a centrifugal pump is described in terms of load ϕ and flow φ coefficients. Hence, the Equation 2.8 should be adopted

$$\begin{aligned}&\dot{V}=f\left(p_{in},p_{out},n\right)=f\left(\phi,\varphi,n\right);\\ &\phi\left(\varphi\right)=\frac{\dot{V}}{nc_{\phi}},\ \varphi=\frac{p_{in}-p_{out}}{n^{2}c_{\varphi}}.\end{aligned} \quad (2.8)$$

where n defines the rotation speed and c_{ϕ}, c_{φ} are characteristics coefficients.

Enthalpy exchanges introduced by the hydraulic actuators have to be evaluated for the calculation of the proper enthalpy flow rate; indeed, the specific enthalpy h in the outlet section has to be coherently recomputed taking into account the exchanged mechanical work calculated in Equation 2.3. Even considering the hydraulic power W_h and the efficiency of the pump $\eta(\phi,\varphi)$, it is possible to compute the mechanical power W_m and the required torque T_{res}. As consequence, also a pump or an

actuator/motor should be modelled as a customized resistive block. For instance, an asynchronous motor can be efficiently modelled considering a known-tabulated speed-torque response T_m while a filtering transfer function should be introduced to model inertial and viscous friction mechanical loads

$$T_m(n) - T_{res} = J_m \frac{dn}{dt} + fn \Rightarrow n = \frac{T_e(n) - T_m}{J_m s + f}; \tag{2.9}$$

where J_m is the motor inertia and f defines the friction factor.

2.2.2 Capacitive components modelling

The mass conservation in Equation 2.1 can be applied to a control volume represented in Figure 2.9 to determine the density ρ, and consequently, knowing the properties of the modelled fluid, is possible to calculate the pressure derivative from the following Equation

$$\frac{dp}{dt} = \beta \left[\frac{1}{\rho} \frac{d\rho}{dt} + \alpha \frac{dT}{dt} \right] = \beta \left[-\frac{1}{v_s} \frac{dv_s}{dt} + \alpha \frac{dT}{dt} \right]; \tag{2.10}$$

where α and β are defined as follows

$$\begin{aligned} \alpha &= -\tfrac{1}{\rho} \left(\tfrac{\partial \rho}{\partial T}\right)_p = \tfrac{1}{v_s} \left(\tfrac{\partial v_s}{\partial T}\right)_p; \\ \beta &= \frac{\rho}{\left(\frac{\partial \rho}{\partial p}\right)_T} = \frac{1}{v_s \left(\frac{\partial \rho}{\partial p}\right)_T} = \frac{-v_s}{\left(\frac{\partial v_s}{\partial p}\right)_T}. \end{aligned} \tag{2.11}$$

In Equation 2.11 appears the α coefficient that takes into account the thermal dilatation of the fluid.

Temperature derivative is calculated from enthalpy balance shown in Equation 2.3, which is written in the simplified form in Equation 2.12

$$\frac{dT}{dt} = \frac{H_{in} - H_{out} - \rho dV/dth + Q_t + L}{V c_p} v_s + \frac{1}{c_p} T \left(\frac{\partial v_s}{\partial T} \right)_p \frac{dp}{dt}; \tag{2.12}$$

Therefore, both pressure and temperature profiles are homogenous in the control volume. They can be calculated integrating 2.10, 2.12 according to the simplified scheme in Figure 2.9.

The exchanges between the capacitive element and the external environment are allowed both by the Q_t (heat exchanged, i.e. the heat flow due to the non-adiabatic

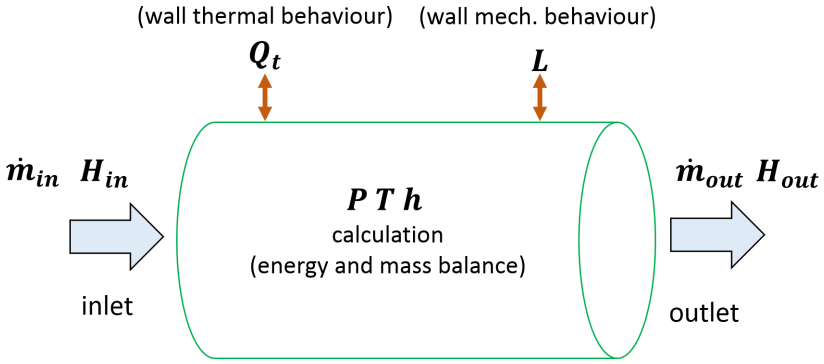

Figure 2.9: Control volume considered for mass and enthalpy balance of a general C element.

capacitive) and by the external work L (i.e. the mechanical work of an hydraulic actuator). The change of the volume capacity V, due to the wall flexibility, is modelled through a wall function $V(p)$. $V(p)$ calculates the internal volume derivative considering the internal pressure coupled with the external mechanical impedance. Therefore, the effect of a generic real pipe wall with an elastic behaviour is modelled, or alternatively (customizing the $V(p)$ function), a simple effect actuator coupled with a mechanical impedance can be modelled.

Also a variable volume or pressurized tanks is modelled as particular case of capacitive elements by properly modelling the $V(p)$ function. It is also interesting to notice that the heat exchange phenomena are modelled through capacitive blocks.

2.3 Modelling of lumped and distributed losses

2.3.1 Lumped losses

These sub-models do not have a friction factor expressed as a function of the total length. These components evaluate the local pressure drop, considering their local geometry. Such local geometries induce a sudden change in the speed and direction of flow. The flow coefficient C_v is deducted from the total friction factor ζ

$$C_v = \frac{1}{\sqrt{\zeta}}; \tag{2.13}$$

The total friction factor is obtained from specific tables and graphs available in literature [63], [64], [65].

2.3.2 Distributed losses

The pressure losses along a straight tube having a constant section of passage are represented by the total friction factor ζ

$$\zeta = \frac{fl}{D_h}; \tag{2.14}$$

where f is the friction factor of a pipe sketch having relative length unit $l/d = 1$, l is the length of the pipe and D_h defines the hydraulic diameter or equivalent (it is defined as the diameter of the circular cross section conduit and, more generally, consists in the ratio between four times the section area and the perimeter).

The flow coefficient C_v is still deducted from Equation 2.13.

In straight pipes, the resistance to motion of a liquid or a gas in laminar motion conditions is due to internal friction forces. This is possible when a layer of liquid or gas has a relative motion comparable with another. These viscous forces are proportional to the flow velocity. Hence, the friction factor depends from the Reynolds Number Re.

When the Re increases, the inertial forces (which are proportional to the square of the speed) tend to dominate. The flow becomes turbulent since there is a significant increase of the resistance to movement. Part of this increase is due to the roughness

of the wall surface, in facts the ducts surfaces are never perfectly smooth, since they present protrusions and recesses with respect to the ideal surface.

In addition, the average value of the protrusions δ is added to the variables that determine the geometric similarity; hence, the friction factor is function of two dimensionless numbers: the Re and the relative roughness. The relative roughness is calculated as the average of all the protrusions (i.e. the absolute roughness) in the inner diameter of the tube, as seen in the Figure 2.10

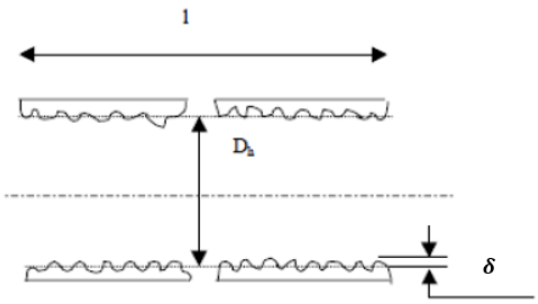

Figure 2.10: Roughness of the wall surface in straight pipes.

Hence, the relative roughness rr is expressed as follows

$$rr = \frac{ar}{D_h}. \tag{2.15}$$

Regards the calculating method of the friction factor f, it uses the dependence to f from Reynolds number Re and the relative roughness rr, through the Colebrook iterative formula

$$\frac{1}{\sqrt{f}} = -2log\left(\frac{rr}{3.7} + \frac{2.51}{Re\sqrt{f}}\right). \tag{2.16}$$

Since the Equation 2.16 is iterative (respect to f), one of its approximations will be used, the Haaland equation 2.17, so to obtain immediately the value of the friction factor:

$$\frac{1}{\sqrt{f}} = -1.8log\left(\left(\frac{rr}{3.7}\right)^{1.11} + \frac{6.9}{Re}\right). \tag{2.17}$$

Finally, the Figure 2.11 highlights the evolution of f in function of the dimensionless coefficients.

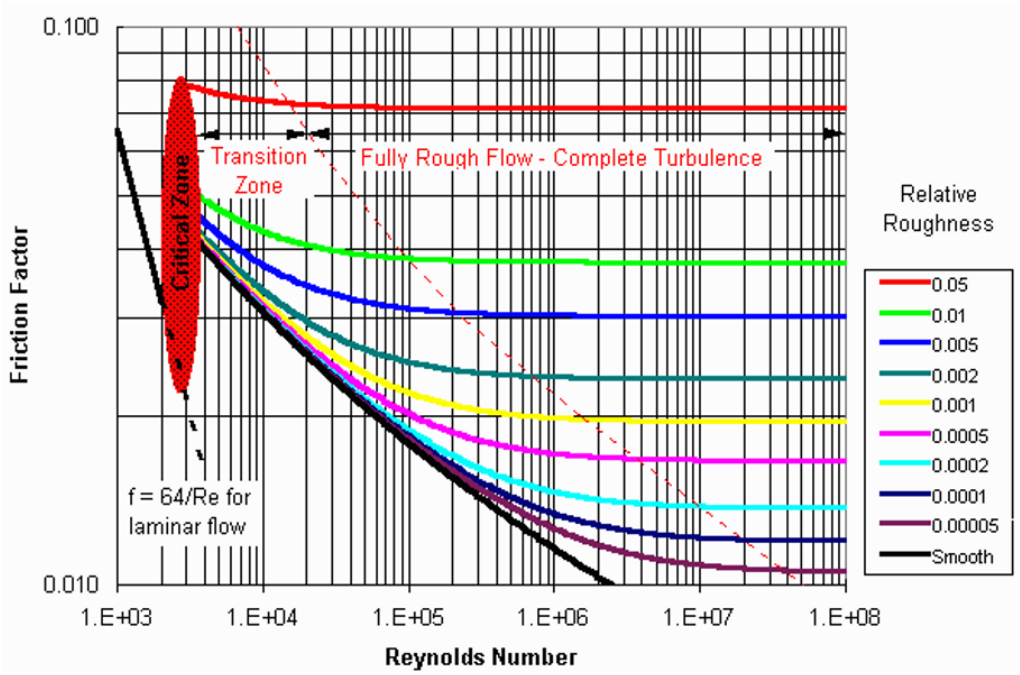

Figure 2.11: Moody diagram.

As can be observed, for the laminar flow the value of f is simply given by $f = 64/Re$, regardless of the relative roughness. Then, a measurement uncertainty zone, corresponding to the transition between laminar and turbulent flow follows. Finally, for the turbulent flow, the relationship between f and Re also depends on the relative roughness with laws more complex not obtainable through theoretical treatises, where f declines with increasing to Re up to a limit value, above which the friction factor is constant.

2.4 Fluid properties

One of the aims of the proposed modelling approach is to simulate the thermal, flow rate and pressure transients of a complex plant, considering off-design conditions, which are often associated to pressure-temperature working ranges where the fundamental properties of the fluids such as viscosity and density could change in an appreciable way. Therefore, the real behaviour of the fluid has been modelled, considering the physical variables as polynomial functions of fluid pressure and temperature and extrapolating the fluid properties respect to reference conditions of pressure p_{ref} and temperature T_{ref}.

The main advantages of the proposed approach are the simplicity of the equations, obtained using Taylor series in the linearization process, and the possibility to describe in a closed form the partial derivative of pressure and temperature (which are more suitable from a computational point of view).

In the following paragraphs, the way in which the main physical variables are modelled is described, respectively, for incompressible and compressible fluids.

2.4.1 Incompressible fluids

The main physical variables employed to describe an incompressible fluid are specific volume, absolute viscosity, specific heat coefficient, thermal conductivity:

Specific volume v_s - It is interpolated with a 2nd order polynomial law

$$\begin{aligned} v_s = \tfrac{1}{\rho} = v_{s0} \left[1 + a_{p1} \left(p - p_{ref}\right) + a_{p2} \left(p - p_{ref}\right)^2 + \right. \\ \left. + a_{t1} \left(T - T_{ref}\right) + a_{t2} \left(T - T_{ref}\right)^2 + a_{pt} \left(P - P_{ref}\right) \left(T - T_{ref}\right)\right] ; \end{aligned} \tag{2.18}$$

where v_{s0} defines the reference value of v_s and $a_{p1},\ a_{p2},\ a_{t1},\ a_{t2},\ a_{pt}$ are the coefficients of the polynomial law.

Absolute viscosity μ - It is approximated by an exponential law whose exponent is interpolated with a 2nd order polynomial law

$$\mu = \mu_0 10^{\psi}, \psi = b_{p1} \left(p - p_{ref}\right) + b_{t1} \left(T - T_{ref}\right) + b_{t2} \left(T - T_{ref}\right)^2 ; \tag{2.19}$$

where μ_0 defines the reference value of μ and $b_{t1},\ b_{t1},\ b_{t1},\ b_{t2}$ are the coefficients of the polynomial law.

Specific heat coefficient c_h - It is interpolated with a 2nd order polynomial law

$$c_h = c_{h0}\left[1 + c_{p1}\left(p - p_{ref}\right) + c_{t1}\left(T - T_{ref}\right) + c_{t2}\left(T - T_{ref}\right)^2 + c_{pt}\left(p - p_{ref}\right)\left(T - T_{ref}\right)\right]; \tag{2.20}$$

where c_{h0} defines the reference value of c_h and $c_{p1},\ c_{t1},\ c_{t2},\ a_{pt}$ are the coefficients of the polynomial law.

Thermal Conductivity λ - Sensitivity against pressure is neglected

$$\lambda_p = \lambda_{p0}\left[1 + d_{t1}\left(T - T_{ref}\right) + d_{t2}\left(T - T_{ref}\right)^2\right]; \tag{2.21}$$

where λ_{p0} defines the reference value of λ_p and $d_{p1},\ d_{p2},\ d_{t1},\ d_{t2},\ d_{pt}$ are the coefficients of the polynomial law.

2.4.2 Compressible fluids

A compressible fluid can be modelled according to the following gas equation

$$P = \rho RT; \tag{2.22}$$

where R is a constant which is different for each gas and its value can be approximated from 2.22 considering the standard conditions of density ρ_0, pressure p_0 and temperature T_0

$$R = \rho_0\left(p_0 T_0\right); \tag{2.23}$$

Therefore, density ρ (and obviously specific volume) can be computed according to Equation 2.22. Concerning the other physical variables, their calculation is very similar with respect to the incompressible fluids. In particular, the absolute viscosity μ and thermal conductivity λ are calculated according to Equation 2.19, 2.21 shown in the previous paragraph 2.4.1.

The gas compressibility is expressed by the following Equation

$$\beta = \frac{\rho \partial p}{\partial \rho}. \tag{2.24}$$

where β indicates the Bulk modulus.

The specific heat at constant pressure c_p is interpolated with a 2nd order polynomial law as a function of pressure

$$c_p = e_{p0}\left[1 + e_{t1}\left(T - T_{ref}\right) + e_{t2}\left(T - T_{ref}\right)^2\right]; \tag{2.25}$$

where e_{p0} defines the reference value of c_p and $e_{t1},\ e_{t2}$ are the coefficients of the polynomial law. Finally, the link between specific heat at constant pressure c_p and specific heat at constant volume c_v has been modelled

$$c_v = c_p - R,\ \gamma = \frac{c_p}{c_v}; \tag{2.26}$$

where γ represents the specific heats ratio.

2.5 Modelling examples

In this section several fluid plant components, belonging to a dedicated library developed during the research activity for an industrial partner, are presented to better clarify the proposed appraoch.

2.5.1 Hydraulic Orifice

This Resistive element models a generic uncontrolled hydraulic orifice, whose layout, as visible in the developed library, is shown in Figure 2.12.

Figure 2.12: Layout of the hydraulic orifice element.

The inputs of this model are represented by the temperatures T_{in}, T_{out}, pressures p_{in}, p_{out} and enthalpies h_{in}, h_{out} that are calculated by the inlet and outlet adjacent capacitive elements, while the outputs are defined by the mass flow rate $\dot{m}$ and enthalpy flow rate H. In particular, the mass flow rate $\dot{m}$ and enthalpy flow rate H are equal in module but have opposite sign between input and output.

The algebraic Equation describing the component behaviour in terms pf volumetric flow rate $\dot{V}$, neglecting the inertial effects, is the following:

$$\dot{V} = \frac{\dot{V}_{nom}}{\sqrt{\Delta p_{nom}}} \Delta p = C_v A \sqrt{\frac{2\Delta p}{\rho}}; \tag{2.27}$$

where A represents the orifice section and $\dot{V}_{nom}$ is the nominal volumetric flow rate. The flow coefficient C_v is used to include the losses due to friction and the local kinetic energy losses. Generally, it may be introduced, for example, to consider friction losses in pipes, or local resistances due to geometric or directional flow changes of the pipes.

The corresponding mass flow rate $\dot{m}$ and enthalpy flow rate H can be computed according to Equations 2.7.

2.5.2 Pneumatic Orifice

This Resistive element models a generic uncontrolled pneumatic orifice, whose layout is shown in Figure 2.13.

Figure 2.13: Layout of the pneumatic orifice element.

The kinetic energy of the upstream flow is denied. The mass flow rate of the compressible flow passing through the orifice is defined as a function of input pressure and temperature according to the following formula

$$\dot{m} = C_v C_m A \frac{p_{in}}{\sqrt{T_{in}}}; \tag{2.28}$$

where A represents the orifice section, C_v defines the flow coefficient and C_m is an additional coefficient employed to distinguish between supersonic and subsonic flow conditions:

- Sonic condition ($p_{out}/p_{in} > p_{cr}^c$):

$$C_m = \frac{\sqrt{2\gamma}}{\sqrt{R\,(\gamma-1)}} \sqrt{\left(\frac{p_{out}}{p_{in}}\right)^{2/\gamma} - \left(\frac{p_{out}}{p_{in}}\right)^{(\gamma+1)/\gamma}}. \tag{2.29}$$

- Subsonic condition ($p_{out}/p_{in} > p_{cr}^c$):

$$C_m = \frac{\sqrt{2\gamma}}{\sqrt{R\,(\gamma-1)}} p_{cr}. \tag{2.30}$$

In particular, critical pressure p_{cr}^c is defined as follows

$$p_{cr}^c = \left(\frac{2}{\gamma+1}\right)^{1/(\gamma-1)}. \tag{2.31}$$

2.5.3 Heat exchanger

The element shown in Figure 2.14 represents a generic heat exchanger where the exchanged thermal power depends from the difference between external and actual component temperatures. The cooler element is realized in a capacitive element between two orifices, constituting an R-C-R chain; therefore, it is externally "seen" as a Resistive element. To this end, this block is associated with drop losses and a certain flow. In addition, the volume associated to the cooler is defined according to the corresponding length and section.

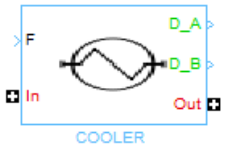

Figure 2.14: Layout of the heat exchanger element.

As for the orifice element, the inputs of this model are represented by the temperatures T_{in}, T_{out}, pressures p_{in}, p_{out} and enthalpies h_{in}, h_{out} that are calculated by the inlet and outlet adjacent capacitive elements, while the outputs are defined by the mass flow rate $\dot{m}$ and enthalpy flow rate H. In particular, the mass flow rate $\dot{m}$ and enthalpy flow rate H are equal in module but have opposite sign between input and output.

The R orifice Equations have already been illustrated in the previous paragraph 2.5.1 while, concerning the C tank dynamics, pressure, temperature and specific enthalpy can be computed as respectively shown in Equations 2.10, 2.12 and 2.3.

The heat exchanged with the external environment is computed using the convection formula

$$Q = h_c A \left(T_{env} - T\right); \tag{2.32}$$

where T_{env} and T are respectively external and actual component temperatures, h_c is the convection coefficient and A is the exchange surface.

2.5.4 Gas-charged accumulator element

This block (in Figure 2.15)describes the dynamics of a thermal-fluid accumulator in which a separated volume contains a pressurized gas. This element is determined by an orifice (Resistive) which is included between the Capacitive tank, and the piping of the fluid circuit. Therefore, this block is an R-C element connected to the network from the R side.

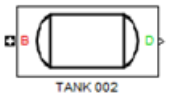

Figure 2.15: layout of the gas-charged accumulator.

Again, the R orifice Equations have already been illustrated in paragraph 2.5.1 while, concerning the C tank dynamics, pressure, temperature and specific enthalpy can be computed as respectively shown in Equations 2.10, 2.12 and 2.3.The inputs of this model are represented by the temperature T, pressure p and enthalpy h that are calculated by the adjacent element of the circuit whose the tank is connected, while the outputs are defined by the mass flow rate $\dot{m}$ and enthalpy flow rate H.

The gas contained in the accumulator follows the law of polytropic gases:

$$pV^{\gamma} = const.; \tag{2.33}$$

where the constant is defined by the precharge pressure p_{prec} and accumulator volume. It is assumed that the hydraulic fluid inside the accumulator has the same pressure of the gas.

For the interaction between compressible and incompressible fluids the accumulator is considered as a hydraulic piston with two separate chambers in which the volume variations of a chamber influences the volume of the other one

$$p_{prec}V^{\gamma} = p_{init}V_{gas}^{\gamma} \Rightarrow V_{gas} = V_{gas}\sqrt[\gamma]{\frac{p_{prec}}{p_{init}}}; \tag{2.34}$$

and therefore the equivalent piston run r_p can be expressed through the following formula

$$r_p = V_{gas}A. \tag{2.35}$$

In particular, the gas volume V_{gas} is calculated according to Equation 2.36

$$V_{gas} = \left[V - V \left(\frac{p_{prec}}{p_{init}} \right)^{\frac{1}{\gamma}} \right] + A \int (\dot{r}_p)\, dt; \tag{2.36}$$

while the equivalent piston run is computed as follows

$$r_p = J_p A \int [p_{gas} - p]\, dt = J_p A \int \left[\frac{(p_{prec} V^{\gamma})}{V_{gas}^{\gamma}} - p \right] dt. \tag{2.37}$$

where J_p defines the piston inertia.

Chapter 3

RT control of auxiliary lubrication systems

In the Oil & Gas industry, the testing of auxiliary lubrication plants represents an important preliminary activity before the whole turbo-machinery train (including the auxiliary lubrication plant) can be put in operation. Therefore, the employment of both efficient and accurate plant models becomes mandatory to synthesize satisfactory control strategies both for testing and normal operation purposes. For this reason, this chapter focuses on the development of an efficient RT model and control architecture to describe and regulate auxiliary lubrication plants. In particular, according to the Bond-Graph modelling strategy introduced in the previous chapter 2, an efficient lumped parameter model of the lube oil unit has been developed to properly optimize the description of such system.

The code (developed through Matlab-Simulink software), which is implemented for a fixed, discrete step solver, has been compiled and uploaded on a commercial RT platform (MicroAutoBoxII produced by dSpace®), employed to control the Pressure Control Valve (PCV) of the physical plant, for which a new controller has been developed.

The modelling approach and the control strategy have been developed in collaboration with GE Nuovo Pignone S.p.a. while the experimental data were acquired in a plant located in Ptuj (Slovenia).

3.1 Introduction to the test-case

A growing interest in the auxiliary lubrication systems employed in the Oil & Gas plants has been noticed in the last few years, because they can significantly affect the turbo-machines operation. In particular, lubrication units are fundamental in the hydrodynamic bearings lubrication [66, 67], which are mandatory to sustain the rotating machines and to avoid potential instability phenomena, as shown by Genta [47, 48]. Furthermore, these plants are very important not only in classical rotor-dynamic and fluid-dynamic fields, but also from an automation point of view [68], because bearings pressure must be controlled within a certain operating range to ensure a reliable plant operation.

For RT applications, an efficient and integrated design of turbo-machinery auxiliary lubrication plants should involve both the physical models [36], including all the integrated mechatronic components (e.g. electric and fluid actuators, pumps, valves, sensors etc.) and the control algorithms [37]. However, such model-based approach appears to be poorly followed, especially in RT applications, in particular for all those components described by complex mathematical models, such as the Pressure Control Valve (PCV), Temperature Control Valve (TCV), Main Pressure Control Valve Actuator, Extraction Control Valve Actuator, Current-to-Pressure Converter (CPC), etc. [38].

Usually, the typical plants components (e.g. valves or hydraulic bearings) of lubricant supply plants are based on simplified lumped parameter models[46], especially in RT applications and, consequently, very simple and non-optimized controllers are implemented. At the same time, in the rotor-dynamic field, bearings are generally regarded as lumped parameters spring-damper systems [47, 48, 49]. This approach is very efficient but, obviously, not very accurate.

On the other hand, modern lubrication studies (based on Computational Fluid Dynamics techniques, CFD) assess with a high accuracy level the main components performances. For example, in bearing performances analyses, 3D CFD analyses are required to achieve reliable results for highly loaded Thrust Bearings [39], Journal Bearings [40], TPJBs [41] and dynamically loaded supports [42] (i.e., bearings of connecting rods for automotive engines). In addition, CFD studies, about particular valves commonly present in industrial plants [43], can be found. Pneumatic plants are studied with a high accuracy degree: as well, for instance, boilers [44] or steam plants dynamics [45] are considered.

However, in complex plants the accurate modelling and the subsequent employment of model-based control techniques of these systems results in an high computation times, that is not acceptable for RT simulations. In addition, both efficient and accurate models usually focus on the modelling of components or plants behaviour, neglecting the development of proper control systems (for instance automatic synthesis instruments or control optimization procedures appear to be generally neglected [69, 70]).

Continuous development of technologies for the fast prototyping of RT code has really contributed to speed up the diffusion of complex HIL testing techniques, able to support complex models of plant components and advanced control systems. For instance, HIL approach is usually applied in the automotive area [20, 29, 21], and it could be widely employed in the rotor-dynamics or energy fields. To this aim, as shown in chapter 2, a Matlab-Simulink library was developed for the integrated simulation of thermal hydraulic plants, such as the auxiliary lubrication circuits.

Therefore, both a model-based approach for the simulation of a complete auxiliary lubrication plant and a PID control optimization approach based on the flexible simplex technique for the control of the plant have been carried out. More in detail, an accurate lumped parameter model was developed, especially in transient operation, characterized by an high accuracy level, however with a greater efficiency, hence optimizing the trade-off between results accuracy and execution efficiency. In particular, the bond-graph approach was adopted 2.1.2, to describe mono-dimensional flows and to better approximate the 1D distributed models through high efficiency lumped ones, optimized for RT simulation and consequently HIL testing of the plant. Concerning the plant control, the main problem highlighted by the industrial partner, GE Nuovo Pignone, was the improvement of the Pressure Control Valve (PCV) regulator performances and, consequently, of the plant pressure and of PCV actuator behaviour. To this end, an innovative model-based methodology is proposed, including both identification and control optimization techniques (based on flexible simplex strategies [71, 72, 73].

Starting from the real data of the plant, provided by the industrial partner, using the proposed approach, the new dynamic plant model was implemented by means of the aforementioned approach (described in chapter 2), characterizing each component through the real characteristics.

In the second phase, the transfer function of the PCV actuator has been

obtained through classical identification techniques [74] consisting in a non-parametric identification based on step response tests. According to this actuator transfer function, which is based on experimental data, the real behaviour of the PCV is properly considered in the simulation of the auxiliary lubrication plant.

In the third phase, an innovative optimization strategy based on flexible simplex strategies for the PCV regulator, with improved accuracy and performance stability, has been developed and tested in the full plant model.

Finally, the performances of the developed PCV regulator have been validated tested through the comparison with the real plant data, using the new PCV regulator directly on the real plant.

To reach these goals, both a suitable electronic cabinet equipped of a RT platform (MicroAutoBoxII produced by dSPACE®), on which new models can be implemented, and the corresponding RT code of the controller are developed, implemented and successfully tested on the field. Finally, according to the internal GE Nuovo Pignone testing procedure, the whole auxiliary lubrication plant has been tested under real operative conditions with the proposed controller.

The whole model approach and the control strategy have been developed and validated in collaboration with Ge Nuovo Pignone S.p.a. which provided the required technical and experimental data [75] needed for the strategy validation. The data are referred to a suitable testing system built at the testing center located in Ptuj (Slovenia).

3.2 Plant description

The lube oil console consists of three pumps: main volumetric pump, auxiliary centrifugal pump (actuated by two asynchronous motors) and emergency centrifugal pump (controlled by a DC motor). A pressure safety valve has been inserted downstream the volumetric pump to limit the plant pressure and then fix the flow rate supplied by the main pump. Then, an orifice is installed, which simulates the usual pressure drop of a cooler and is applied in parallel with the emergency pump; these pipes are connected through a 3-way valve. Beyond this valve, a filtering stage and a Pressure Control Valve (PCV) are installed. The PCV is a regulated pressure control valve for the regulation of the downstream pressure, with a bypass branch placed in parallel (in the following section the PCV control will be described in detail). Finally, two orifices in parallel are placed after the PCV to simulate the oil flow through the bearings and the hydraulic bleed of the gear box. Additional orifices, check-valves and bypass valve are added to the plant to simulate other known lumped losses or failures.

The fluid which flows through the plant is a mono-dimensional, isotropic, incompressible, viscous and laminar flow of a Newtonian lubricant called ISO VG 32, given by *GE Nuovo Pignone S.p.a.*. This mineral oil is characterized by a kinematic viscosity μ in a range between 28.8 and 35.3 mm^2/s at 40 $^\circ C$.

3.2.1 General architecture of the auxiliary plant model

The model, which was built in Matlab software, has been discretized according to the procedure shown in chapter 2. In particular, the resulting architecture is depicted in Figure 3.2.

The main sub-models that are employed to describe the dynamics of the auxiliary plant are the following:

- Main, Auxiliary and Emergency pumps (R elements): These elements are complex resistive blocks in which, as shown in section 2.2.1, are included the main equations of electric drives (AC and DC motors). The outputs of this kind of sub-models are determined by the mass flow rate $\dot{m}$ and the enthalpy flow rate H, while the inputs are upstream and downstream temperatures T_{in}, T_{out}, pressure p_{in}, p_{out} and enthalpy h_{in}, h_{out}.

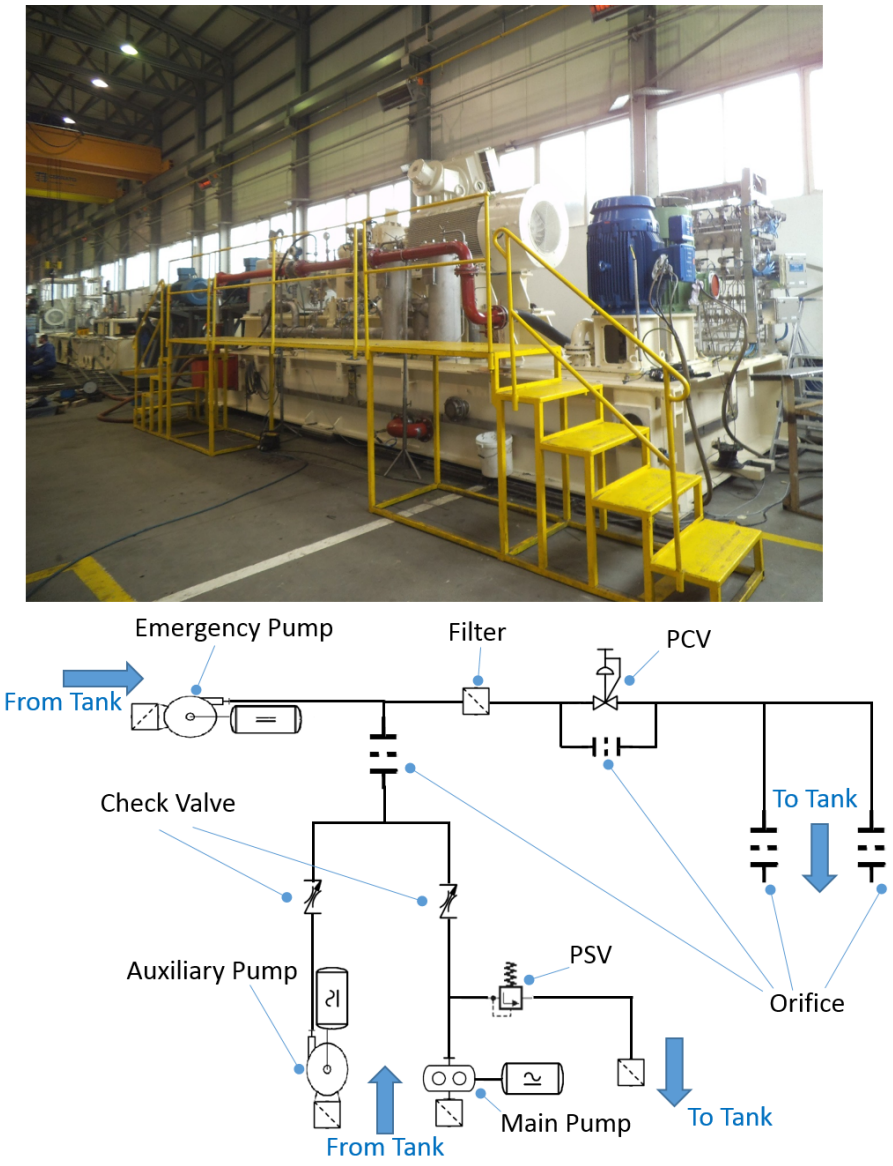

Figure 3.1: Real plant and functional scheme of the lubrication testing system in Ptuj (SLO).

- Hydraulic pipes (C elements): The pipe element models the capacitive effects present in a fluid circuit. Since it is a fully capacitive element, it does not calculate the distributed load losses. Consequently, it can be used when it is assumed that the piping lengths are small enough, thus the corresponding losses of the real plant can be negligible. Finally, heat exchange with the external environment is neglected to reduce the computational load of the whole model. Each pipe receives as inputs the mass flow rates $\dot{m}_{in}$, $\dot{m}_{out}$ and enthalpy flow rates H_{in}, H_{out} from adjacent resistive blocks (valves, filters, pumps, orifices...) while

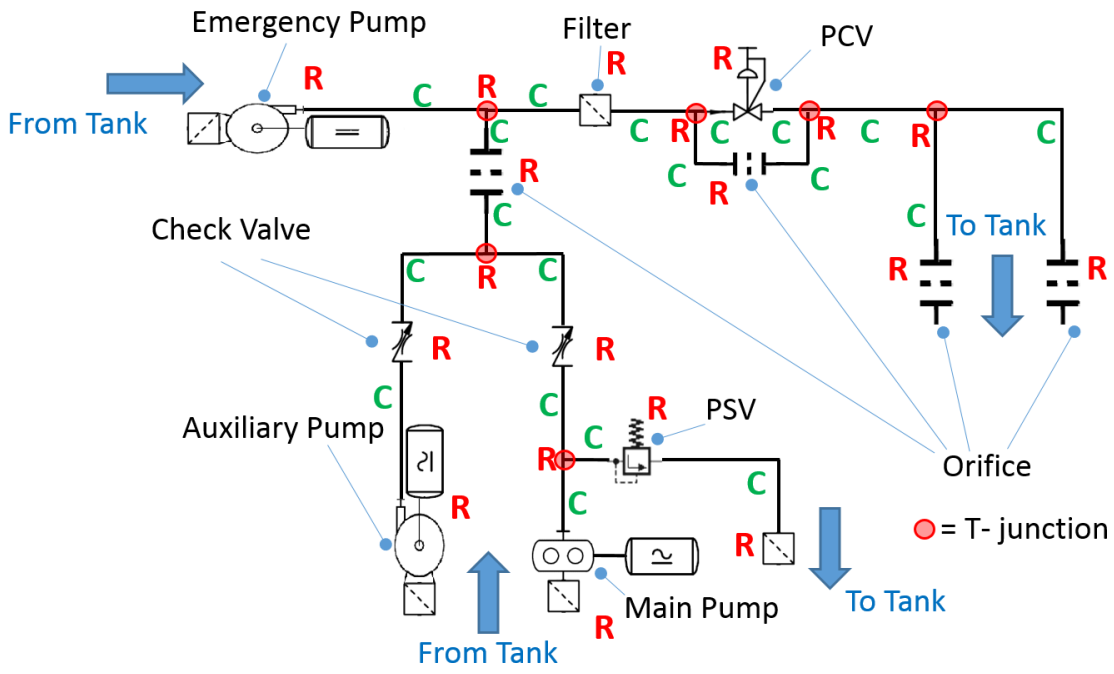

Figure 3.2: Simplified architecture scheme of the studied auxiliary plant with corresponding discretization in capacitive (C green capital letters) and resistive (R red capital letters).

dynamically computes pressure P, temperature T and specific enthalpy h.

- Valves, orifices, filters (R elements): This kind of elements model lumped load losses in fluid plants. According to chapter 2, the outputs are defined by the mass flow rate $\dot{m}$ and the enthalpy flow rate H, while the inputs of these model are represented by upstream and downstream temperatures T_{in}, T_{out}, pressure P_{in}, P_{out} and enthalpy h_{in}, h_{out}.

Thus, the Matlab-Simulink layout of the complete model is shown in Figure 3.3.

3.2.2 Model of the auxiliary and emergency pumps

The auxiliary and emergency pumps are centrifugal pumps, which are peculiar Resistive components. The model inputs are represented by the inlet/outlet pressure p_{in}, p_{out}, temperature T_{in}, T_{out} and enthalpy h_{in}, h_{out}, while the computed outputs are the mass flow rate $\dot{m}$ and enthalpy flow rate H exchanged with the adjacent capacitive components. In addition, since it is driven by an electric motor, the pump model receives the angular speed n and provides the volumetric flow rate $\dot{V}$ and the resistant torque T_{res}.

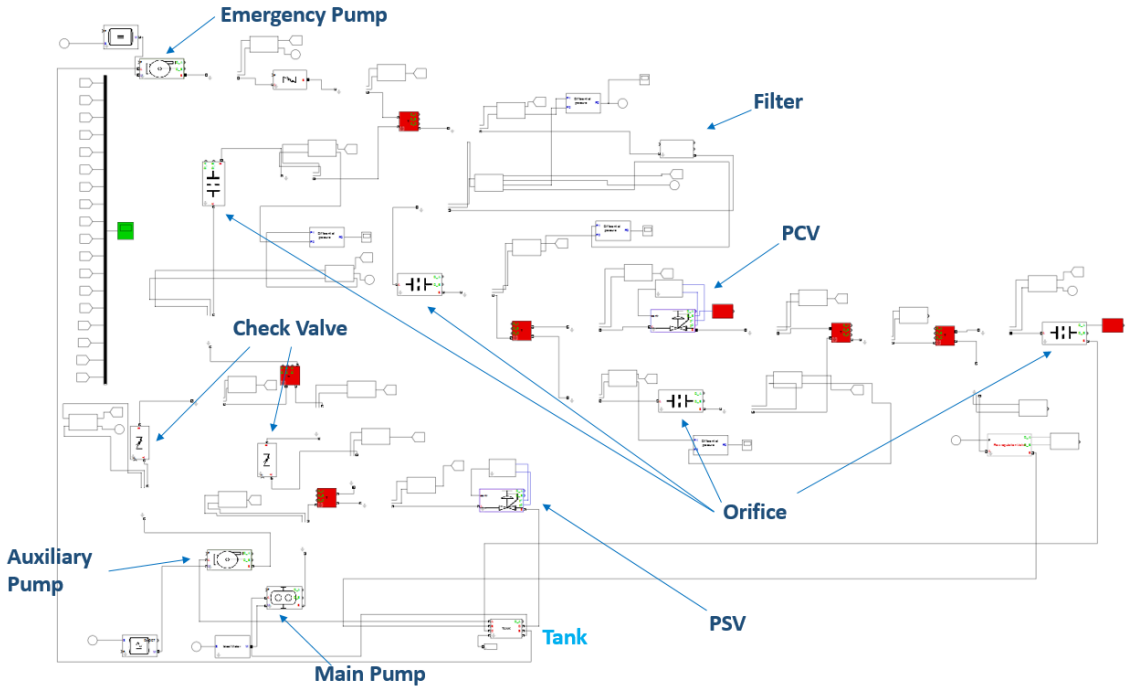

Figure 3.3: Matlab-Simulink layout of the auxiliary lubrication plant.

Generally the centrifugal pump is characterized by two fundamental curves:

- The flow rate-prevalence curve.
- The power-flow rate curve.

The first characteristic curve is employed to compute the volumetric flow rate $\dot{V}$. The pump flow rate-prevalence curve is plotted experimentally for points, at constant speed, by plotting in the x-axis the prevalence $\Delta p/(\rho g)$ and in the y-axis the flow rate $\dot{V}$ in a system of orthogonal Cartesian axes. The prevalence decreases with increasing flow rate (and vice-versa). Consequently, when the flow rate is zero, the prevalence reaches the maximum value.

The second characteristic curve is utilized to calculate the developed power. The power W is the product of the flow rate $\dot{V}$, by the prevalence Δp and the density of the fluid ρ

$$W = \rho \dot{V} \frac{\Delta p}{\rho g} = \dot{V} \frac{\Delta p}{g}. \tag{3.1}$$

The pump power-flow rate curve is plotted experimentally for points, at constant speed, by plotting in the x-axis the flow rate $\dot{V}$ and in the y-axis the power W in a system of orthogonal Cartesian axes. Therefore, the power increases as the volumetric flow rate grows.

In order to eliminate the rotational speed dependence in the proposed model, both curves were rendered dimensionless. Hence, the prevalence dimensionless coefficient χ is given by the ratio of the prevalence itself and the square of the rotational speed; the flow rate dimensionless coefficient ϕ is given by the ratio of the flow rate and the rotational speed; finally, the power coefficient P_W is calculated through the ratio of the power and the cube of the rotational speed. The dimensionless characteristics are plotted in Figure 3.4.

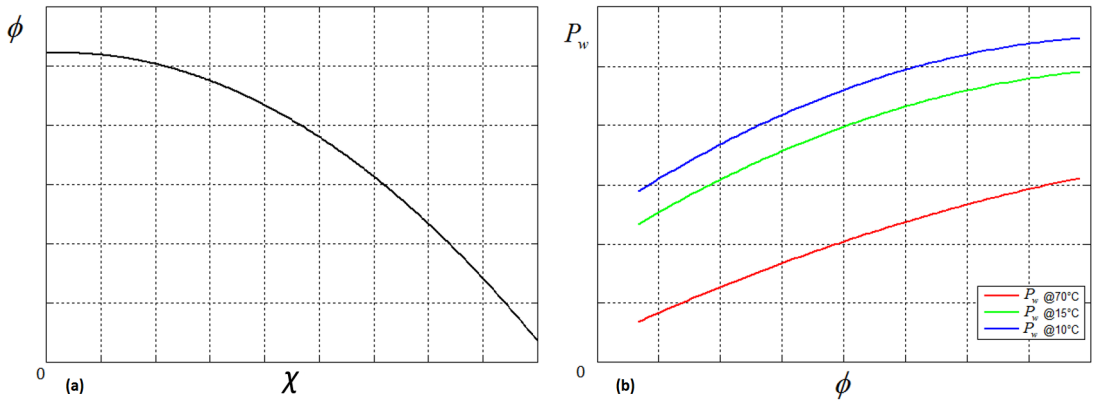

Figure 3.4: Dimensionless characteristics: (a) flow rate-prevalence (ϕ-χ) and (b) power-flow rate (P_W-ϕ).

The dimensionless characteristic power-flow rate, as shown in Figure 3.4 (b), also depends from temperature. Consequently, the inputs of the second curve are both the dimensionless flow rate ϕ and the temperature T.

Even if, in the developed architecture, the resistive components have an isenthalpic behaviour, due to the pump efficiency losses, the outlet enthalpy flow rate must be calculated as visible in the following formula

$$H_{out} = \dot{m}_{out} \left[h_{in} + V \left(p_{out} - p_{atm} \right) \right]. \tag{3.2}$$

3.2.3 Model of the AC motor

This element, whose model is strictly coupled with the centrifugal pump one, represents a simplified model of an asynchronous electric motor, whose electrical and inertial characteristics are statically defined by means of a Matlab script file.

First, the synchronous velocity n_s is computed as follows

$$n_s = n\frac{60}{2\pi}\frac{100}{N_{ref}}; \tag{3.3}$$

where N_{ref} represents the motor nominal speed. The ratio between motor torque T_m and nominal torque value T_{nom} is given by the formula

$$\frac{T_m}{T_{nom}} = \frac{n}{n_s}; \tag{3.4}$$

where a known-tabulated speed-torque response T_m is implemented.

The resisting torque is calculated from the developed power W_m and angular velocity n

$$T_{res} = \frac{W_m}{n}. \tag{3.5}$$

Finally, the angular velocity n is computed through Equation 3.6, in which a filtering transfer function has been introduced to model inertial and viscous friction mechanical loads

$$J_m\dot{n} = T_m - T_{res} - fn \Rightarrow n = \frac{T_e\,(n) - T_m}{J_m s + f}; \tag{3.6}$$

where J_m is the motor inertia and f defines the friction factor.

3.2.4 Model of the main pump

The main pump is a volumetric pump, which is a peculiar Resistive component. The model inputs are represented by the inlet/outlet pressure p_{in}, p_{out}, temperature T_{in}, T_{out} and enthalpy h_{in}, h_{out}, while the computed outputs are the mass flow rate $\dot{m}$ and enthalpy flow rate H exchanged with the adjacent capacitive components. In

addition, since it is driven by an electric motor, the pump model receives the angular speed n and provides the resistant torque T_{res}.

Other important parameters that the determine the component operation are the displacement c, volumetric efficiency η_v and mechanical efficiency η_m. The flow losses are obtained from the angular speed of the shaft n, from the displacement c and from the inlet pressure p_{in}. The mass flow rate through the pump $\dot{m}$ and the enthalpy flow H are calculated from the temperature T_{in} and the pressure input p_{in}. In particular, the equations that describe the behavior of the component and that allow to find the mass flow and the enthalpy flow are

$$\dot{m} = n\rho c\eta_v; \tag{3.7}$$

$$H = \dot{m}h_{in}T_{res}n; \tag{3.8}$$

where the resistant torque T_{res} is calculated through the following formula

$$T_{res} = c\left(p_{in} - p_{out}\right)\frac{\eta_v}{\eta_m}; \tag{3.9}$$

3.2.5 Model of the DC motor

This element, whose model is strictly coupled with the volumetric pump model, represents a very simplified model of a generic DC electric motor in which the angular velocity n varies linearly with respect to the resistant torque T_{res}. To completely define its behavior the free angular velocity (without resistive load) n_0 and the angular velocity n_g obtained at a generic value of torque T_g have to be provided.

The input is represented by the resistant torque T_{res} of the connected volumetric pump while the output is the angular velocity n. Consequently, the equations that describe the behavior of the component in terms of angular velocity is the following:

$$n = n_0 + \frac{n_g - n_0}{T_g}T_{res}; \tag{3.10}$$

3.2.6 Model of the plant pipes

The basic pipe element models the effect of capacities present in a circuit. In particular, several simplifying assumptions are considered:

- It does not model heat exchanges between piping and external environment;
- Distributed load losses are neglected, therefore it can be used when the lengths are small enough to be regarded negligible.

The Equations associated with this component, respectively 2.10, 2.12 and 2.3, allow to compute pressure, temperature and enthalpy variations in the piping section. Therefore, it can be considered as a simple C component.

However, a more complex version of the piping model was developed to include the gravitational effect: the effect of the piezometric altitude on the fluid inside the pipe. This characteristic is quite useful to simulate particular plant geometries (for instance, the bearings load may be situated at a different altitude from the auxiliary plant). This way, the more complex component results in a composition of three elements: Capacitive-Resistive-Capacitive. This way, a central resistive element allows to model the hydraulic losses and the gravitational effect on the pipe, which, externally, is still "seen" as a C element. Therefore, the distrubuted losses are computed considering the equations expressed in section 2.3.2.

3.2.7 Model of the orifices and filters

The model employed to describe the orifice has already been described in paragraph 2.5.1.

Concerning the filter, this element follows the approach of resistive elements 2.2.1. The mass flow rate is computed depending on the type of regime:

- Laminar regime:

$$\dot{m} = \rho \dot{V} \sqrt{\frac{\Delta p}{\Delta p_{nom}}}. \tag{3.11}$$

- Turbulent regime:

$$\dot{m} = \rho \dot{V} \frac{\Delta p}{\Delta p_{nom}}. \tag{3.12}$$

Moreover, the component model allows to simulate the filter failure which is simply obtained by a different initialization of the nominal drop Δp_{nom}. In facts, from a physical point of view, it represents a major pressure drop associated to this component which is due to a partial filling (e.g. caused by dirt in the filter).

3.2.8 Model of the check-valves

This Resistive component allows to simulate the behavior of a check valve which has a spring with linear characteristic. It incorporates a 1st order dynamic element whose working frequency reaches about 10-15 Hz. In addition it is supposed adiabatic, since all the energy dissipated by the check valve is transferred to the fluid.

The pressure drop for this component is evaluated as follows

$$\Delta p = p_{in} - p_{out} - p_{cr}; \tag{3.13}$$

where p_{cr} defines the pressure value which has to be exceeded in order to allow the fluid flow through the element. In particular, the mass flow rate through the component is computed according to the following Equations

- If $\Delta p > 0$:

$$\dot{m} = \rho(max\{T_{in}, T_{out}\}) f(\Delta p). \tag{3.14}$$

- If $\Delta p < 0$:

$$\dot{m} = 0. \tag{3.15}$$

where ρ represents the fluid density and $f(\Delta p)$ defines a the valve characteristic which depends from the pressure drop of the valve.

3.2.9 Model of the T-junctions

This element allows to model a "T" shaped junction, also modelling the concentrated losses arising within this three-way connection. Therefore, this element models a Resistive block.

The nominal flow $\dot{V}_{nom}$ defines the nominal flow calculated with respect to which the pressure drop associated with the block; moreover, the ratio between the major and the minor diameters is employed to increase the pressure loss generated by the further narrowing of the piping section.

The direction of the fluid flow is determined by the pressure at the three terminals so that the balance among them should be maintained. In particular, this element implements two orifices. Each one of these orifices computes its own mass flow rate ($\dot{m}_{in1}$, $\dot{m}_{in2}$) and enthalpy flow rate (H_{in1}, H_{in2}) and, finally, the output mass flow rate $\dot{m}_{out}$ and enthalpy flow rate H_{out} are calculated through Equations 3.16 and 3.17.

$$\dot{m}_{out} = \dot{m}_{in1} + \dot{m}_{in2}; \tag{3.16}$$

$$H_{out} = H_{in1} + H_{in2}. \tag{3.17}$$

3.2.10 Model of the Pressure Safety Valve

This Resistive component allows to simulate the behavior of a pressure safety valve, characterized by a mono-dimensional flow. Similarly to the check valve model, it simulates the presence which of a spring with linear characteristic, thus incorporating a 1st order dynamic element whose working frequency reaches about 10-15 Hz. In addition it is supposed adiabatic, since all the energy dissipated by the check valve is transferred to the fluid.

The pressure drop for this component is evaluated as follows

$$\Delta p = p_{in} - p_{out} - p_{cr}; \tag{3.18}$$

where p_{cr} defines the pressure value which has to be exceeded in order to allow the fluid flow through the element. In particular, the mass flow rate through the component is computed according to the following Equations

- If $\Delta p > 0$:

$$\dot{m} = \rho(max\{T_{in}, T_{out}\})f(\Delta p). \tag{3.19}$$

- If $\Delta p < 0$:

$$\dot{m} = 0. \tag{3.20}$$

where ρ represents the fluid density and $f(\Delta p)$ defines a the valve characteristic which depends from the pressure drop of the valve.

3.2.11 Model of the Pressure Control Valve

The Pressure Control Valve (PCV) can be approximated as a variable orifice controlled by a standard PID in order to vary its flow coefficient in function of the downstream pressure to be controlled. The PCV used in this lubrication testing system is characterized by a maximum flow coefficient $C_v = 113$ and its actuator is moved with equipercentual characteristic; this valve has been made available by Masoneilan [76]. The PCV model (R element) is a variable orifice in which the mass-flow rate $\dot{m}$ $[kg/s]$ is calculated as a function of the maximum flow coefficient C_v $[-]$, the valve opening x_c $[-]$, the pressure drop ΔP $[Pa]$, the density ρ $[kg/m^3]$ and a coefficient SG called "Specific gravity" $[-]$:

$$\dot{m} = x_c \cdot \rho \cdot C_v \sqrt{\frac{\Delta p}{SG}}; \tag{3.21}$$

while the enthalpy flow rate is computed using the following Equation:

$$H = h\dot{m}. \tag{3.22}$$

Then, the formula 3.21 is applied to the actuator real dynamics identified as described in Equation 3.24. The valve opening x_c (manipulated variable) is calculated by a simple PID controller in function of the error between the PCV downstream pressure P_{out} (controlled variable) and the set point pressure P_{ref}. Consequently, the

opening percentage x_c is computed as follows

$$x_c(s) = e_p(s)\left[k_p + \frac{k_i}{s} + \frac{k_d s}{1 + \frac{k_d}{k_p N} s}\right], \tag{3.23}$$

where k_p, k_i, k_d define respectively the proportional, integral and derivative gains while the constant $N > 0$, introduced to guarantee the feasibility of the controller, is chosen so that that the pole in $s = -Nk_p/k_d$ is out of the control band (at high frequency). The logic scheme of the PCV model is shown in Figure 3.5:

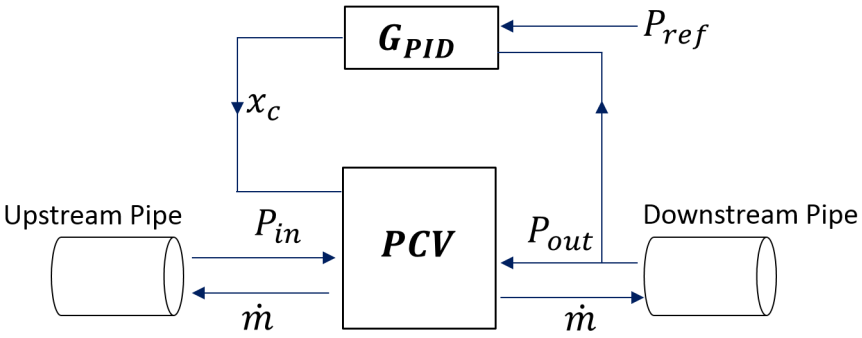

Figure 3.5: Scheme of the PCV model.

3.3 Control Design

3.3.1 Preliminary testing of the PCV

This preliminary test campaign, which is not included in the functional test procedure, concerns the data acquisition of the PCV dynamic behaviour according to several step tests. In particular, the PCV opening position and downstream pressure were acquired to perform the valve identification described in the next section. The following experimental data have been obtained by the industrial partner at the testing site located in Ptuj (Slovenia). These preliminary results have been obtained through a PID control system which was manually tuned by the industrial partner[77], whose gains are shown in Table 3.1, while the main features of the adopted testing computer and algorithm are expressed in Table 3.2.

Table 3.1: Features of the preliminary PID control system.

Gain	Value
Proportional gain k_p	10 $[1/bar]$
Integral gain k_i	0.03 $[1/(s \cdot bar)]$
Derivative gain k_d	3 $[s/bar]$

Table 3.2: Main features of the testing computer and of the adopted solver for the RT control system.

Computer	
Operative system	Windows 7®
CPU clock frequency	2.4 GHz
RAM memory	8 Gb
Solver	
Solver name	ODE1
Solver type	Fixed Step
Sampling time	0.001 s

In Figure 3.6 and 3.7 both pressure and position trends are shown. Both the PCV opening position and, consequently, the regulated header pressure demonstrate an oscillatory behaviour, therefore a proper tuning of the control system seems to be

mandatory in order to perform the desired tests. In facts, in the subsequent sections the optimized results will be shown.

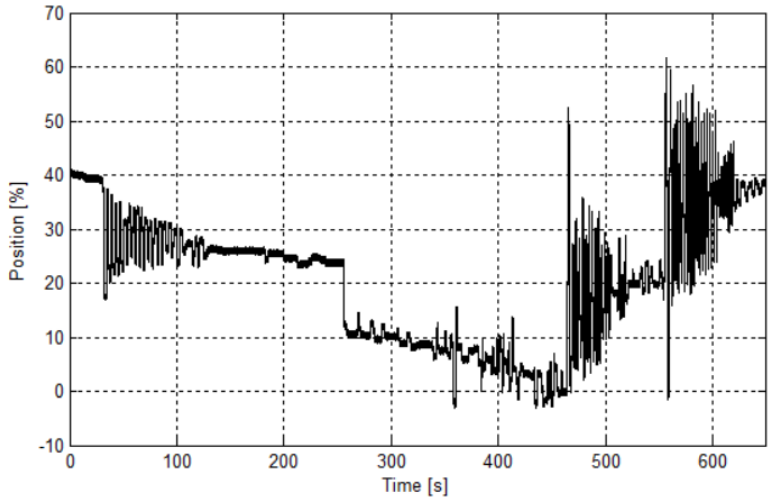

Figure 3.6: Experimental behavior of the PCV opening position trend.

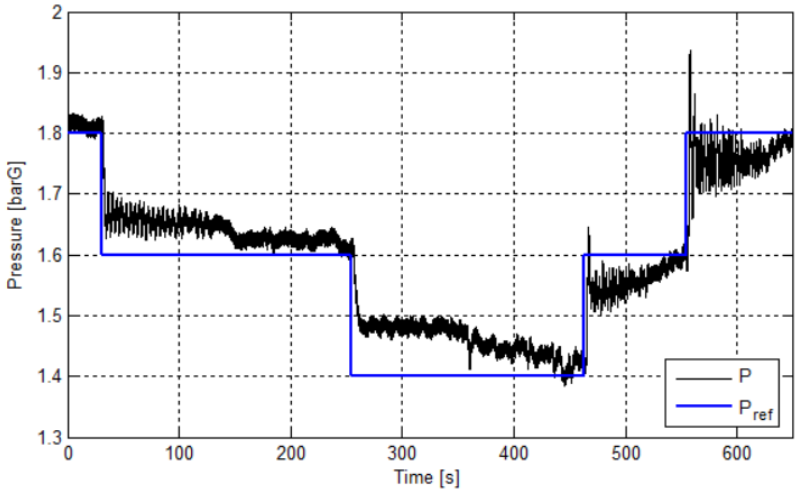

Figure 3.7: Experimental behavior of the header pressure trend.

The Control System functional scheme is represented in Figure 3.8: it is composed by two control loops, one of which is a pressure control loop and the other is a position one.

In particular, the desired set-point, represented by the reference pressure P_{ref} $[barG]$, is compared with the actual header pressure P $[barG]$ (controlled variable), measured downstream the PCV. The error e_P $[barG]$ is then processed by the Pressure regulator G_{PID}, object of the further optimization (see the following section), whose output

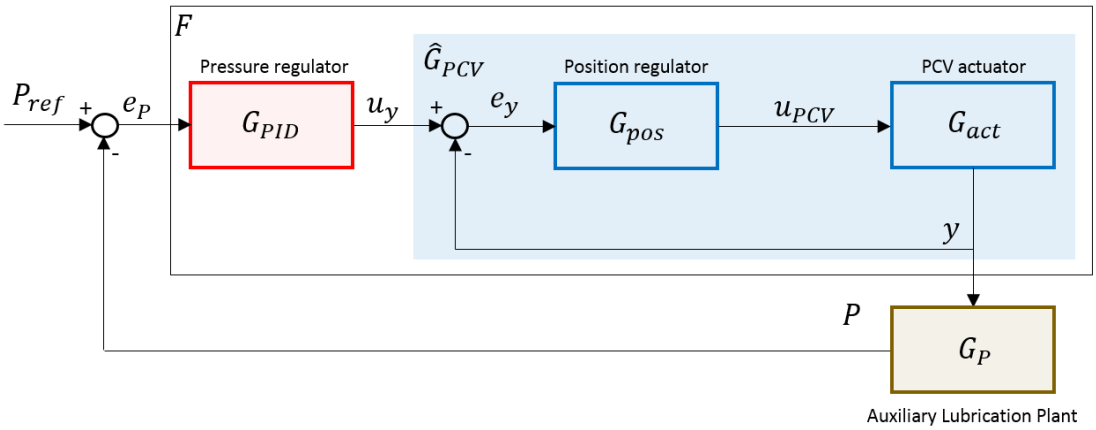

Figure 3.8: Functional scheme of the PCV Control loops.

is represented by the PCV reference position y_{ref} $[-]$ (which is the set-point of the inner control loop). The PCV dynamics $\hat{G}_{PCV}$, (which is unknown and therefore to be identified) could be schematized in two separate processes: the first one is represented by the Positioner regulator G_{pos} that, according to the position error $e_y = y_{ref} - y$ $[-]$ produces the command u_{PCV} (the manipulated variable of the inner control loop, internal to the PCV and unknown/not measurable) which makes the PCV actuator G_{act} move to the position y $[-]$ (the manipulated variable). The position y $[-]$ influences the plant G_p in terms of the oil passage downstream the valve, and, finally, the controlled variable (pressure P).

The tuning of the proper control system could be improved by the numerical model of both the lube oil plant and the PCV, because their dynamics highly affects the parameters of the control system. Therefore, the Control Design procedure can be resumed in three steps:

- *Realization of the plant model*: the whole plant P dynamics affects also the PCV actuator and controller.
- *Identification of the PCV transfer function*: a linear model of the PCV $\left(\hat{G}_{PCV}\right)$ should be identified in order to capture the component dynamics, according to the acquired experimental data.
- *Tuning of the control parameters*: according to the plant model and the identified PCV transfer function, an optimization procedure, based on the flexible simplex techniques, can be applied to find the best gains for the controller G_{PID}.

3.3.2 Identification of the PCV

The PCV dynamics has been acquired with the proposed testing setup and according to the P_{ref} step variation from $1.8\,barG$ to $1.6\,barG$ of the PCV shown in the first 50 seconds of Figure 3.7. The control adopted for these test is not optimized yet (see the previous section) and is performed through a classic PID regulator manually tuned from the industrial partner (Table 3.1), without using any optimization technique to improve the accuracy of the controller action. The identification procedure of the PCV has been performed with the Matlab *System Identification Toolbox*. In particular, the employed techniques include maximum likelihood, prediction-error minimization schemes, and subspace methods [78].

The Matlab *System Identification Toolbox* takes in input the experimental pressure error e_p and the measured opening position y (shown in Figure 3.6) and brings out the transfer function F (Figure 3.9 (a)) that models the dynamics of pressure regulator G_{PID}, and PCV dynamics, described by the closed loop transfer function $\hat{G}_{PCV} = \frac{G_{pos} \cdot G_{act}}{1+G_{pos} \cdot G_{act}}$ (see Figure 3.9 (b) and Equation 3.24).

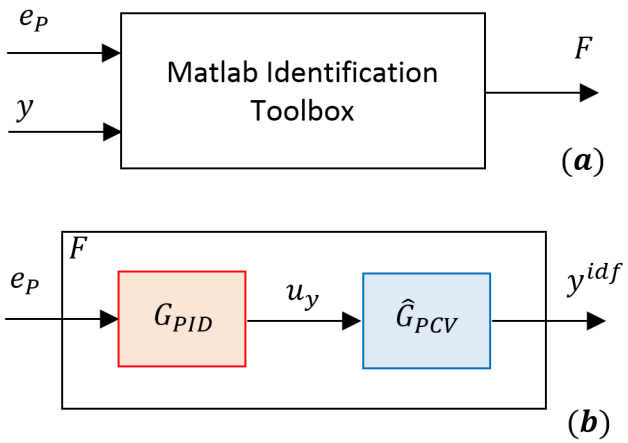

Figure 3.9: Identification of the transfer function F (a) and computation of y^{idf} (b).

The whole PCV dynamics (of both internal regulator G_{pos} and actuator G_{act}) is represented by the identified transfer function shown in Equation 3.24.

$$\hat{G}_{PCV}(s) = \frac{F(s)}{G_{PID}(s)} = \frac{k}{1+\tau s} \tag{3.24}$$

where $k = 1.296\ [-]$ and $\tau = 0.9794$ s.

The identified trend of the PCV opening position y^{idf} has been obtained considering the error pressure e_P as input of the identified F. The comparison between the

opening position trends, obtained from experimental data y (see Figure 3.6) and y^{idf}, represented in Figure 3.10 show a good matching in terms of amplitude and phase of the signals. In particular, the experimental data shown in Figure 3.10 corresponds to a P_{ref} step variation from $1.8\ barG$ to $1.6\ barG$ of the PCV: the adopted control logic in this case is that indicated in Table 3.1), that consists in a classic implementation of a PID regulator manually tuned.

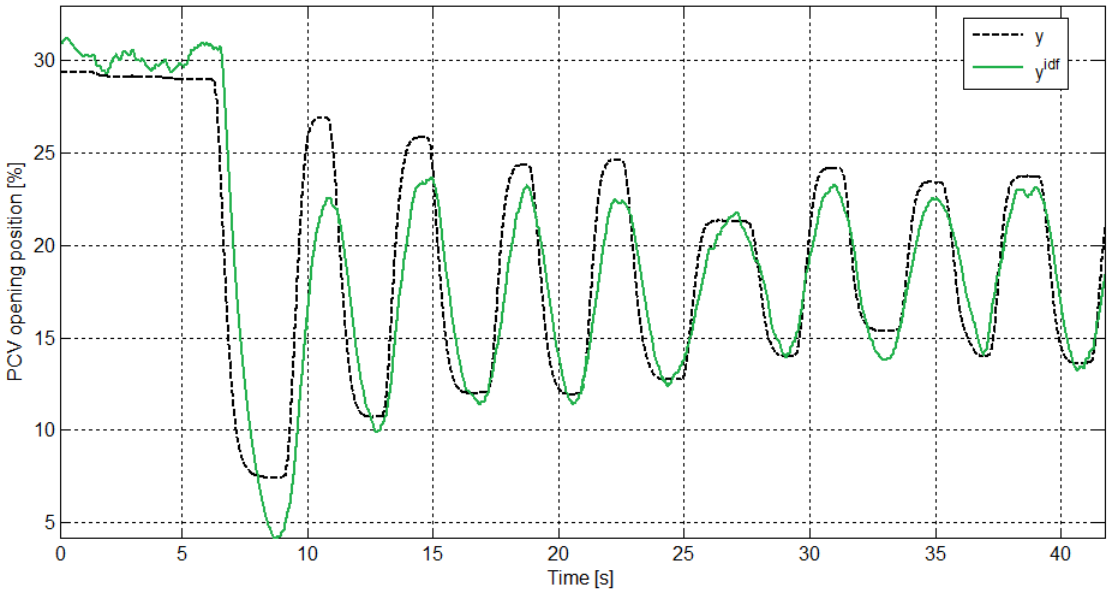

Figure 3.10: Comparison between the opening position trends obtained from experimental data y and identification y^{idf}, corresponding to P_{ref} step variation from $1.8\ barG$ to $1.6\ barG$ of the PCV

3.3.3 Optimization of the PCV PID regulator

The parameters optimization of the pressure regulator, referred to the Figure 3.8, represents a novelty in the energy field and an important aspect in order to improve the trend of the regulated header pressure. More precisely, the flexible simplex technique has been adopted [71, 72, 73], which is quite useful for two reasons:

- derivative free algorithm;
- high numerical efficiency, especially for low dimension problems.

In facts, the proposed method aims at obtaining a vector of parameters (here the PID control gains) which minimizes a given non-linear function (here depending from the

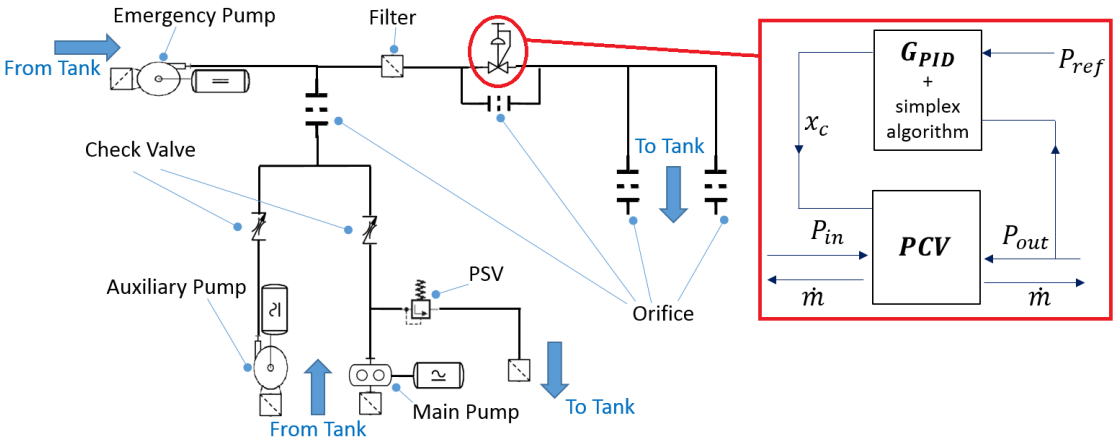

Figure 3.11: Functional scheme of the plant and the PCV.

pressure error). In particular, this technique aims at minimizing a cost function: the parameter used for the optimization is the IAE (Integral Absolute Error), indicated in Equation 3.25. In particular, it is computed through the simulation of the whole model of the auxiliary lubrication plant (shown in Figure 3.11) during the tracking of the same reference pressure p_{ref} (Figure 3.7) with a nominal flow-rate of 2000 lpm.

$$IAE = \int_0^{T_0} |e_p(t)|\, dt, \qquad e_p(t) = p_{ref} - p(t) \tag{3.25}$$

where $T_0 = 650$ s (in according with Figure. 3.7), p_{ref} is the set pressure, $p(t)$ indicates the PCV downstream pressure while $e_p(t)$ is the difference between these two amplitudes.

The simplex algorithm has been developed in Matlab-Simulink environment and needs to define the starting values of the PID parameters from which it begins to operate: to this aim, the parameters of the preliminary PID control system have been used (see Table 3.1). In order to improve the optimization procedure, the simplex algorithm provides optional parameters, whose features and working setup are illustrated in Table 3.3. The obtained PID parameters are listed in Table 3.4. Results, that will be described in the following section, have shown the good operating of the proposed procedure as control strategy, implemented with a first identification phase of the PCV dynamic behaviour and a second one of controller optimization through flexible simplex techniques. Results described in chapter 3.5 highlight the efficiency and accuracy of the proposed approach.

Table 3.3: Description of the adopted configuration for the optional parameters and tolerances of the flexible simplex algorithm.

Option	Description	Value
Option1	Display of the intermediate results: 1/0 (Y/N)	1
Option2	Precision required for the optimized parameter at the solution	0.1
Option3	Precision required for the cost function at the solution	0.1
Option14	Maximum number of iterations after which the research of the minimum is stopped	500

Table 3.4: Features of the optimized PID control system.

Gain	Value
Proportional gain k_p	11.2562 $[1/bar]$
Integral gain k_i	0.1287 $[1/(s \cdot bar)]$
Derivative gain k_d	10.3621 $[s/bar]$

3.4 Experimental Testing

3.4.1 Functional test procedure

The functional test procedure is characterized by a first phase in which only the auxiliary centrifugal pump is activated and the diameters of the last orifices are set to have a circuit flow rate equal to the nominal one; then this flow rate is increased by 20% and subsequently decreased to a value equal to 70% of the nominal one. During these tests the PCV is always able to control the downstream pressure unless the flow rate is equal to 70% of the nominal one, where it should be fully closed. At this point, the test procedure continues by searching the minimum flow rate for which the PCV restarts to regulate.

For the successive tests, the following testing conditions are considered: the last orifices are set to have a circuit flow rate equal to the nominal one. Maintaining the auxiliary centrifugal pump activated, the main volumetric pump is initially turned on by rotating the motor at a velocity equal to 20% of the normal operating one. The motor rotational velocity is then increased up to 80% and 100% of the normal operating velocity.

Finally, first the auxiliary centrifugal pump is switched off, maintaining the motor rotational velocity equal to the nominal one, and then the main volumetric pump is turned off too, simultaneously activating the emergency centrifugal pump. The last test requires to set the last orifices in order to have a circuit flow rate equal to 50% of the nominal one, only with the emergency centrifugal pump activated. This functional test procedure is summarized in Table 3.5.

3.4.2 Testing Apparatus

The control signal and the measured data are processed by MicroAutoBox II, which is a commercial RT platform produced by dSPACE ®, and many electronic components that equip the electric cabinet, while the tunable simulation parameters (gains, numeric conversions...) and the measured data can be managed in a Human Machine Interface (HMI) realized with the dSPACE ® software Control Desk ®. The HMI, whose layouts for the management of the PCV control logics and plant sensors acquisition are respectively shown in Figures 3.13 and 3.14, is located on a Host PC

Table 3.5: Functional test procedure.

	Main Volumetric Pump	Auxiliary Centrifugal Pump	Emergency Centrifugal Pump
Test 1	no	activated (nominal flow rate)	no
Test 2	no	activated (120% nominal flow rate)	no
Test 3	no	activated (70% nominal flow rate)	no
Test 4	no	activated (nominal flow rate)	no
Test 5	activated (20% normal operating velocity)	activated (nominal flow rate)	no
Test 6	activated (80% normal operating velocity)	activated (nominal flow rate)	no
Test 7	activated (normal operating velocity)	activated (nominal flow rate)	no
Test 8	activated (normal operating velocity)	no	no
Test 9	no	no	activated (nominal flow rate)
Test 10	no	no	activated (50% nominal flow rate)

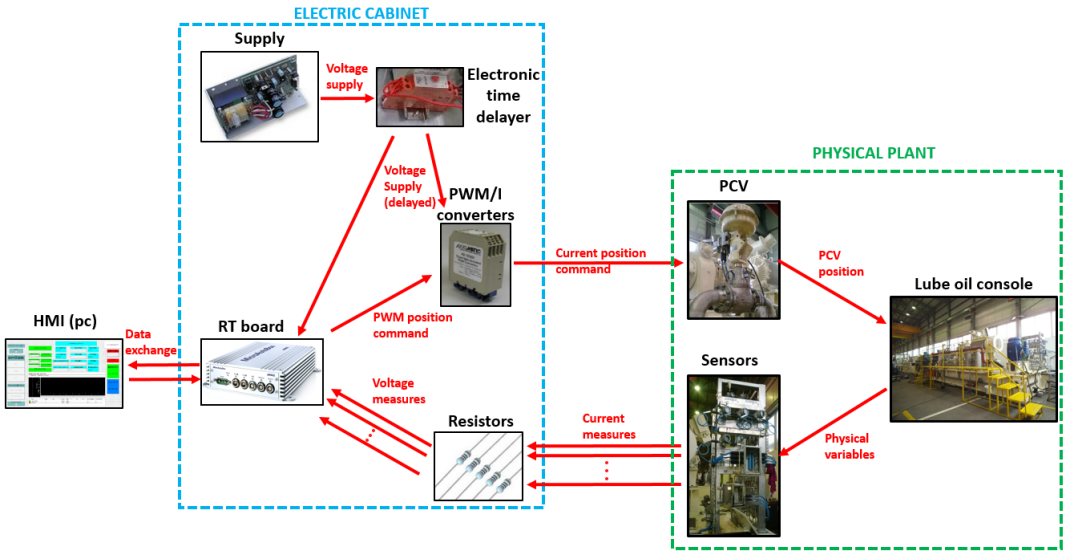

Figure 3.12: Testing apparatus architecture.

employed for data acquisition and test management. The the logic architecture is shown in Figure 3.12, while electric cabinet layout is depicted in Figure 3.15.

The inputs of the electric cabinet are represented by the $4 - 20\ mA$ electric current signals provided by the transmitters installed on the physical plant shown in Figure

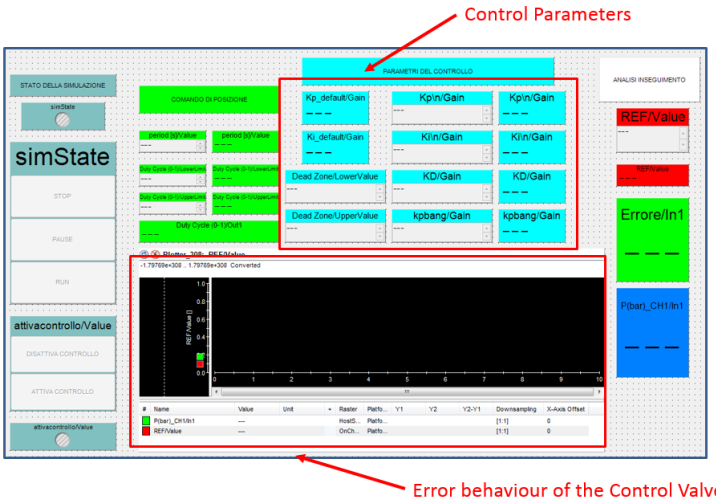

Figure 3.13: Dedicated HMI: layout of the PCV control logics.

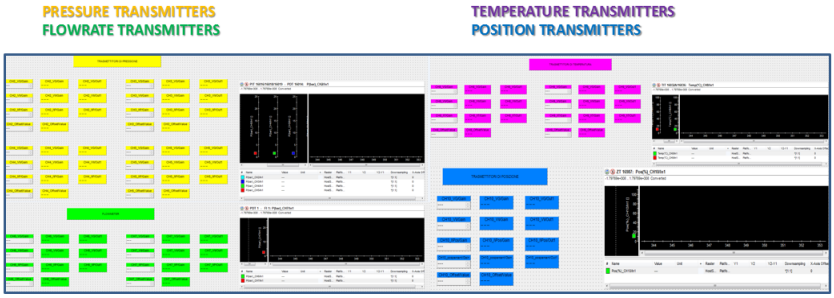

Figure 3.14: Dedicated HMI: layout of the plant sensors acquisition.

3.16. In particular, these signals are referred to physical variables described in Table 3.6.

The command output is represented by the $4 - 20\,mA$ electric signal employed to command the PCV positioner, an electronic-pneumatic component whose internal control system sets the actuator position to the given reference (its input command signal produced by the electric cabinet).

In more detail, the electric cabinet is composed by the following components:

- *MicroAutoBox II*: it is the RT platform for performing fast function prototyping, whose main features are described in Table 3.7. It operates without user intervention, just like an ECU (Electronic Control Unit), which can be used for different rapid control prototyping (RCP) applications. The control and measurement system is developed in Matlab-Simulink® 2013a. In particular,

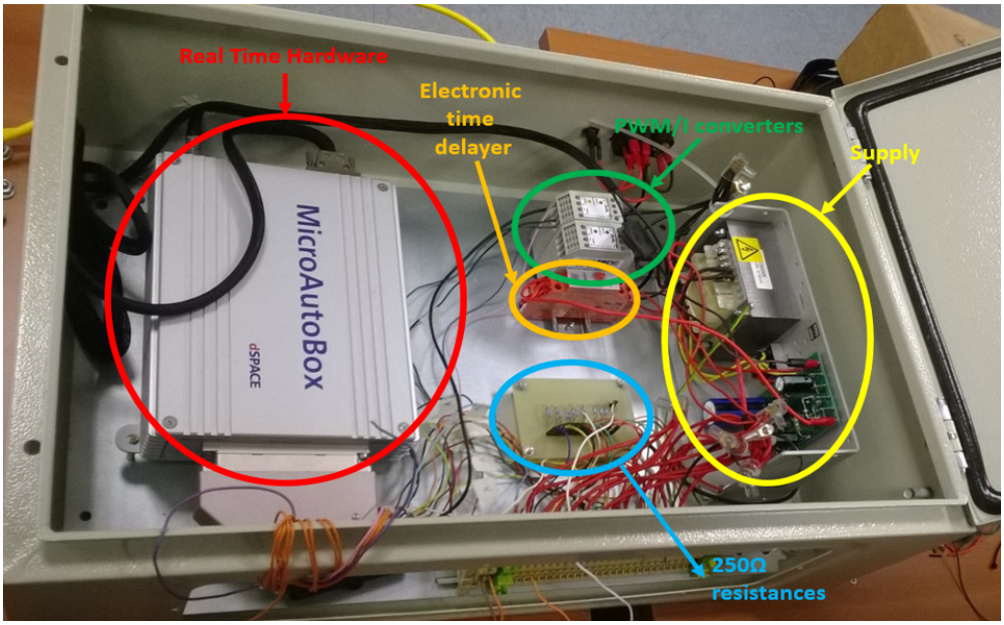

Figure 3.15: Electric cabinet and components.

Figure 3.16: Transmitters installed on the physical plant.

Table 3.6: Acquired signals.

Header pressure
Main pump discharge pressure
Auxiliary pump discharge pressure
Emergency pump discharge pressure
Filters differential pressure
Tank temperature
Header temperature
PCV position feedback
Load flow-rate
Flow-rate on the bypass line

the PID control logic has been uploaded on the MicroAutoBox II hardware that, therefore, is able to send the control signal to the other electronic components and contemporary receive in RT the data from the plant. The output consists in the PWM control signal to the PWM/I converters while the inputs are the voltage signals from the $250\ \Omega$ resistors.

Table 3.7: Main Features of the chosen RT board.

Model	MicroAutoBox II 1401/1511
Processor	900 MHz
I/O Design Voltage	5/4.5 V
Memory	16Mbit (main) +16Mbit (flash)
CAN modules	4
Host and RT I/O interfaces	Ethernet connection (100/1000 Mbit/s)
ADC I/O channels	16/4
GPIO pins	40/40
PWM inputs/outputs	40/40

- *PWM/I converters*: the PWM/I converters are electronic components employed to convert the Pulse Width Modulation signal,provided by the RT platform, into a $4 - 20\ mA$ current signal, which is sent to the PCV positioner.
- *Supply*: the supply system converts the $220V_{DC}$ voltage into a stabilized $24V_{DC}$ voltage, which is used to supply the MicroAutoBox II and the PWM/I converters.
- *Electronic time delayer*: An electronic time delayer produces a fixed time delay of the $24V_{DC}$ voltage from the Supply system to the other components. It is

useful to avoid undesired power shut-downs due to the inrush currents of the components.

- $250\ \Omega$ *resistors*: Ten $250\ \Omega$ electric resistances are equipped in order to convert the $4 - 20\ mA$ current signals from the plant sensors in $1 - 5\ V$ voltage signals that can be acquired by the input stage of the RT platform.

3.5 Validation and Results

3.5.1 Steps test: Numerical Simulation

The following section focuses on the simulation results obtained according to the simulation of the whole plant model with different PID parameters. This numerical test in not included in the functional test procedure. It is required to compare the different PID performances, and in particular to show that the optimized PID has a better behavior respect to the non-optimized one. This way, the optimized PID can be employed to regulate in the real component to perform the functional test procedure, which will be object of the next section 3.5.2.

In particular, the control is evaluated in terms of the following parameters:

- Rising time T_r;
- Falling time T_f;
- Settling time $T_{a,\epsilon}$;
- Static error of pressure e_p.

The following figures (3.17 and 3.18) show the behaviors of the pressure downstream the PCV, with standard and optimized PID regulators, respectively in falling and rising steps of the reference pressure P_{ref}.

In particular, while the rising time T_r and falling time T_f remain very similar, the settling time $T_{a,\epsilon}$ and the static error of pressure e_P relative to the optimized gains simulation are remarkably reduced respect to the standard one. The obtained parameters values are resumed in Table 3.8.

Table 3.8: Comparison between T_r, T_f and e_P obtained from standard and optimized PID gains.

PID gains	Mean T_r	Mean T_f	Mean e_P	Mean $T_{a,\epsilon}$
Standard	$2\ s$	$4\ s$	$0.02\ bar$	$200\ s$
Optimized	$2\ s$	$4\ s$	$< 0.01\ bar$	$8\ s$

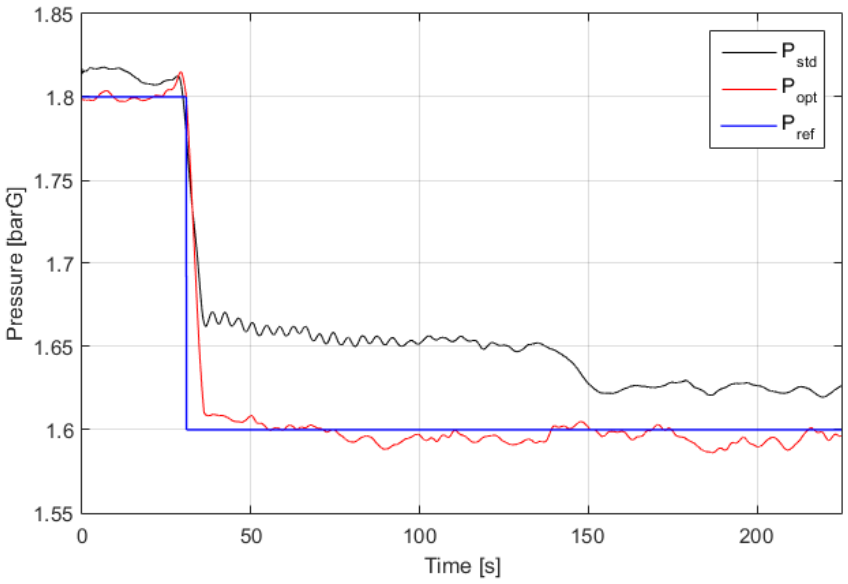

Figure 3.17: Comparison between the pressure trends, obtained from standard (std) and optimized (opt) PID gains, with respect to a decreasing step of P_{ref}.

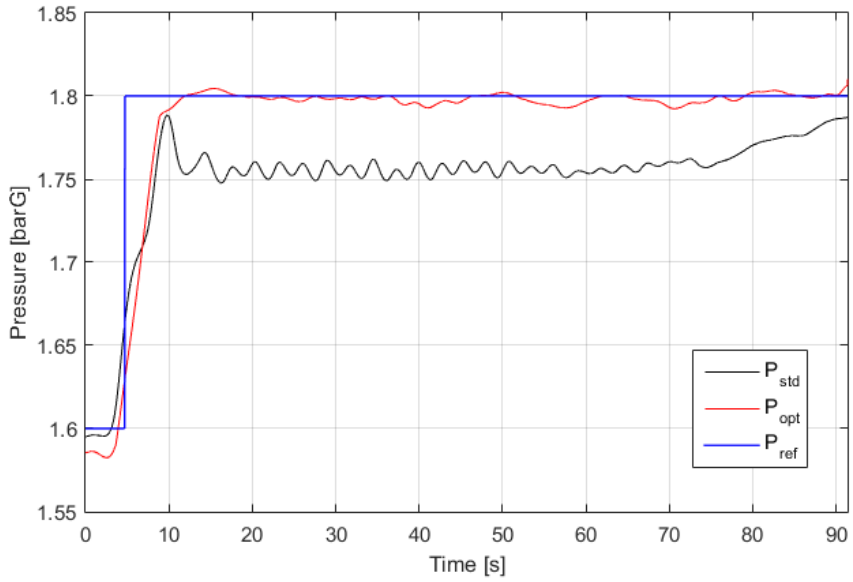

Figure 3.18: Comparison between the pressure trends, obtained from standard (std) and optimized (opt) PID gains, with respect to an increasing step of P_{ref}.

3.5.2 Experimental Data Comparison

In this section, the comparisons between the numerical results of the whole plant (simulated through the Thermal-Hydraulic Library components) and the experimental

data acquired during the official tests performed in Ptuj, Slovenia have been carried out. According to the Tables 3.5 and 3.9, the numerical simulations follow the real functional procedure. These comparisons aim at evaluating the optimized controller performance in terms of the whole plant.

Table 3.9: Testing phases.

	Main Volumetric Pump	Auxiliary Centrifugal Pump	Emergency Centrifugal Pump	Flow rate [lpm]	Main pressure [barG]	Auxiliary pressure [barG]	Emergency pressure [barG]
Test 1		X		2000		6.6	
Test 2		X		2400		6.15	
Test 3		X		1400		6.95	
Test 4		X		2000		6.6	
Test 5	20%	X		2000	5.8→6.4	6.6→7	
Test 6	80%	X		2000	6.4→7	7	
Test 7	X	X		2000	7→7.45	7	
Test 8	X			2000	7.5		
Test 9			X	1500			2
Test 10			X	1000			2.2

Figures 3.19, 3.20 and 3.21 express the experimental validation of the numerical model with respect to the real plant. Both the numerical simulations and the experimental tests have been performed through the optimized PID controller. The highlighted areas represent a test part which is not defined in the test procedure and therefore is not simulated during the validation phase.

According to the previous subsection, the control model is also validated in terms of TTH components of the whole plant (e.g.: pump, check valve, orifice,...). Figure 3.19 shows the comparison between the measured and simulated header pressure (i.e. the downstream PCV pressure). Figure 3.20 and Figure 3.21 show respectively the comparison between the measured and simulated flow rate and the comparison between the main, auxiliary and emergency pump pressures; since the flow rate and the pumps pressures are directly influenced by the PCV pressure, the successful outcome of this validation demonstrates the proper operation of the PCV controller synthesized in the previous sections. The yellow labels indicate the corresponding test number.

The numerical simulations of the plant were carried out through the testing computed and algorithm shown in Table 3.10. It should be noticed that, because the feasibility of RT simulations is a mandatory specification, the developed code has been optimized to privilege robustness when used with fixed step solvers and limited

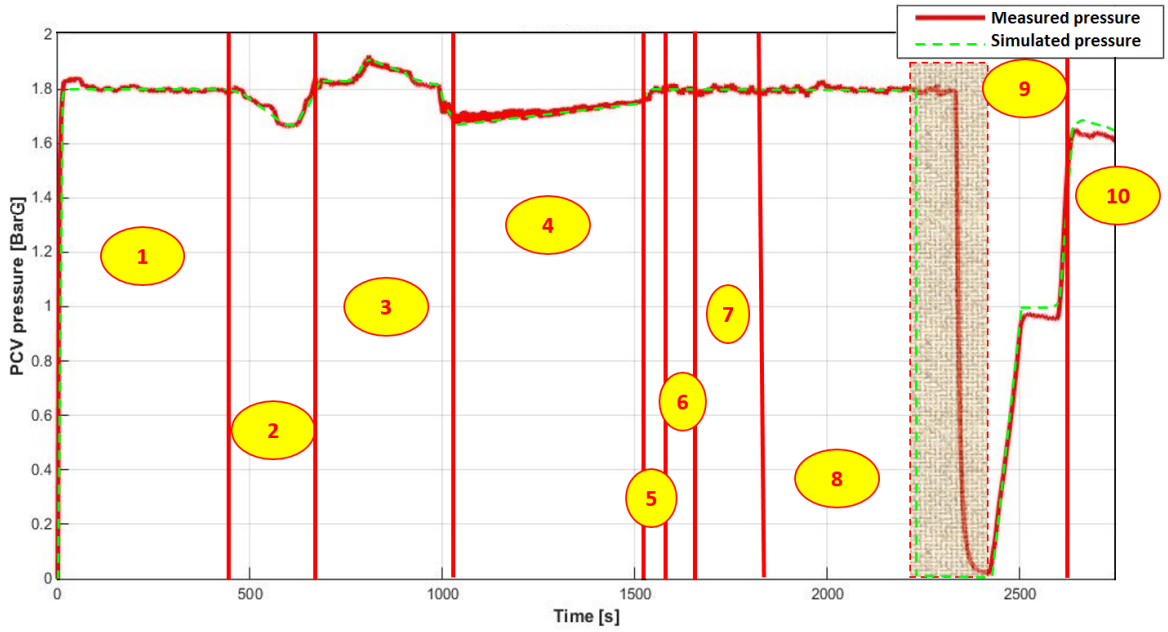

Figure 3.19: Comparison between the measured and simulated header pressure.

computational resources, which involve the use of low sampling-solving frequencies. Therefore, for the present application, implicit solvers proved to be more stable than the explicit ones; in particular, the ODE14x [79] is an extrapolation solved based on linearly implicit Euler method [80, 81] and has been preferred because it represents the best compromise in terms of stability and numerical efficiency. Therefore, considering the simulation times, the ratio between the simulated test time (i.e. about 2700 s) and the time needed by the computer to carry out the simulation is less than 1:3, which, considering the large amount of components present in this plant and consequently in the model, can be considered a satisfactory result, very close to the desired 1:1 "RT ratio".

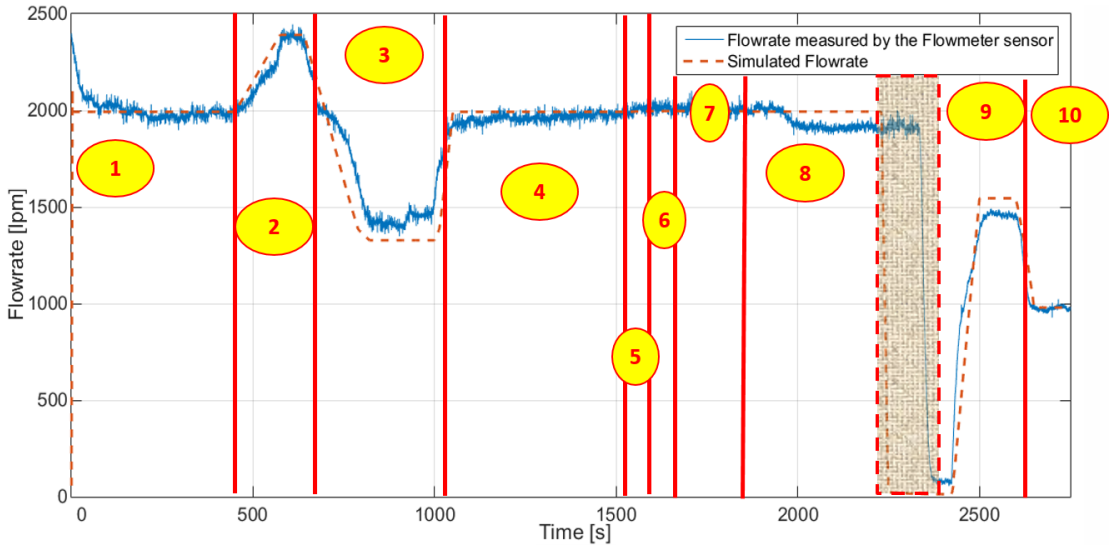

Figure 3.20: Comparison between the measured and simulated flow rate.

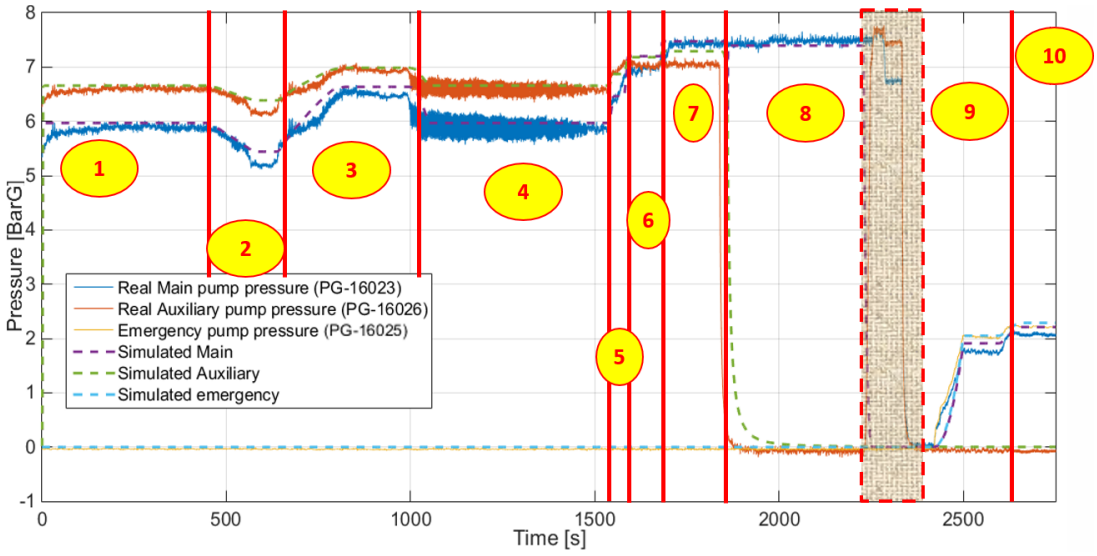

Figure 3.21: Comparison between the main, auxiliary and emergency pump pressures obtained from experimental data and numerical simulation.

Table 3.10: Main features of the testing computer and of the adopted solver for the plant simulation.

Computer	
Operative system	Windows 7®
CPU clock frequency	2.4 GHz
RAM memory	8 Gb
Solver	
Solver name	ODE14x
Solver type	Fixed Step
Sampling time	0.0005 s

Chapter 4

HIL testing of a Turbine Bypass Valve controller

In this chapter, a numerically efficient model for the RT simulation of a steam plant is presented. To this aim, the modelling approach described in the previous chapter 2 has been employed to develop a lumped parameter model of the steam plant. The proposed model has been used to develop a HIL test rig of turbine bypass controllers and (eventually) valve positioners, which was the aim of the industrial partner (Velan ABV S.p.A.).

The simulation code (developed through Matlab software), which is implemented for a fixed, discrete step solver, has been compiled for a RT target to be executed in Real Time on a low-cost (and low-performances) industrial hardware. In particular, for this application, a Texas Instrument DSP was chosen. Considering the low performances of the chosen hardware, the modelling and RT implementation activities aimed at obtaining the best compromise between accuracy and efficiency.

Therefore, in this chapter, the modelling and RT implementation aspects of both model and related control system are treated. Moreover, the whole HIL architecture for the execution of the experimental activities and results of the proposed test rig are discussed.

The work proposed in the following sections belongs to the project *High Efficiency Valves* (CUP:D55C12009530007) which is financed by the program POR CREO FESR of Regione Toscana (European Funds for Regional Industrial R&D projects).

4.1 Introduction to the problem

Efficiency and, more generally, cost optimization of energy production are important specifications for the development of power generation units [45].

However, a growing interest is noticed in the improvement of the performance in transients and off-design operating conditions [82] (e.g. the cyclic operation). This interest is mainly justified by industrial and economic reasons such as the delocalization of energy production and the increasing global liberalization of the energy market. One of the most important causes of the delocalization of the energy production (especially in western Europe) is the growing use of renewable energy sources. Also, integration and management of renewable energy sources into total sites, as proposed for example by Varbanov and Klemes [83] should offer a way to mitigate these troubles, but not to change the trend toward a more flexible exercise of both power plants and grids. Another important aspect is the globalization and liberalization of the energy market [33].

Liberalization involves the availability of different power sources, countries and producers. With a free energy market even an intermittent use of the plant should become remunerative, considering fluctuations of the energy price. This is one of the most cited reasons to optimize, as much as possible, the control and behavior of power plants during the start-up phase [84].

For large steam or combined cycle power plants, a flexible use of the plant involves higher reliability, availability, and duration of components which are more subjected to potentially dangerous thermomechanical stresses. These features can be achieved introducing turbine bypass systems.

4.1.1 Turbine Bypass Systems

Turbine bypass valves (TBVs, in Figure 4.1 [85]) are typically used to smoothly adjust temperature and pressure gradients affecting the plant transients and off-design operating conditions, which can negatively affect safety and reliability of potentially critical components such as heat exchangers or turbines [86]. In particular, these results are obtained by adjusting the pressure and the temperature of the fluid by two distinct valves, respectively defined as DTP (Discrete Tortuos Path, which refers to the construction technology of these valves [87, 88]) control valve and spray water control

valve.

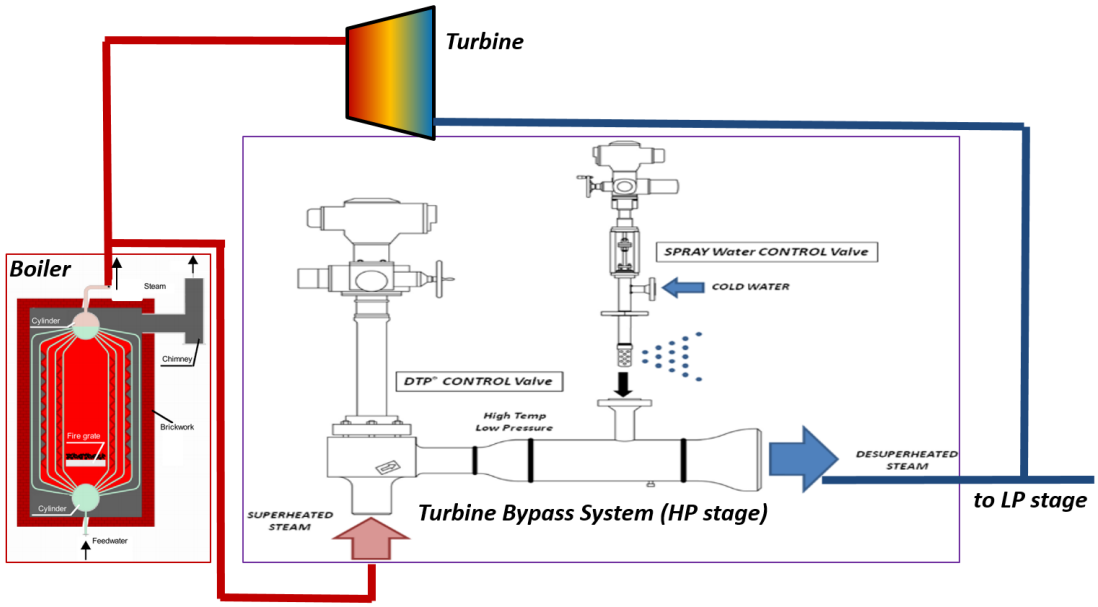

Figure 4.1: Typical layout of a turbine bypass system (e.g. HP stage), courtesy of Velan ABV [87].

The system architecture is heavily influenced by features and performances of the valves used to adjust pressure and temperature: useful technical information concerning valve structure and performances are available from the sites of some of the most important industrial suppliers [87, 89, 90].

Typical applications of bypass systems are in large fossil fired steam plants [91], in combined gas-steam turbine power plants [45] or even in nuclear plants [92].

4.1.2 Hardware In the Loop Approach

To improve the response of the turbine bypass systems (TBSs) an efficient design of both actuators and control system is mandatory. In particular, the TBS control parameters have to be optimized with respect to plant features including the dynamical response of valves and their positioners. To this aim, HIL testing could represent a powerful tool to identify and optimize the dynamical performances of valve actuators and positioners and to mutually tune them with respect to the higher level control of the TBS system.

A preliminary scheme of the proposed HIL test rig is described in Figure 4.2: the

actuators and positioners of the turbine bypass valves are the components that are really installed and tested on the rig; the valve reference commands are generated by a RT model of the plant including the TBS controller. The corresponding response of the valve actuators in terms of position feedback is acquired in Real Time; once the plug positions are acquired by the control board the simulated opening states of the valves are known and the RT model of the plant is updated and able to calculate new values of valve commands for the next computational step, closing the simulation loop. The rig is completed by a host pc which is used to implement the rig Human Machine Interface (HMI) and, more generally, to manage the rig (pre-processing and post-processing of test results and data storage).

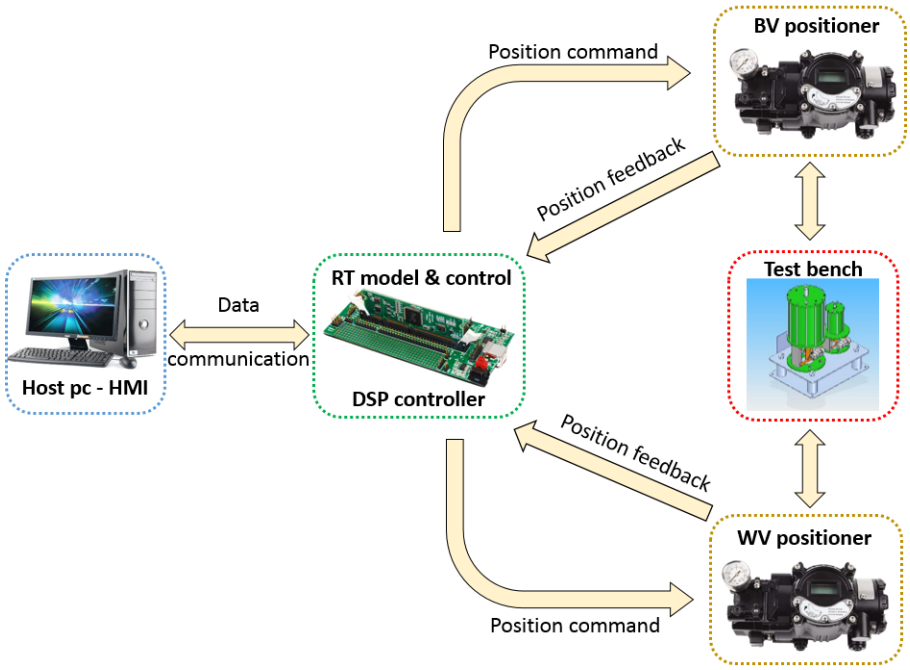

Figure 4.2: Preliminary HIL architecture in which both DTP and spray water valves are simulated.

The way in which the RT models of both plant and controllers are developed and implemented is very important for the future use of the rig in terms of expandability and customization.

Simulation and optimization of TBSs are still the object of recent research: for example, in [91] and [92] simulation tools dedicated to specific power plant configurations and technologies have been proposed. With respect to these previous works, the idea of developing a modular, object oriented model is proposed, in which

every component of the simulated plant can be seen as an individual block of a library that can be used to assemble different plant layouts. In literature there are some previous works [93, 59] concerning the development of dynamical models mainly applied to the optimization of control aspects. However, they are mostly devoted to off-line standard simulations and not to RT applications. In particular, RT applications involve an efficient and robust fixed-step implementation of the model which is not considered in the above mentioned examples [93, 59]. To this end, the plant is modeled as a lumped system in which each component is implemented as a lumped element.

The aim of the proposed HIL application is to test the behavior of tested positioners, also during the start-up and the shut-down phases of the plant; during the plant start-up, pressure and temperature of the steam flow drastically change and all the plant is working in off-design conditions which are smoothly but continuously changing; so, the use of linearized models with respect to a known mean operating point could cause appreciable errors that can be avoided by using a nonlinear plant model.

It is also interesting to notice that, to simplify as much as possible the RT implementation, the number of plant states that are integrated in the time domain have been reduced as much as possible. For this reason, the behavior of some plant states is calculated by interpolating tabulated data that are referred to the steady-state response of the simulated plant in off-design conditions. The tabulated data are calculated using an off-line steady-state model previously developed and validated in [94, 95, 96].

In 2014, Sindareh-Esfahani published two works [97, 98] on these topics, concerning both simulation, control and identification of a steam generator during a cold plant start-up. Since a complete model of the boiler dynamical behavior is quite unsuitable for RT implementation, a simplified approach was preferred [99]. In particular, the dynamical model is derived from the work of Astrom and Bell [44].

In order to verify the suitability of the chosen approach, some simulations on a specific benchmark case study [100] have been carried out. Benchmark simulations are directly performed in Real Time using the same DSP that has been used for the HIL test rig. The adopted benchmark is referred to a double pressure level, fossil fired, steam power plant. Despite to the age of the publication, this kind of benchmark was preferred since it was directly referred to the simulation of a plant start-up with a General Electric MARK architecture which is still quite diffused.

Therefore, the aim is to demonstrate that the RT plant model can be used to simulate different kind of plant control layouts without losing reliability, numerical

stability, and ease of use. In particular, results of RT simulations are compared with the corresponding pressure, flow and temperature profiles calculated in [100]. The aim of this comparison is not to simply evaluate the performance of the controllers but, mainly, the robustness of the proposed HIL approach. Finally, the results of experimental activities performed on the test rig are described.

4.2 Model of the steam plant

4.2.1 General architecture of the steam plant model

Figures 4.3 and 4.4 show respectively the general architecture of the steam power plant chosen as benchmark [100] and the functional scheme of the implemented boiler.

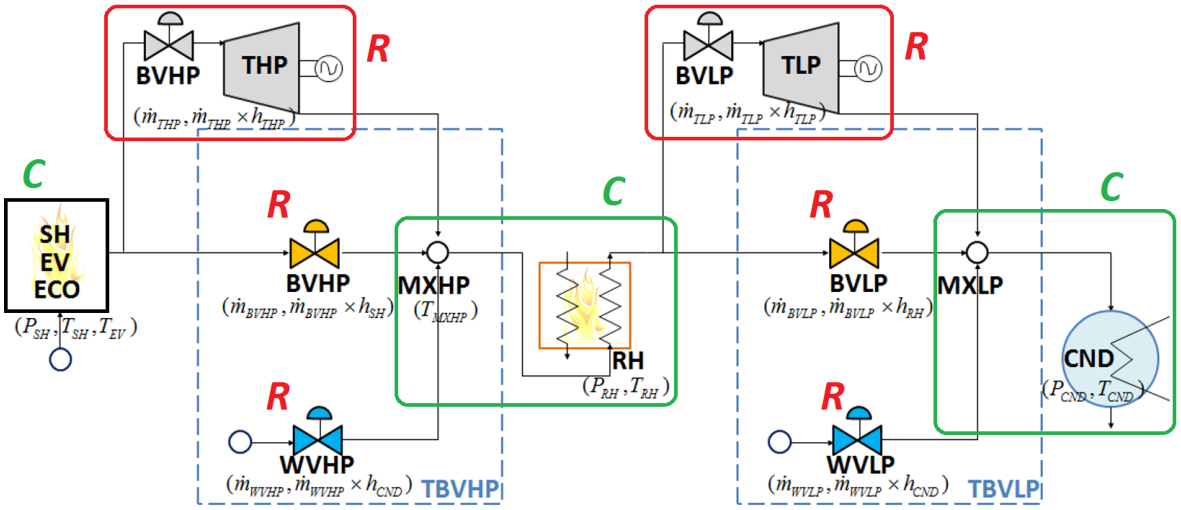

Figure 4.3: Simplified architecture scheme of the studied steam plant with adopted symbols and variables and corresponding discretization in capacitive (C green capital letters) and resistive (R red capital letters).

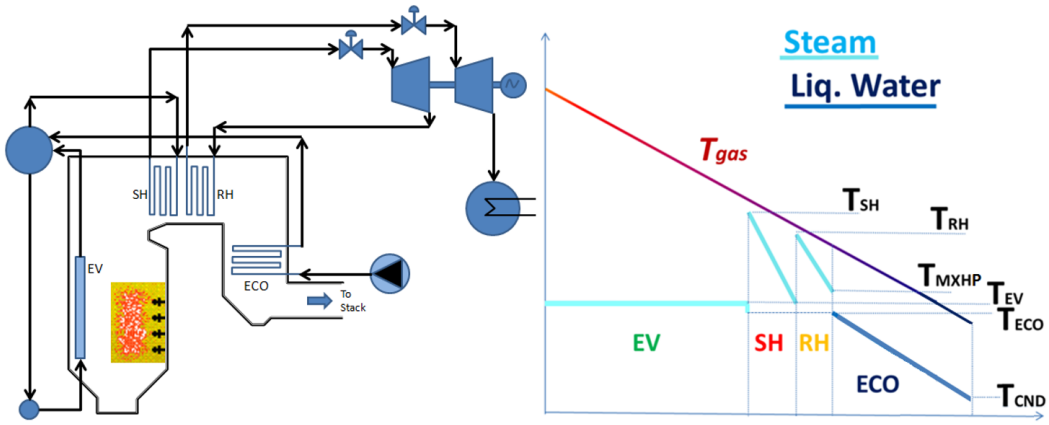

Figure 4.4: Simplified boiler plant scheme adopted for the simulation and temperature versus heat exchanged diagram.

The dynamical behavior of the continuous fluid system has been represented

considering the equations governing the balance of mass 2.1, momentum 2.2, and energy 2.3 and, more generally, the modelling approach described in chapter 2 was adopted. In particular, the plant is composed by the following components:

- The boiler (C element): The boiler is represented by a block including evaporator (EV), economizer (ECO), and superheater stage (SH). In the boiler model, the pressure P_{SH} and the temperature T_{SH} of the outlet flow rate of the superheater are calculated as functions of the heat $Q_{SH} + Q_{EV}$ provided by an external source (the burner) and by the steam flow $\dot{m}_{BVHP} + \dot{m}_{THP}$ required by the connected high-pressure turbine and bypass valve.

- High-pressure turbine, THP, with its regulating valve TVHP (R element): the steam flow of the turbine $\dot{m}_{THP}$ is calculated as a function of P_{SH}, T_{SH}, and P_{RH} which are calculated by adjacent capacitive blocks. The relationship between the computed flow rate $\dot{m}_{THP}$ and the pressure drop $(P_{SH} - P_{RH})$ considers both the states of the valve TVHP (open/closed) and of the turbine.

- Bypass and spray valves (respectively BVHP and WVHP) of the bypass system for the high-pressure level (R elements): the computed steam flow through BVHP $\dot{m}_{BVHP}$ and the water flow through WVHP $\dot{m}_{WVHP}$ are calculated as functions of the pressure drop across the valves and their opening state in terms of equivalent area.

- Mixer MXHP and reheater RH Block (C element): this block represents the mixing of different flows coming from THP, BVHP and WVHP. In addition, the reheating in the RH stage is modeled. The inlet flow rates $\dot{m}_{BVHP}$,$\dot{m}_{WVHP}$, and $\dot{m}_{THP}$ are calculated by the turbine and valves resistive blocks. Performing mass and enthalpy balances is possible to calculate the corresponding pressure P_{MXHP} and temperature T_{MXHP} of the mixed flow. Neglecting pressure drops in the reheater stage ($P_{MXHP} = P_{RH}$) and knowing the heat flow Q_{RH} from the boiler is possible to calculate the outlet temperature T_{RH}.

- Low-pressure turbine, TLP, with its regulating valve TVLP (R element): the steam flow of the turbine $\dot{m}_{TLP}$ is calculated as a function of P_{RH}, T_{RH} and P_{CND} which are calculated by adjacent capacitive blocks. The relationship between the computed flow rate $\dot{m}_{TLP}$ and the pressure drop $(P_{RH} - P_{CND})$ considers both the states of the valve TVLP (open/closed) and of the turbine.

- Bypass and spray valves (respectively BVLP and WVLP) of the bypass system for the low pressure level (R elements): the computed steam flow rate through BVLP $\dot{m}_{BVLP}$ and the water flow through WVLP $\dot{m}_{WVLP}$ depend both on the inlet and outlet pressure conditions and on the valves opening states.

- Condenser CND and low-pressure mixer stage MXLP (C element): this block represents the condenser which is modeled as an imposed boundary pressure condition P_{CND}. The temperature of the mixed flow T_{MXLP} is obtained by merging $\dot{m}_{BVLP}$, $\dot{m}_{WVLP}$, and $\dot{m}_{TLP}$ through a simple enthalpy/energy balance.

The proposed approach is modular, so it can be easily applied to the simulation of plants with different layouts.

4.2.2 Model of the steam generator

The aim of the proposed model is the HIL testing of components such as the valve positioners and, therefore, a simplified model has been developed. On the other hand, the dynamical effects, as the huge thermal capacity of the evaporator, cannot be completely neglected. Moreover, in the proposed approach the following simplifications are assumed:

- The level of the water in the boiler drum is perfectly controlled so, considering the presence of the boiler pressure control too, the mass flow rate of feeding water provided by the pump to the boiler drum is equal to the corresponding steam mass flow rate produced.

- Pressure losses into evaporator and superheater are completely neglected $P_{EV} = P_{SH}$.

- Enthalpy of the feeding water is assumed to be known and constant, including the contribution of the pump.

- The calculation of the outlet temperatures of superheater T_{SH} and reheater T_{RH} are approximated using tabulated results from static off-line simulations of the plant in off-design conditions. Off-line simulations are performed with a previously developed model [94].

If these assumptions are verified, the application of mass and energy conservation to a lumped element produces the balance equation 4.1 which has been previously introduced [44]:

$$\frac{P_{SH}}{dt} = \frac{[Q_{ECO} + Q_{EV} - (\dot{m}_{BVHP} + \dot{m}_{wVHP}) \cdot (h_{EV} + h_{FW})]}{\left[\rho_{w,EV} \cdot V_{w,EV} \cdot \frac{h_{w,EV}}{dP_{SH}} + (C_{EV} + C_{SH}) \cdot \frac{T_{EV}}{dt}\right]}. \tag{4.1}$$

By integrating equation 4.1, it is possible to calculate the pressure of both evaporator and superheater [44]. Mass flow rates are calculated by connected resistive elements. In addition, the temperature of the evaporator (T_{EV}) is known as it depends from P_{EV} (assumed to be equal to the one calculated in the previous computational step). The steam properties are calculated considering tabulated data taken from Wagner et al. [101]. Moreover, the heat flows exchanged in the economizer (Q_{ECO}), the evaporator (Q_{EV}), and the superheater (Q_{SH}) have to be calculated, as they are the control variables of the control system implemented within the boiler model.

The control input of the boiler is supposed to be the fuel mass flow rate. For an assigned fuel/air ratio of the burner, the mass flow rate of hot gas produced by the burner is proportional to the consumed fuel. To optimize computational resources for a RT application, a tabular approach was preferred: a previously validated model ([94, 95, 96]) for the performance analysis in steady-state conditions is used to determine temperatures and exchanged heat fluxes of the plant considering different off-design conditions. These simulations are performed off-line. The boiler geometry is imposed; moreover, the thermodynamic, heat transfer, and momentum equations are used. Fluid properties in each section of boiler and heat exchanger are calculated in design analysis, but it changes in off-design conditions according the approach proposed in [95, 96]. In off-design analysis, the heat transfer coefficient depends on the mass flow rate and on the fluid properties. Correlation for the heat transfer coefficient can be defined using Nusselt and Reynolds number (exponent between 0.5 and 0.8).

The boiler plant is composed by an evaporator a superheater, a reheater section, and finally an economizer (Figure 4.4) where the evaporator is put in fire zone to take advantage of flame radiation. Figure 4.5 shows the steam and gas temperature trends in the boiler stages. Fixing the heat exchanging surfaces of the boiler stages, only three parameters can be changed: the burner gas mass flow rate ($\dot{m}_{GAS}$), evaporator/superheater pressure ($P_{EV} = P_{SH}$), and reheater pressure P_{RH}.

Some simulation results are shown in Figures 4.5 and 4.6. The outlet steam temperature of superheater depends on pressure of the same element, but there is

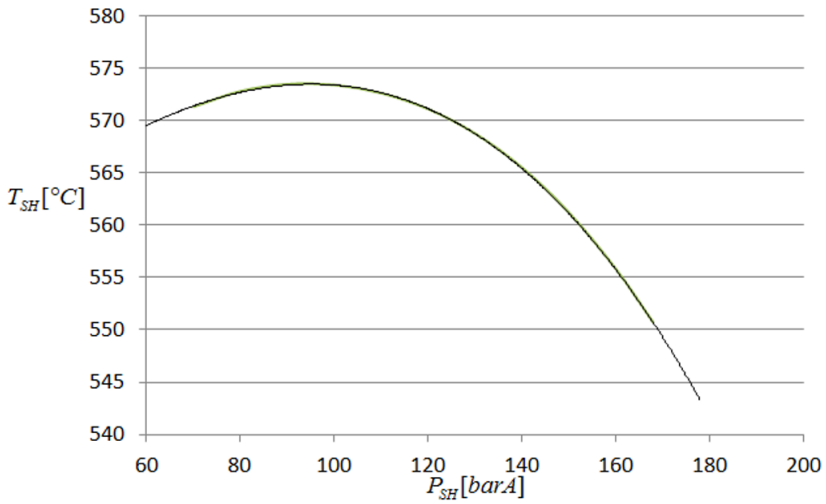

Figure 4.5: Calculated (interpolated from off-design steady-state simulations) outlet temperature T_{SH} as function of P_{SH} for an assigned value of $\dot{m}_{GAS}$ (the nominal value).

only a minor effect of reheat pressure because the reheater is downstream with respect to evaporator and superheater, so it has an effect only on the economizer. Varying the superheater pressure, some phenomena occur: the latent heat exchanged into evaporator varies and the mean logarithms difference temperature into evaporator varies, too. Thus, the heat exchanged changes and the steam temperature from superheater is like in Figure 5. The reheater temperature (Figure 4.6) depends on superheater and reheater pressures, in fact the superheater is upstream with respect to reheater and so the evaporator (and superheater) pressure influences the exit temperature from reheater. Varying the reheater pressure, the exhaust condition of high-pressure turbine changes, and hence the steam temperature at inlet of reheater varies, too. It should be also noticed from Figure 6 that the dependency of T_{RH} with respect to a variation of P_{RH} is quite weak. Heat fluxes exchanged along the various sub-sections of the steam generator (Q_{ECO}, Q_{EV} and Q_{SH}) and outlet temperatures of steam from superheater and reheater elements (T_{SH}, T_{RH}) are calculated using on-line interpolation of tabulated data from off-design simulations.

The complete model [94] runs off-line, producing in few minutes a tabulated surface of results which can be used to evaluate on-line the desired plant properties. The main advantage of the proposed approach is the simplicity and the capacity of simulating the delays effects introduced by the thermal inertia of water and metal parts of the evaporator. Thermal inertia of the evaporator greatly contributes to influence the plant dynamics during transients. On the other hand, superheater and reheater are modeled

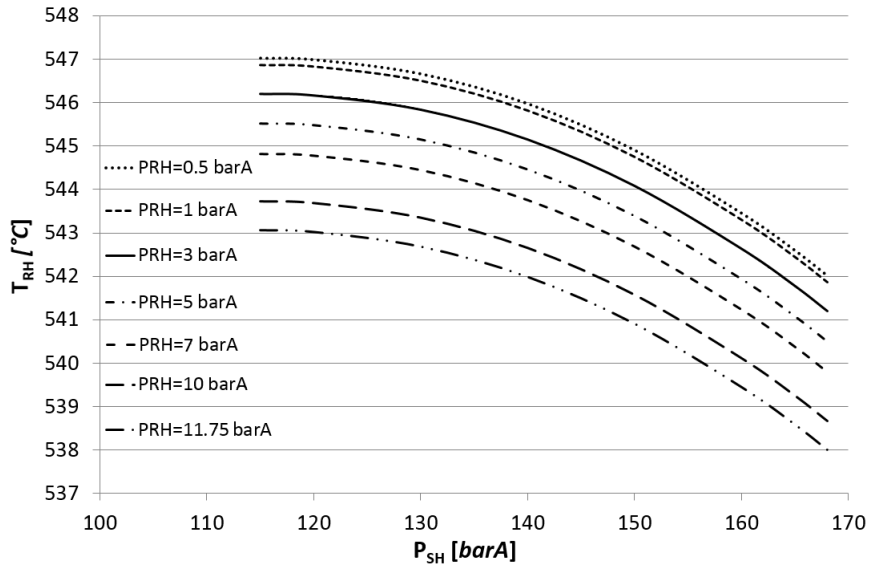

Figure 4.6: Calculated (interpolated from off-design steady-state simulations) outlet reheater temperature T_{RH} as function of P_{SH} and P_{RH} for an assigned value of $\dot{m}_{GAS}$ (the nominal value).

considering tabulated data of off-design simulations. As consequence, the contribution of these components to the plant dynamics is treated with a much more approximated approach.

4.2.3 Model of the bypass valves

The HP bypass valve BVHP and LP bypass valve BVLP generate an adjusted pressure drop (isenthalpic lamination) respectively across the HP and LP pressure levels of the plant. The mass flow rates [kg/s] of BVHP and BVLP are calculated according to the following equations, which are empirical fits to experimental data derived from technical documentation [87, 102]:

$$\dot{m}_{BVHP} = x_{c,BVHP} C_{v,BVHP} F_p N_6 \sqrt{\gamma_{SW} P_{SH} X_{BVHP}} \cdot \left(1 - \frac{X_{BVHP}}{3 x_t F_k(\gamma)}\right) \frac{1}{3600}; \tag{4.2}$$

$$\dot{m}_{BVLP} = x_{c,BVLP} C_{v,BVLP} F_p N_6 \sqrt{\gamma_{SW} P_{RH} X_{BVLP}} \cdot \left(1 - \frac{X_{BVLP}}{3 x_t F_k(\gamma)}\right) \frac{1}{3600}. \tag{4.3}$$

The behavior of spray water valves is modeled using equations 4.4 and 4.5, which describe the water mass flow rates $\dot{m}_{WVHP}$, $\dot{m}_{WVLP}$ [kg/s] derived from [87, 102] as

well:

$$\dot{m}_{WVHP} = \frac{\sqrt{1000 v_{sFW} \left(P_{FW} - P_{RH} - \Delta P_{rgHP}\right) \frac{0.865 \rho_{FW}}{3600}}}{\frac{1}{C_{vWVHP}^2} + \frac{1}{C_{vRGHP}^2}}; \tag{4.4}$$

$$\dot{m}_{WVLP} = \frac{\sqrt{1000 v_{sFW} \left(P_{FW} - P_{CND} - \Delta P_{rgLP}\right) \frac{0.865 \rho_{FW}}{3600}}}{\frac{1}{C_{vWVLP}^2} + \frac{1}{C_{vRGLP}^2}}. \tag{4.5}$$

Moreover, both the DTP valves and the spray water ones are composed by an array of stacked perforated discs which are grouped in sets. A single set is composed of a $3\,mm$ thick full disc (spacer) and by two perforated, milled discs ($5\,mm$ thick for BVHP and BVLP; $3\,mm$ thick for WVHP and WVLP), rotated through a particular angle. The C_v trend along the height direction of the set defines the set characteristics, while the sum of the set characteristics produces the valve characteristics. Hence, valves characteristics have been modeled through a look-up table, reproducing a sum of broken lines of the set characteristics. Finally, the opening/closing dynamics of the valve actuators are realized by simple first-order filters with a time constant of $3.3\,s$ [87].

4.2.4 Model of the turbines

Turbines have been modeled implementing a simplified algebraic model [103] which is still widely adopted for the modeling of turbine control systems [98, 104].

Since steam turbines operate in chocking conditions, the equations defining the mass flow and relative enthalpies of the HP and LP turbines are respectively 4.6 and 4.7:

$$\dot{m}_{THP} = K \frac{P_{SH}}{\sqrt{T_{SH}}}, \; H_{THP} = \dot{m}_{THP} h_{THP}; \tag{4.6}$$

$$\dot{m}_{TLP} = K \frac{P_{RH}}{\sqrt{T_{RH}}}, \; H_{TLP} = \dot{m}_{TLP} h_{TLP}. \tag{4.7}$$

where K $\left[\frac{kg \cdot K^{1/2}}{s \cdot bar A}\right]$ is defined according to a look-up table to simplify the regulation that, in a steam plant is performed by the turbine valves TVHP and TVLP. Hence, the mass flow regulation is simulated adjusting this value to reproduce the turbine behavior during the plant start-up.

Values of Isentropic efficiencies of the turbines η_{IsHP} and η_{IsLP} are considered respectively equal to 0.75 for THP and 0.72 for TLP. From the efficiency expression 4.8, the enthalpies h_{THP} and h_{TLP} are calculated:

$$\begin{aligned} h_{THP} &= h_{SH} - \eta_{IsHP}\left(h_{SH} - h_{THPIs}\right), \\ h_{TLP} &= h_{RH} - \eta_{IsRP}\left(h_{RH} - h_{TLPIs}\right); \end{aligned} \tag{4.8}$$

where h_{THPIs} and h_{TLPIs} are the specific enthalpies calculated considering an ideal isentropic expansion corresponding to an unitary efficiency ($\eta_{Is} = 1$). The specific enthalpies of the outlet turbine flows are used by the connected capacitive components to update their local temperature calculations.

4.2.5 Models of mixer-reheater and mixer-condenser blocks

The superheated steam downstream the BVHP and THP is mixed with the atomized cold water from the valve WVHP. The mixing of these flows has been implemented in a capacitive element by merging energy and mass conservation equations. The enthalpy of the mixed flow 4.9 is then obtained:

$$h_{MXHP} = \frac{\dot{m}_{THP}h_{THP} + \dot{m}_{BVHP}h_{SH} + \dot{m}_{WVHP}h_{FW}}{\dot{m}_{THP} + \dot{m}_{BVHP} + \dot{m}_{WVHP}}. \tag{4.9}$$

Pressure drops in the reheater stage are neglected ($v_{s,MXHP} = v_{s,RH}$, $P_{MXHP} = P_{RH}$). Consequently, the specific volume 4.10 and pressure 4.11 are calculated as follows:

$$v_{s,MXHP} = v_{s,RH} = -\int v_{s,RH}^2 \frac{\dot{m}_{THP} + \dot{m}_{BVHP} + \dot{m}_{WVHP} - \dot{m}_{TLP} - \dot{m}_{BVLP} - \rho_{RH}\dot{V}_{RH}}{V_{RH}} dt \tag{4.10}$$

$$P_{MXHP} = P_{RH} = \int \left(\rho_{RH}R\dot{T}_{RH} - \rho_{RH}^2 R T_{RH}\dot{v}_{s,RH}\right) dt \tag{4.11}$$

Once the pressure P_{MXHP} is known, it is possible to calculate the temperature T_{MXHP} of the mixed flow rate from tabulated steam properties [101] since both pressure and enthalpy conditions are known.

The same approach is also followed to model the mixer-condenser block: hot steam from BVLP and TLP is mixed with the atomized cold water from the valve WVLP. The mixing of these flow rates has been implemented in a capacitive element, so the

enthalpy h_{MXLP} can be calculated:

$$h_{MXLP} = \frac{\dot{m}_{TLP} h_{TLP} + \dot{m}_{BVLP} h_{RH} + \dot{m}_{WVLP} h_{FW}}{\dot{m}_{TLP} + \dot{m}_{BVLP} + \dot{m}_{WVLP}}. \tag{4.12}$$

Assuming that P_{CND} is imposed as a boundary condition, the temperature of the mixed flow T_{MXLP} is calculated from steam tabulated properties as a function of known pressure and enthalpy conditions.

4.3 Simulated benchmark plant and control scenarios

Turbine bypass systems are used to smoothly control the plant start-up which is modeled considering three phases: bypass start-up, turbine run-up, bypass shutdown.

During the bypass start-up, the boiler gradually starts to produce steam which is not used to feed turbines, since TBVHP and TBVLP are closed. All the steam flow passes in the bypass system. Flow rates, pressures, and temperatures are smoothly increased. Once the minimal pressure and temperature conditions are reached, a second phase, turbine run-up, begins: the turbine valves are gradually opened while an appreciable part of the flow rate is still passing in the bypass system. Once the turbine stages are correctly initialized the bypass system has to be gradually excluded. This phase is also called bypass shutdown: bypass and spray valves BVHP, BVLP, WVHP, and WVLP are gradually closed. Therefore, at the end of this phase, all the steam produced by the boiler is processed by the turbines.

During the plant start-up various control strategies can be followed [100]. The adopted control strategies mainly differ in the way is supposed to be controlled the boiler and, more generally, the plant with respect to the functionality of the turbine bypass system. In particular, the boiler can be mainly pressure or flow regulated. Typically on a real plant both the control strategies of the boiler are adopted because both the approaches have their own benefits and weak points: for instance, the sliding pressure control is preferable for plants operating with partial loads, since the inlet turbines valves are maintained fully opened in steady-state condition, improving the plant efficiency. Therefore, the pressure varies ("slides") depending on the actual load condition.

Thus, two different simulation scenarios are proposed, called Strategy "A" and "B", in which is assumed that the boiler is always pressure controlled (Strategy "A") or flow regulated (Strategy "B").

4.3.1 Strategy "A"

The boiler pressure ($P_{EV} = P_{SH}$) is controlled as visible in the simplified scheme of Figure 4.7. P_{EV} is determined by increasing and decreasing the heat flow provided to the boiler. The boiler controller is modelled as a proportional, integral, and derivative (PID) regulator. Bypass valves BVHP and BVLP control the steam flow rates through

the two stages of the plant. As a consequence, small changes of the heat provided to the boiler produces null or negligible changes in terms of steam flows, with respect to appreciable variations of the boiler pressure P_{EV}.

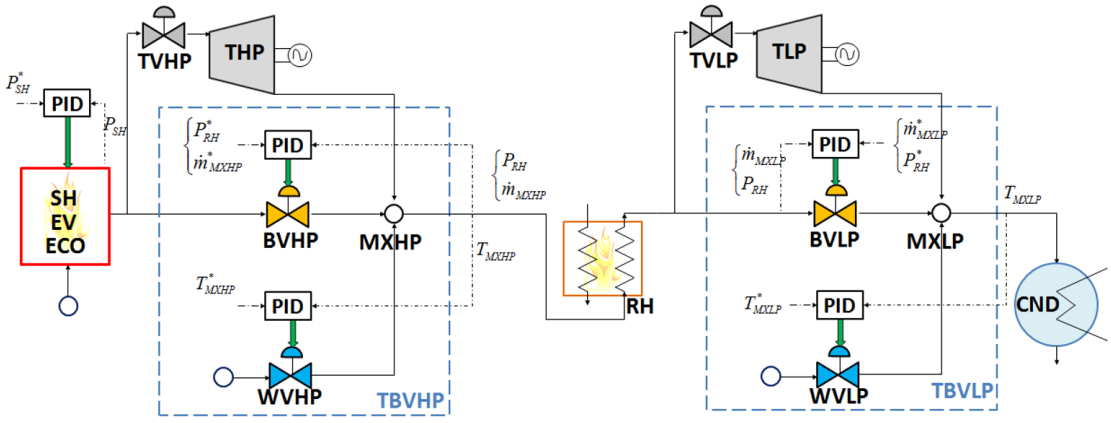

Figure 4.7: Simplified scheme of Strategy "A" control.

In particular, different control strategies are supposed to be applied with respect to three phases of the plant initialization described above. During bypass start-up and turbine run-up phases, BVHP controls the reheater pressure P_{RH}, while the total steam flow $\dot{m}_{CND}$ which is discharged in the condenser is determined by BVLP. Both control loops are supposed to be controlled using simple PID regulators. $\dot{m}_{CND}$ differs from the corresponding steam flow produced by the boiler $\dot{m}_{SH}$ only for the contribution of the water injected by the two spray waters WVHP and WVLP. WVHP and WVLP regulate respectively T_{MXHP} and T_{MXLP} to protect the reheater and the condenser from excessive thermal loads and gradients. In this way, it is possible to smoothly start the plant while the turbines are still excluded (bypass start-up) and in the following turbine run-up where TVHP and TVLP are opened.

During the bypass shut-down, the controllers smoothly transfer their functions, adopting a bumpless switching strategy [105, 106]: BVHP regulates the mass flow rate $\dot{m}_{MXHP}$ through the whole high-pressure stage and, consequently, through the reheater; BVLP regulates the pressure in the reheater P_{RH}. In addition, during the bypass shut-down, both the water spray valves WVHP and WVLP continue to regulate respectively temperatures T_{MXHP} and T_{MXLP}.

4.3.2 Strategy "B"

In this second case, as shown in the scheme of Figure 4.8, bypass valves BVHP and BVLP are used to control the pressure levels of both boiler P_{SH} and reheater P_{RH}. As a consequence, a variation of the heat provided by the boiler produces a null or negligible variation in the boiler pressure P_{EV} with respect to the corresponding variation of the produced steam flow $\dot{m}_{SH}$. For this reason, the boiler is modeled as a flow controlled system in which a simplified PID regulator adjusts the heat flux provided by the burner to roughly control $\dot{m}_{SH}$. The Outlet mean temperatures of the HP and LP stages T_{MXHP} and T_{MXLP} are regulated with the same approach described for the Strategy "A": spray valves WVHP and WVLP regulate respectively T_{MXHP} and T_{MXLP} by injecting a variable amount of cold water in the steam flow. As in the previous case, all the loop controllers are implemented as simple PID.

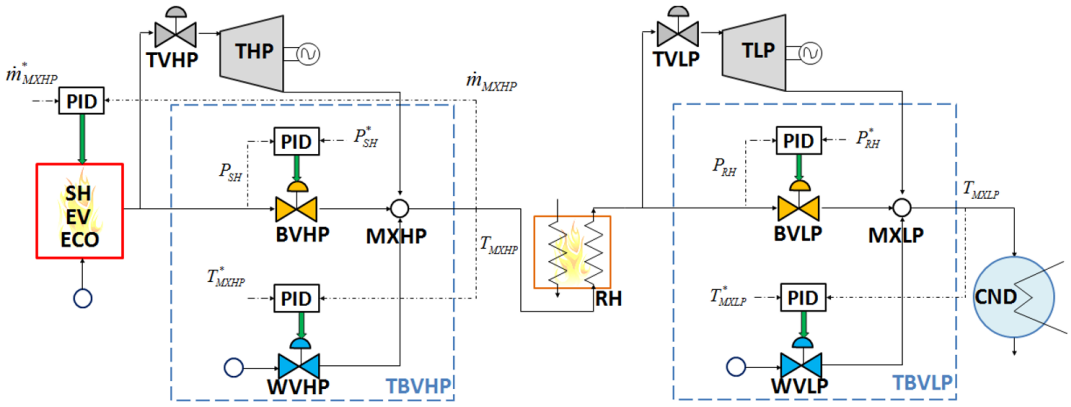

Figure 4.8: Simplified scheme of Strategy "B" control.

4.3.3 Benchmark plant: Reference data and performances

The research doesn't aim at a strict comparison of the performances of the two control strategies. Both controllers are implemented to verify the generality and the robustness of the proposed plant model with respect to the simulation of different control strategies and plant operating conditions. Both the proposed control strategies are applied to the same benchmark plant described in Figure 4.3, whose main features available in bibliography are described in Table 4.1.

The same bibliographic reference [100] gives also some results, shown in Table 4.2, concerning the start-up of the plant whose boiler is supposed to be pressure controlled

Table 4.1: Main features of the simulated plant [100].

Data	Value	Units of measure
Plant type	Oil-fired generating unit	-
Power	4×500	MW
Nominal steam flow	$1,343,664$	kg/h
Nominal throttle pressure	16.8	MPa
Nominal superheater temperature	538	$°C$
Nominal reheater temperature	538	$°C$

(Strategy "A"). These values are referred to a time history which is defined with respect to initial conditions in which $P_{EV} = 68\ bar$.

Table 4.2: Behaviour in the transient phases of the reference plant.

	Time (s)	0	200	1,000	3,000	3,300	3,600
	Unit	Variable	Bypass Start-up			Turbine Run-up	Bypass Shut-down
HP level							
	$[kg/s]$	$\dot{m}_{MXHP}$	0	30	35	60	125	125
	$[kg/s]$	$\dot{m}_{TBVHP}$	0	30	35	60	60	0
	$[kg/s]$	$\dot{m}_{THP}$	0	0	0	0	65	125
LP level							
	$[kg/s]$	$\dot{m}_{MXLP}$	0	35	43	75	130	125
	$[kg/s]$	$\dot{m}_{TBVLP}$	0	35	43	75	75	0
	$[kg/s]$	$\dot{m}_{TLP}$	0	0	0	0	60	125
HP level							
	$[bar]$	P_{SH}	68	68	85	117	117	123
	$°C$	T_{SH}	571	571	572	573	572	572
	$°C$	T_{MXHP}	300	300	300	300	300	300
LP level							
	$[bar]$	P_{RH}	3.7	4	5.3	5.3	11.75	
	$°C$	T_{RH}	440	455	500	538	538	538
	$[bar]$	P_{CND}	0.285	0.285	0.285	0.285	0.285	0.285
	$°C$	T_{MXLP}	210	210	210	210	210	210

4.4 RT implementation

The complete model of the plant described in the previous sections has been implemented in Real Time. For this reason, it was chosen for the RT Implementation a commercial digital signal processing (DSP) board TI C2000-F28335 [107] (Figure 4.9) whose main features are described in Table 4.3.

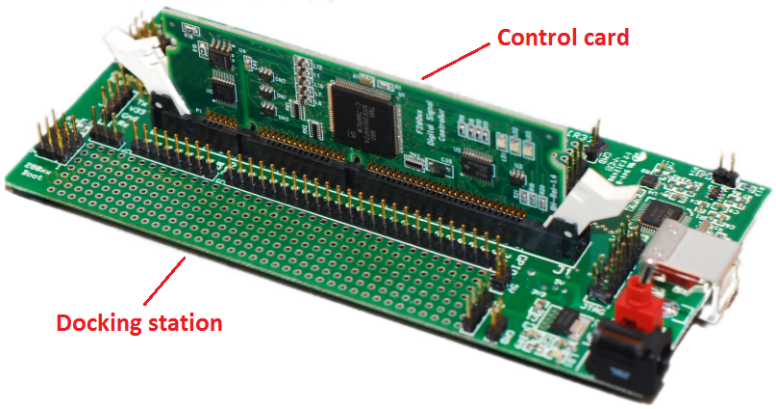

Figure 4.9: DSP board TI C2000-F28335.

The chosen DSP board is supported by Matlab Real Time Workshop™ [79] and, consequently, the Simulink code can be easily compiled and download for RT execution on the board. Also, the cost of the proposed board is very low with respect to a possible industrial application and it has been successfully used for the development of model based controllers of plants [108]. Finally, the chosen board provides a wide range of analog and digital I/O to be easily integrated in mechatronic complex systems including sensors, actuators, and a communication bus (CAN and Serial communication modules).

The docking station (Figure 1.5-13) supplies the control card that contains the microcontroller and performs the communication with an external PC via USB connection which allows to program the microcontroller and manage the data transfer. Also, makes it possible to manage its inputs and outputs. In particular, the serial communication between the code uploaded on the board and the PC host is realized through two separate channels: a first channel is used for reading the data from the microcontroller through a suitable HMI present on the host PC; a second channel was instead created specifically for writing operations, by connecting the appropriate microcontroller pin to (TTL-232R-PCB) TTL to USB Serial Converter PCB, again

Table 4.3: Main features the Texas Instrument Delfino C2000-F28335 DSP board [107].

Data	Value	Units
Model	TMS320F28335	-
Processor	150	MHz
I/O voltage	3.3	V
DMA controller	Six channels	-
On-chip memory	$256K \times 16$ Flash	-
PWM outputs	18	-
CAN modules	2	-
SCI modules	3	-
A/D 12-bit channels	16	-
GPIO pins	88 -	
Cost (estimated)	70 (single piece), 20 (mass production)	€

through this graphical user interface on the host PC, the required parameters the proper execution of the tests.

The RT implementation of Simulink models depends on the particular features of the chosen hardware and, consequently, of the corresponding target for which Mathworks Real Time Workshop^{TM} compiles the model, producing a program which is optimized for a specific environment.

According to target specifications, the integration of continuous states in differential equations using Matlab-Simulink integrators is not supported. To avoid potential portability and stability troubles related to specific features of the target, the discrete integration of all the differential equations of the model has been implemented.

Moreover, a multitasking implementation has been adopted: integrated equations are solved by different tasks running with different integration steps. For the discretization of integrated states the bi-linear Tustin method is adopted [109]. A non-secondary advantage granted by the adopted multitasking approach consists in an high numerical efficiency of the generated code: heavy calculations, corresponding to systems with a slow dynamic behavior (e.g. the boiler) are implemented considering a slow integration frequency ($10\ Hz$), reserving higher frequencies ($400\ Hz$) to the simulation of fast transients and dynamics as the ones associated to the closed loop controllers of valves and to safety and communication tasks of the system. The structure of the Simulink model is organized in different subsystems whose topology resembles the structure of the simulated plant as visible in Figure 4.10.

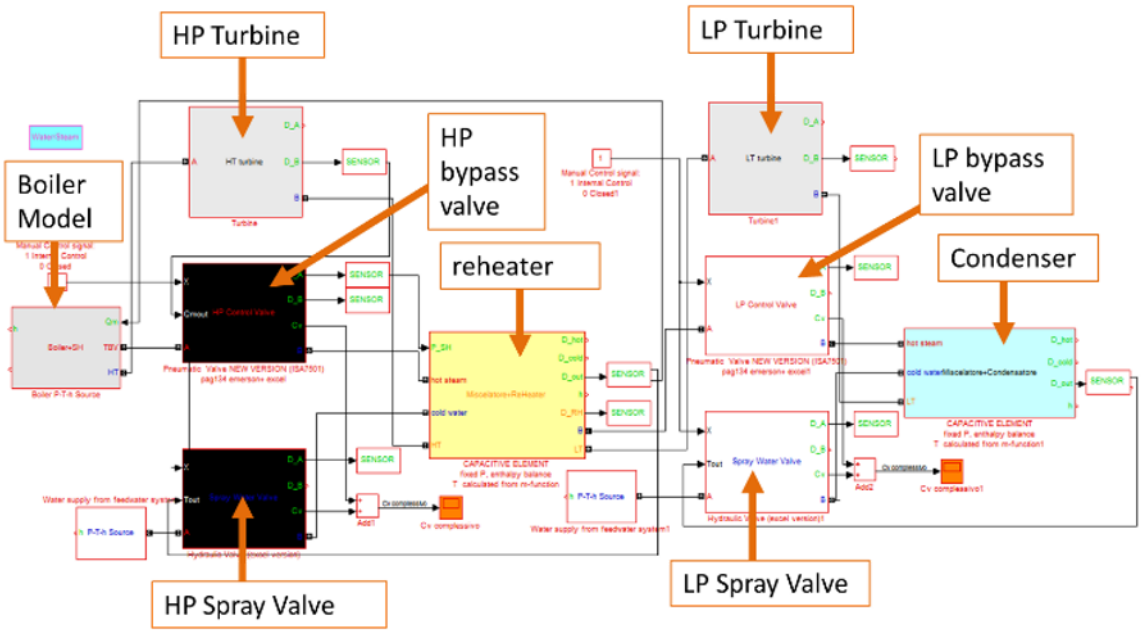

Figure 4.10: Implemented Matlab-Simulink model.

4.5 Preliminary validation of the RT model

To verify stability and reliability of the RT plant model, the results shown in Table 4.2 are compared with the corresponding ones obtained repeating the same simulations with both the control strategies "A" and "B". It should be noticed that the control strategy "A" is the same adopted in the reference test case [100]. The gains of the "A" control system have been tuned to fit the performances of the reference test case taken from literature: in this way it is possible to verify that the proposed model is able to reproduce in Real Time the same behavior exhibited in [100]. The same procedure is repeated considering the control strategy "B" to verify that the model can be easily customized to implement control strategies which are quite different with respect to the proposed one. The gains tuned for PID controllers with strategies "A" and "B" are described in Tables 4.4 and 4.5.

Table 4.4: Gains of the PID controllers for Strategy "A".

			Operating phases			
			Bypass start-up	Turbine run-up	Bypass shut-down	
	PID	Gain	Value	Unit of measure	Unit of measure	Unit of measure
HP level	Bypass valve	k_P	0.5	$1/barA$	$1/barA$	s/kg
		k_I	0.025	$1/sbarA$	$1/sbarA$	$1/kg$
		k_D	0	$s/barA$	$s/barA$	s^2/kg
	Spray valve	k_P	0.01	$1/°C$	$1/°C$	$1/°C$
		k_I	0.001	$1/s°C$	$1/s°C$	$1/s°C$
		k_D	0	$s/°C$	$s/°C$	$s/°C$
LP level	Bypass valve	k_P	0.25	s/kg	s/kg	$1/barA$
		k_I	0.2	$1/kg$	$1/kg$	$1/sbarA$
		k_D	0	s^2/kg	s^2/kg	$s/barA$
	Spray valve	k_P	0.001	$1/°C$	$1/°C$	$1/°C$
		k_I	0.001	$1/s°C$	$1/s°C$	$1/s°C$
		k_D	0	$s/°C$	$s/°C$	$s/°C$

In Figures 4.11, 4.12 and 4.13 are presented the pressure, temperature and mass flow rate profiles, simulated considering both "A" and "B" strategies compared with reference results [100]. Moreover, the maximum relative errors between simulated temperature, pressure, and flow values with respect to the reference of literature are shown in Table 4.6.

Higher errors in terms or regulated temperature are recorded for both control strategies at the beginning of the bypass start-up phase and at the end of the bypass shut-down phase. In the end of the bypass shut-down phases the flow processed by the

Table 4.5: Gains of the PID controllers for Strategy "B".

			Operating phases			
			Bypass start-up	Turbine run-up	Bypass shut-down	
	PID	Gain	Value	Unit of measure	Unit of measure	Unit of measure
HP level	Bypass valve	k_P	0.5	$1/barA$	$1/barA$	$1/barA$
		k_I	0.025	$1/sbarA$	$1/sbarA$	$1/sbarA$
		k_D	0	$s/barA$	$s/barA$	$s/barA$
	Spray valve	k_P	0.01	$1/°C$	$1/°C$	$1/°C$
		k_I	0.001	$1/s°C$	$1/s°C$	$1/s°C$
		k_D	0	$s/°C$	$s/°C$	$s/°C$
LP level	Bypass valve	k_P	0.25	$1/barA$	$1/barA$	$1/barA$
		k_I	0.2	$1/sbarA$	$1/sbarA$	$1/sbarA$
		k_D	0	$s/barA$	$s/barA$	$s/barA$
	Spray valve	k_P	0.001	$1/°C$	$1/°C$	$1/°C$
		k_I	0.001	$1/s°C$	$1/s°C$	$1/s°C$
		k_D	0	$s/°C$	$s/°C$	$s/°C$

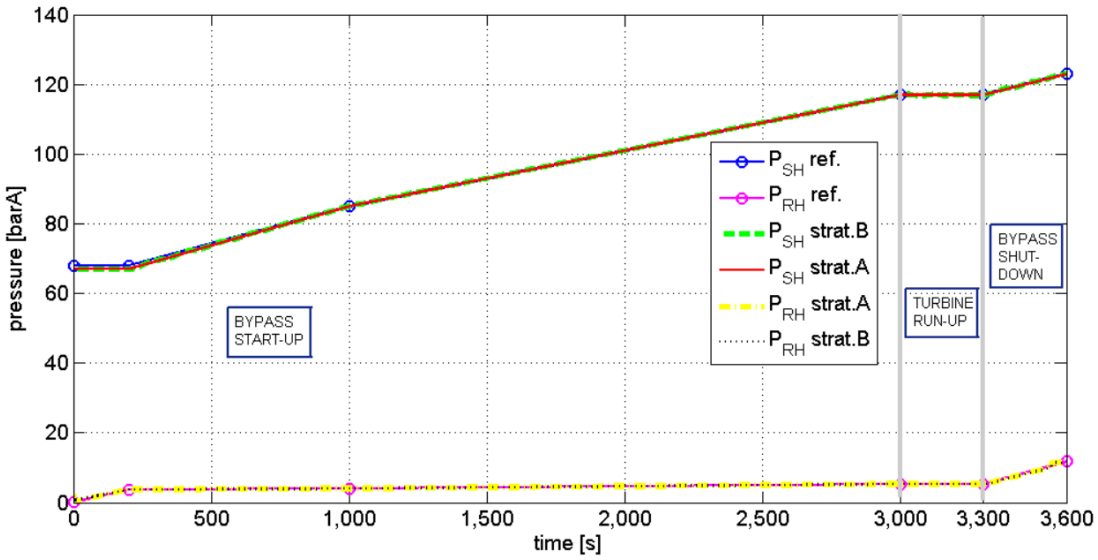

Figure 4.11: Pressure behavior for superheater and reheater stages: comparison between reference values and controlled ones for Strategies "A" and "B".

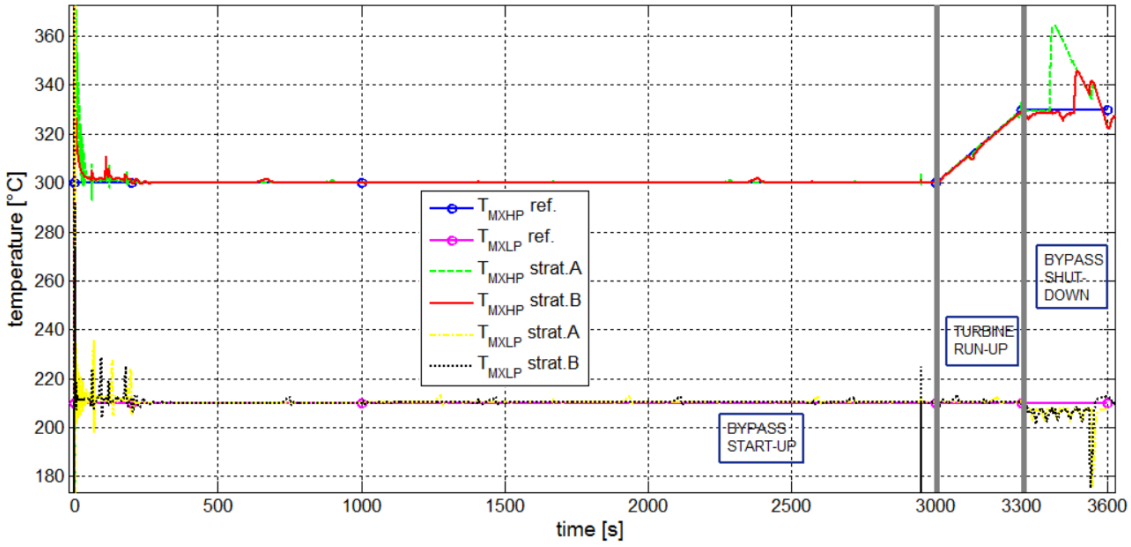

Figure 4.12: Temperature of the outlet mixed flow rate after the bypass turbine stages: comparison between reference values and controlled ones for Strategies "A" and "B".

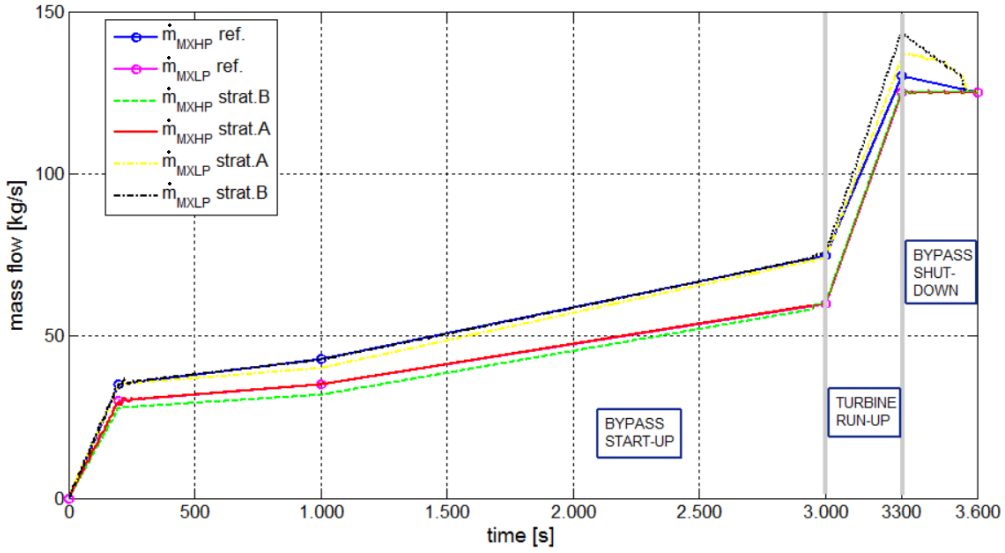

Figure 4.13: Mass flow rate of the outlet mixed flow rate after the bypass turbine stages: comparison between reference values and controlled ones for Strategies "A" and "B".

bypass system is quite small since the bypass is gradually excluded. In future studies, it should be considered the implementation of a more complex control strategy also affecting the way in which the turbines are regulated during this phase. Also, in the beginning of the bypass start-up phase the flow processed by the bypass system is quite small with respect to the nominal one.

It can be noticed that differences between obtained simulation results with the same control strategy proposed in [100] are quite small. Therefore, the model should be considered validated with respect to the reference literature case study. Moreover, also Strategy "B" is validated with respect to both Strategy 'A" and the reference case study.

Table 4.6: Behavior of the relative error between simulated values and reference ones [100].

	Bypass Start-up	Turbine Run-up	Bypass Shut-down
$\dot{m}_{MXHP}$ (strat. "A")	$< 4\%$	$< 0.1\%$	$< 0.1\%$
$\dot{m}_{MXHP}$ (strat. "B")	$< 0.1\%$	$< 0.1\%$	$< 0.2\%$
$\dot{m}_{MXLP}$ (strat. "A")	$< 0.5\%$	$< 3.5\%$	$< 6.5\%$
$\dot{m}_{MXLP}$ (strat. "B")	$< 0.7\%$	$< 6.5\%$	$< 8.5\%$
P_{SH} (strat. "A")	$< 0.1\%$	$< 0.1\%$	$< 0.1\%$
P_{SH} (strat. "B")	$< 0.1\%$	$< 0.1\%$	$< 0.1\%$
P_{SH} (strat. "A")	$< 0.1\%$	$< 0.1\%$	$< 4\%$
P_{SH} (strat. "B")	$< 0.1\%$	$< 0.1\%$	$< 4\%$
T_{MXHP} (strat. "A")	$< 0.4\%$	$< 0.2\%$	$< 2\%$
T_{MXHP} (strat. "B")	$< 0.2\%$	$< 0.3\%$	$< 0.9\%$
T_{MXLP} (strat. "A")	$< 0.2\%$	$< 0.2\%$	$< 3\%$
T_{MXLP} (strat. "B")	$< 0.2\%$	$< 0.4\%$	$< 3\%$

4.6 Architecture of the test rig

Aim of the rig is to test the dynamical response of the positioners and the corresponding actuators of both DTP and spray water valves reproducing their interaction in Real Time with the simulated plant and control systems. In addition, the simulated plan control system can be calibrated and improved on the rig considering the real response of the tested components.

The positioners and their corresponding actuators, visible in Figures 4.14 and 4.15, are the real components that have to be materially tested on the rig. The layout of the HIL test rig is shown in Figure 4.16 and it should be considered as a peculiar case with respect to the more general scheme of Figure 2. In particular, to verify the functionality of the rig, the testing of the HP stage positioners is performed. The simulated plant, interacting with the control valves, is supposed to be controlled according to the Strategy "B". As shown in Figure 4.16, at each computational step, the RT model of the plant calculates the reference commands for both HP spray water and DTP bypass valves; the reference commands are transmitted as analogic current signals ($4-20\ mA$) to the tested valve positioners shown in Figure 4.14.

Figure 4.14: Young Tech series 3400-3450 smart positioner; an example of 4/3 3/3 pneumatic position controller typically used to pilot pneumatic actuators.

The tested positioners are able to measure the position of the corresponding actuators that are interfaced with mechanical devices properly regulated to reproduce the preload and the mechanical impedance of the moved valves (equivalent preload stiffness and damping). The position feedbacks are acquired as current signals ($4-20\ mA$) by the DSP board on which is running the plant model. Consequently, a new simulation step is calculated considering the measured positions of the tested valves and their corresponding effects on the simulated plant.

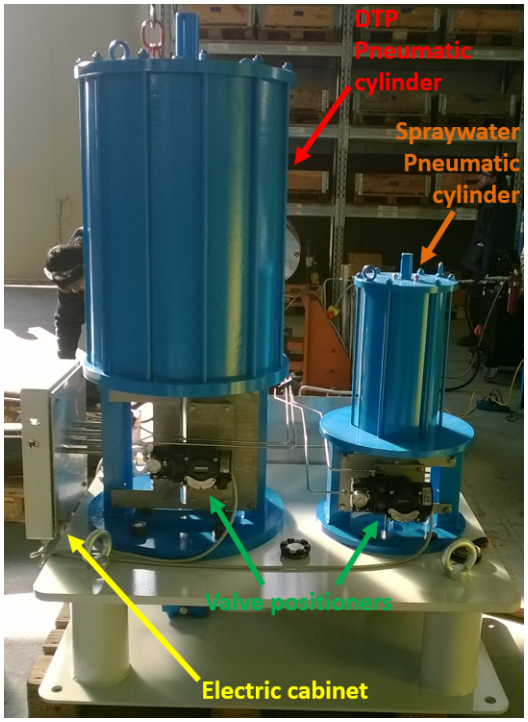

Figure 4.15: Tested actuators and positioners of TBV control systems during preliminary testing activities of the rig.

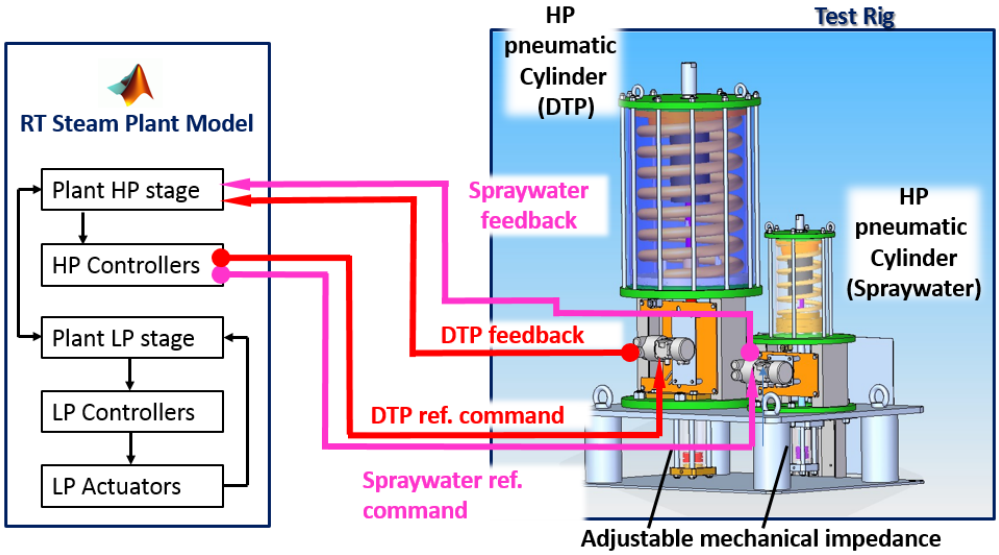

Figure 4.16: Architecture of the test rig for TBV control systems applied to the testing of positioners and actuators of the HP stages of the simulated plant (Strategy "B").

With respect to the general scheme of Figure 4.3, the RT model of the plant implemented in the scheme of Figure 14 has to be slightly customized: the simulation blocks corresponding to tested actuators have to be removed. Moreover, the RT application has to manage the communication with the tested systems in term of outputs (the reference commands of the HP valves) and inputs (valve position feedback signals).

An external PC communicates with the DSP board using dedicated USB connections. The external PC is used to provide the rig of an HMI (in Figure 4.17). The interface was designed in Matlab and then compiled to generate a standalone application (.exe) that can run on a generic calculator, on different operating systems and without the Matlab software. The executable has been obtained through *MCR Installer* (Matlab Compiler Runtime), which is available (free) on the net. In this way, it is ensured a better portability of both the code and the system that has been simulated through this software. The interface is designed to accomplish the following specifications:

- Management of the host-to-DSP communication settings;
- Management of the control gains: a panel allows to change the gains of the control system during the execution of the test;
- On-line visualization of both the physical and simulated variables;
- Storage of test data.

The main advantage of the rig shown in Figure 4.15 is the possibility to virtually verify performances of valve control and actuation systems and their mutual interactions with the rest of the plant. Benefits in terms of costs, time to market, and reliability of the tested product are quite evident and largely justify research investments. It can be noticed that the proposed system is modular, so it is possible to build a more complex layout in which the LP actuators can be connected and tested with the corresponding LP stage model, and therefore, in which the whole plant model is considered. In addition, different control strategies can be tested on the rig.

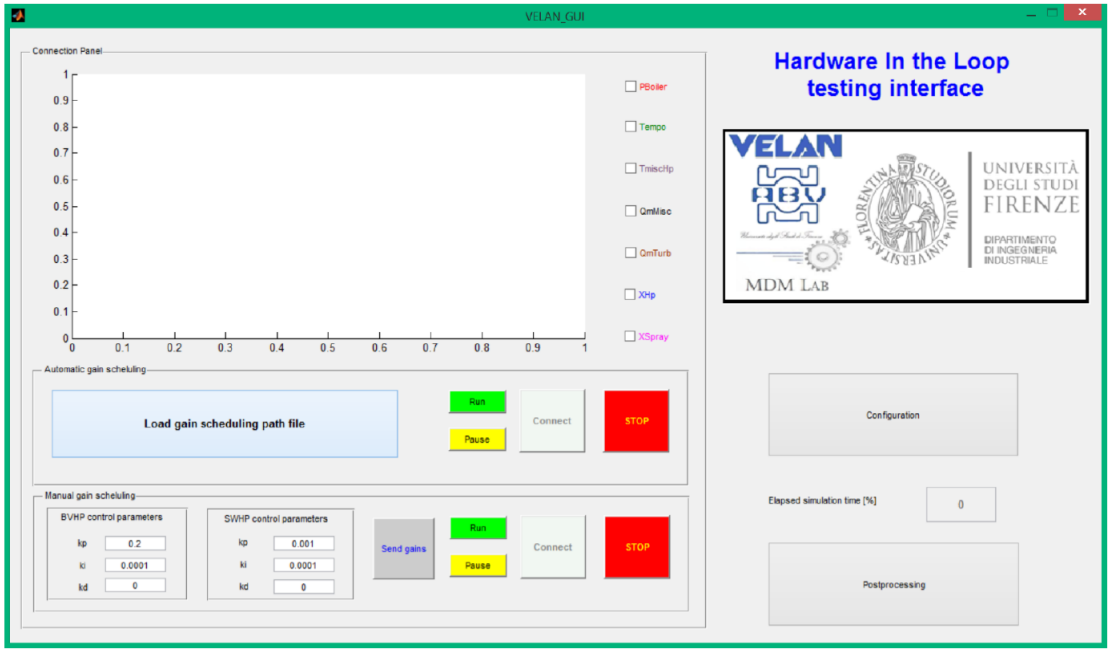

Figure 4.17: Graphical User Interface for the HIL testing of TBV controllers.

4.7 Experimental results

The experimental activities have been organized in two phases. First, tested positioners and actuators are calibrated and identified. Then, in a second phase, HIL tests are performed and also the simulated plant controllers are calibrated with respect to the performances of the chosen actuators. In this way, it is possible to verify the potential uses of the proposed approach to mutually tune actuators, positioners, and plant controllers in a controlled environment with a clear advantage in terms of costs, safety, and performances.

Compared to the actuator model simulated via software, in real systems several unmodeled phenomena are usually present which can negatively affect the performance and sometimes the stability of the whole system. In such cases, the system under test should be carefully identified to eventually modify the control law with respect to the one adopted in the completely virtual model.

For this reason, one of the possible functionalities of the realized test rig consists in the open-loop evaluation and identification of generic unknown actuators.

In this peculiar application, the transfer functions of the pneumatic cylinders have been identified through open-loop tests. Therefore, the steam plant transfer functions have been linearized to improve the control system performances for the further HIL testing activities.

4.7.1 Identification of valve positioners and actuators

The response of valve and positioners and actuators is the result of a complex interaction between the valve position loop, performed in the positioner, and the behavior of the corresponding pneumatic actuator, which is highly nonlinear. In particular, the orifices which provide air to the pneumatic cylinders have to be tuned to obtain the same rise time both during the opening (filling of the pneumatic cylinder) and the closing (cylinder is discharging) times. Opening and closing times are set according to those values suggested in literature [100]. In Figure 4.18, a simplified scheme of pneumatic plant and tuning orifices is shown.

In this preliminary phase, the internal gains of the positioner loop have to be calibrated as well: the resulting PI controller is tuned with high proportional gain and a tiny integral part to compensate static errors due to friction and fluid losses. This is a

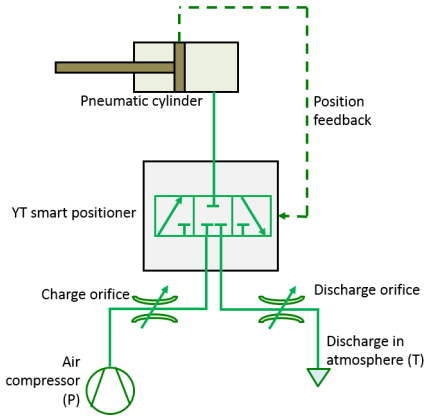

Figure 4.18: Simplified scheme of the pneumatic plant for a single cylinder.

quite common calibration considering that the response of a fluid actuator with respect to the flow provided by the positioner can be approximated using a system with a pole in zero: position of the actuator is proportional to the exerted force since the cylinder is coupled and preloaded with a spring; force is proportional to the actuator pressure which depends from the integral of the inlet mass flow.

The transfer function between reference command given to the positioner and corresponding position of the actuator is then identified by sending a position reference signal, defined as a square wave function whose features are described in Table 4.7.

Table 4.7: Features of the square wave signal.

Low level opening (%)	0
High level opening (%)	100
Time period [s]	50

Identification is performed using a best-fit procedure, which tunes the coefficients of the identified transfer function to minimize the mean square error between experimental and predicted output. As shown in Table 4.8, both the identified closed-loop transfer functions are second-order systems which are quite different from the first-order ones originally expected and used for the simulation described in the section 4.5.

As shown in Figure 4.19, the fitting between the responses of the DTP and spraywater valves (measured data) and the identified transfer functions is quite good.

Table 4.8: Identified closed-loop transfer functions of the positioner with their corresponding actuators.

Input	Output	Identified TF	Nominal TF
Position reference for the positioner of the DTP valve of the HP Stage	Position of the DTP valve of the HP stage	$TF_{BV} = = \frac{0.1587}{s^2+0.6319s+0.1634}$	$TF_{BVnom} = = \frac{1}{3.3s+1}$
Position reference for the positioner of the spray water valve of the HP stage	Position of the spray water valve of the HP stage	$TF_{SW} = = \frac{0.2793}{s^2+0.8571+0.2801}$	$TF_{SWnom} = \frac{1}{3.3s+1}$

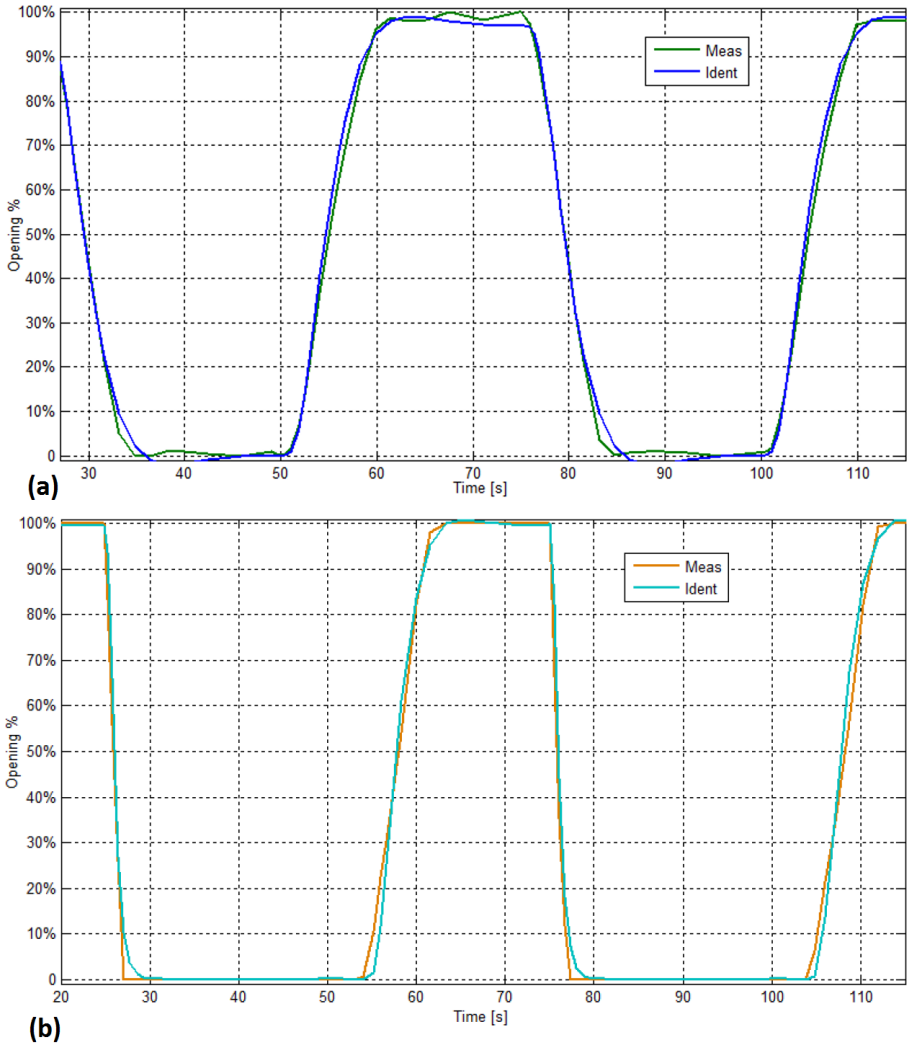

Figure 4.19: Comparison between physical and identified systems responses for the DTP (a) and spraywater (b) pneumatic cylinders.

4.7.2 Tuning of the plant controller

The identified transfer functions TF_{BV} and TF_{SW} (in Table 4.8) are quite different with respect to their expected behavior. Consequently, the HIL tests performed with controllers having the nominal gains described in Table 4.5 produced poor results: the simulated control system was prone to instability troubles and more generally performances were not satisfactory. To better understand and explain the stability margins of the system, a linearization of the plant model was performed with respect to the operating conditions which proved to be more critical for the stability of the system. In particular, the system is linearized with respect to an operating point described in Table 4.9, which corresponds to an intermediate phase of the Bypass Start-up of the turbine bypass system.

Table 4.9: Operating point chosen for the linearization.

Simulation time	P_{SH}	T_{MXHP}	P_{RH}	T_{MXLP}	$\dot{m}_{MXHP}$
$1100\ s$	$86.6\ barA$	$300\ °C$	$4.065\ barA$	$210\ °C$	$36.7\ kg/s$

Since the RT model of the plant was implemented in Simulink the numerical linearization of the system was performed using the tools available in the same Matlab environment (Matlab Identification Toolbox™). In particular, maintaining all the other input constants, a step perturbation on the plant on a desired input is introduced (for instance, the reference command of a DTP positioner). The corresponding outputs are used to perform a numerical identification using the same procedure adopted in section "Calibration and identification of valve positioners and actuators" to identify the transfer function of positioners and actuators. Considering the current configuration of the HIL test rig shown in Figure 4.16, the plant was linearized as a multiple-input-multiple-output (MIMO) system with two inputs and two outputs. The inputs are the reference commands of the positioners of both DTP and spray water valves of the HP stage. Outputs are the regulated super-heater pressure P_{SH} and the determined temperature T_{MXHP}.

Therefore, considering the cross coupling effects, there are four identified transfer functions:

- F_{PP}: describes the dynamic effects on P_{SH} produced by the DTP valve opening;
- F_{PT}: describes the dynamic effects on T_{MXHP} produced by the DTP valve

opening;

- F_{TP}: describes the dynamic effects on P_{SH} produced by the spray water valve opening;
- F_{TT}: describes the dynamic effects on T_{MXHP} produced by the spray water valve opening.

The cross term F_{TP} is null/negligible since the pressure drop across the DTP valve of the HP stage is very high and the valve is chocked working in sonic conditions. As a consequence, the action of the other spray water valve cannot significantly affect the value of the pressure P_{SH}. The other cross-term F_{PT} is not null but is not completely negligible, since the lamination process of the DTP valve produces a variation of the fluid temperature as well. However, from a quantitative point of view, the two pressure and temperature control loops are highly decoupled and the response of the bypass systems are dominated by the diagonal, direct terms F_{PP} and F_{TT} which can be approximated by the first-order linearized transfer functions 4.13 and 4.14:

$$F_{PP} = \frac{153.25}{303.6s + 1}; \tag{4.13}$$

$$F_{TT} = \frac{571.7}{0.157s + 1}. \tag{4.14}$$

In Figures 4.20 and 4.21, the step response of the full nonlinear system is compared with the corresponding approximating linearized function: linearized transfer functions 4.13 and 4.14 seem to be a good approximation of the system behavior with respect to the chosen operating point. Since pressure and temperature control loops of the HP turbine stage are highly decoupled, they can be studied and optimized as two independent single-input-single-output (SISO) systems as represented in the block scheme of Figure 4.22. According to the block scheme represented in Figure 4.22, the open-loop transfer functions L_{PP} and L_{TT} are defined as follows:

$$\begin{aligned} L_{PP} &= PID_{BVHP} TF_{BV} F_{PP}, \\ L_{TT} &= PID_{SWHP} TF_{SW} F_{TT}. \end{aligned} \tag{4.15}$$

Considering the scheme of Figure 4.22, in Figures 4.23 (a) and (b), the bode diagrams of the two open L_{PP} and L_{TT} linearized transfer functions with different gains applied to the PID_{BVHP} and PID_{SWHP} are shown. In particular, two different calibration sets are considered: the nominal one corresponding to the gain values of Table 4.5 and a

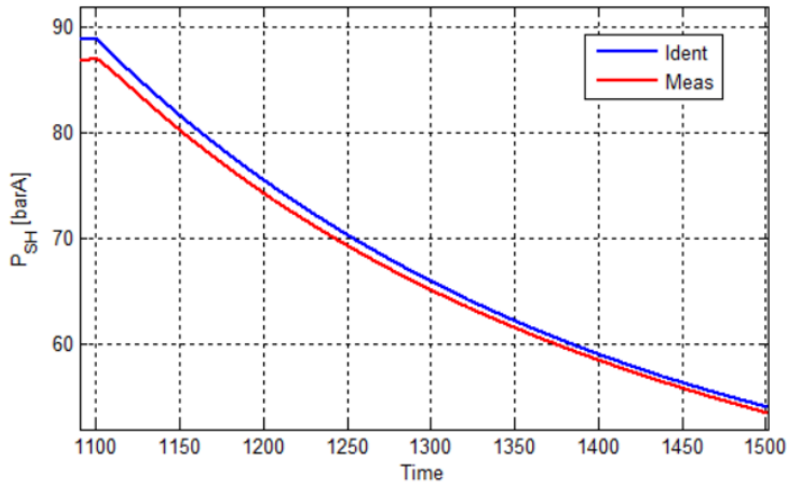

Figure 4.20: Comparison between physical and identified systems responses for the DTP pneumatic cylinder.

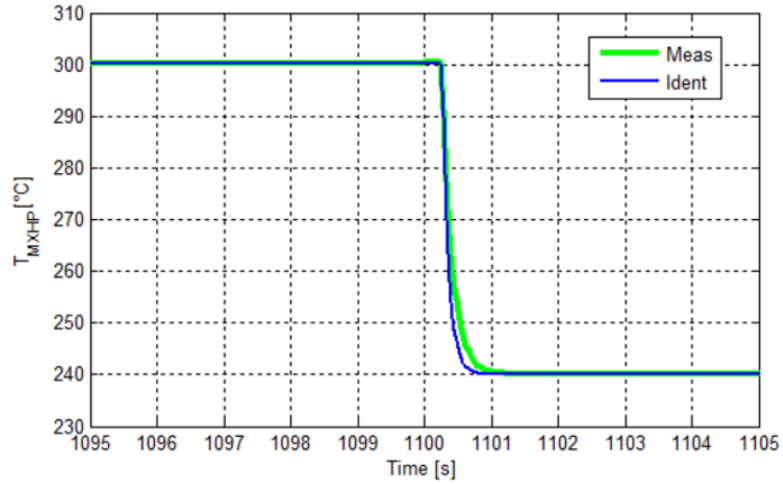

Figure 4.21: Comparison between physical and identified systems responses for the spray-water pneumatic cylinder.

Table 4.10: New calibration set of the PID gains for the HP pressure level of Strategy "B".

			Operating phases			
			Bypass start-up	Turbine run-up	Bypass shut-down	
	PID	Gain	Value	Unit of measure	Unit of measure	Unit of measure
HP level	Bypass valve	k_P	0.2	$1/barA$	$1/barA$	$1/barA$
		k_I	0.0001	$1/sbarA$	$1/sbarA$	$1/sbarA$
		k_D	0	$s/barA$	$s/barA$	$s/barA$
	Spray valve	k_P	0.0005	$1/°C$	$1/°C$	$1/°C$
		k_I	0.00005	$1/s°C$	$1/s°C$	$1/s°C$
		k_D	0	$s/°C$	$s/°C$	$s/°C$

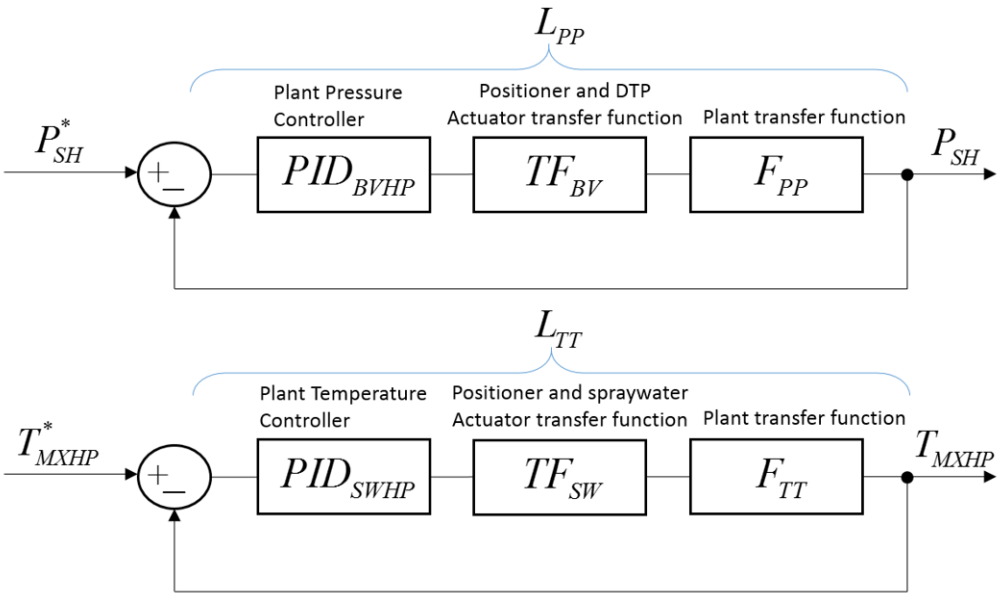

Figure 4.22: Pressure and temperature control loops of the HP stage.

new ones visible in Table 4.10. The new calibration values shown in Table 4.10 are obtained by adopting the flexible simplex technique [71, 72, 73] described in section 3.3.3. To this aim, the vectors of the PID control gains PID_{BVHP} of and PID_{SWHP} which minimize a given non-linear function (depending respectively from the pressure error and temperature error) are obtained. In particular, the cost functions to be minimized are the Integral Absolute Errors of pressure IAE_{BVHP} and temperature IAE_{SWHP} indicated in Equations 4.16 and 4.17. These parameters are computed through the simulation of the steam plant model during the tracking of the reference pressure and temperature

$$IAE_{BVHP} = \int_0^{T_0} |P_{ref} - P_{SH}(t)|\, dt, \tag{4.16}$$

$$IAE_{SWHP} = \int_0^{T_0} |T_{ref} - T_{MXHP}(t)|\, dt, \tag{4.17}$$

where $T_0 = 3600$ s, P_{ref} is the set-point of the superheater pressure, P_{SH} indicates the superheater pressure, T_{ref} is the set-point of the HP mixer temperature and T_{MXHP} defines the HP mixer temperature. The starting values of the PID parameters from which the simplex algorithm begins to operate are the gains of the preliminary PID control system (see Table 4.5)

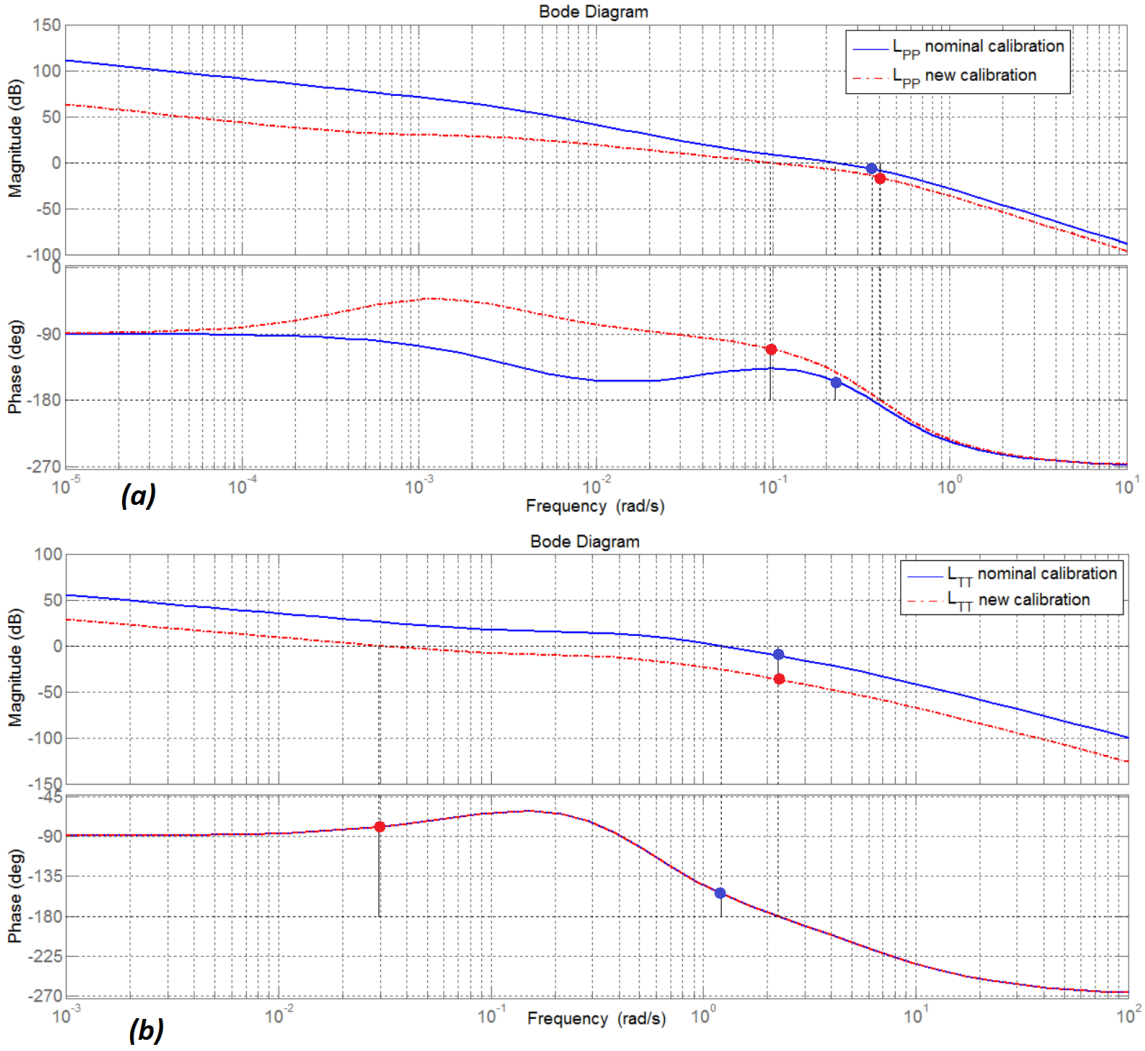

Figure 4.23: Bode diagram and stability margins of L_{PP} (a) and L_{TT} (b) transfer functions with the nominal gains and new PID gains.

It should be noticed that the new calibration values assure increased more robust stability margins for both the pressure loop L_{PP} and the temperature loop L_{TT}. The pressure and temperature loops stability margins are finally reported in Table 4.11.

Table 4.11: Gain and phase margins.

Transfer function	Gain margin	Phase margin
L_{PP} nom. calibration	$6.49\ dB$	$26.6°$
L_{PP} new calibration	$16.3\ dB$	$70.0°$
L_{TT} nom. calibration	$10.7\ dB$	$25.7°$
L_{TT} new calibration	$36.7\ dB$	$101.0°$

4.7.3 HIL testing results

In this section are finally exhibited the results relative to the test rig situated in Capannori (Lu, Italy). The test covers a plant start-up of 3600 s, while on the DSP are uploaded both the complete steam plant model and the control system expressed in Table 4.10).

The position references for the DTP and spray water valves positioners are respectively depicted in Figure 4.24 and 4.25. In both cases, the oscillations (whose amplitude is less than $< 3\%$ and the frequency is inferior than $0.1\ Hz$) are very limited. Moreover, the boiler pressure, the HP mixer temperature and mass flow rate behaviors are respectively illustrated in Figure 4.26, 4.27 and 4.28, with respect to their own reference signals. In Table 4.12, the mean relative errors are finally expressed between reference signals and outputs for the main plant variables, both for the simulated model and the HIL test shown in this sections. HIL test show greater errors, due to the relevant complexity of the testing apparatus, unmodeled dynamics of pneumatic plant or electrical noise in the electronic logics. Anyway, these errors can still be considered very limited with respect to the industrial requirements.

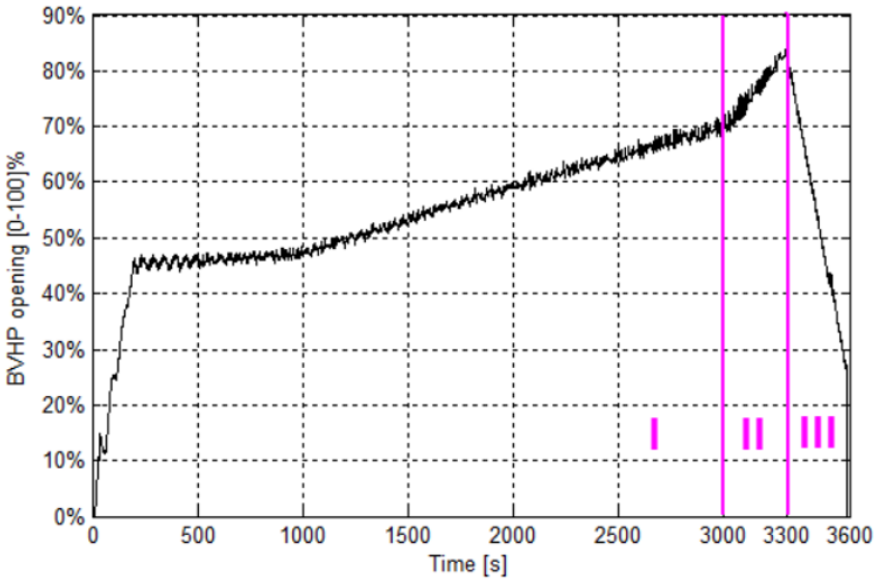

Figure 4.24: Reference of the DTP valve positioner during Bypass Start-up (I), Turbine Run-up (II), and Bypass Shut-down (III) phases.

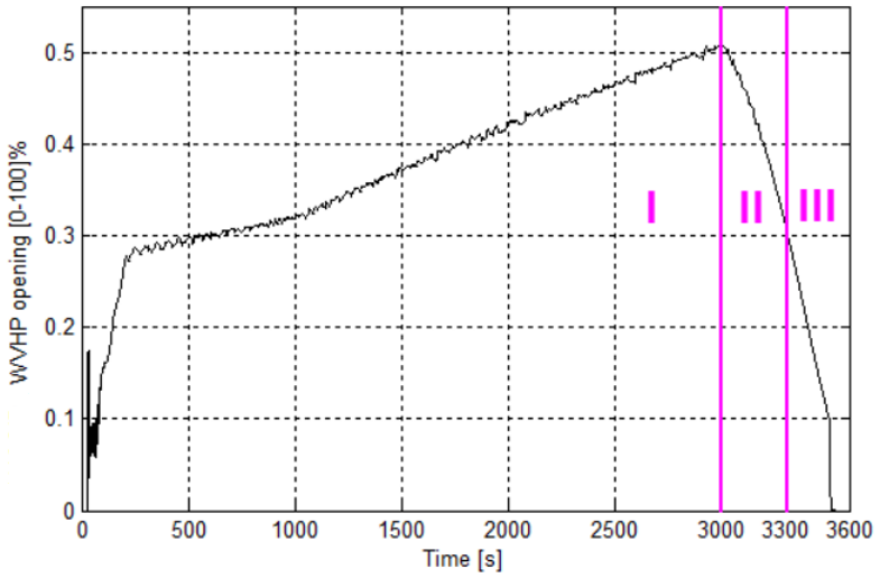

Figure 4.25: Reference of the spray water valve positioner during Bypass Start-up (I), Turbine Run-up (II), and Bypass Shut-down (III) phases.

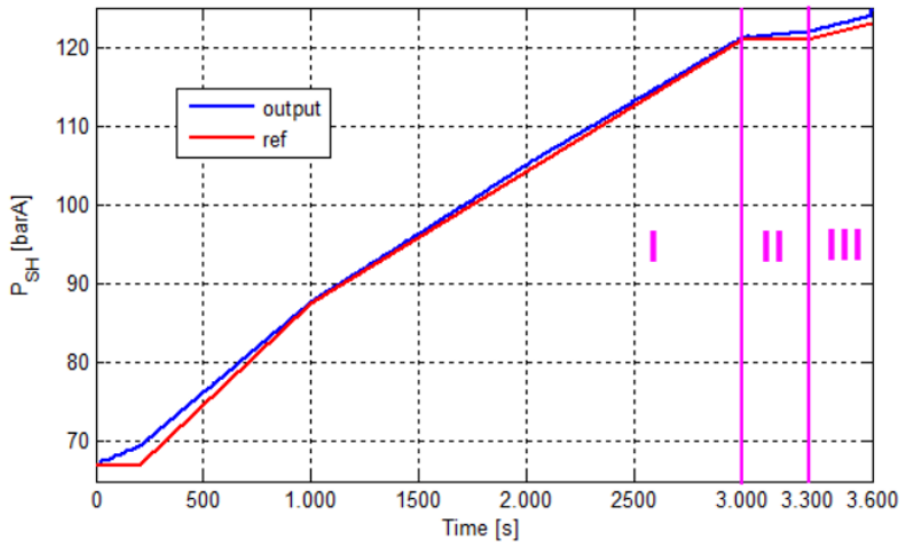

Figure 4.26: P_{SH} behavior comparison between reference value and controlled output.

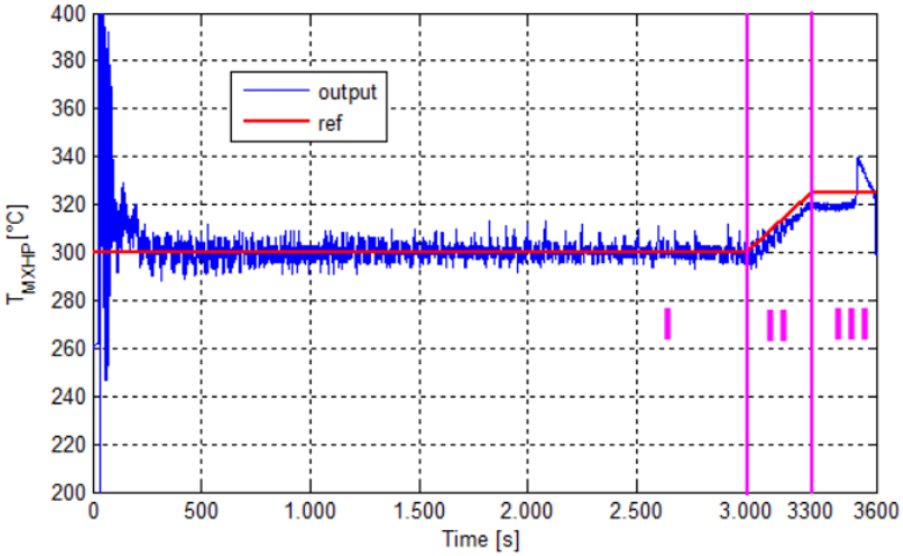

Figure 4.27: T_{MXHP} behavior comparison between reference value and controlled output.

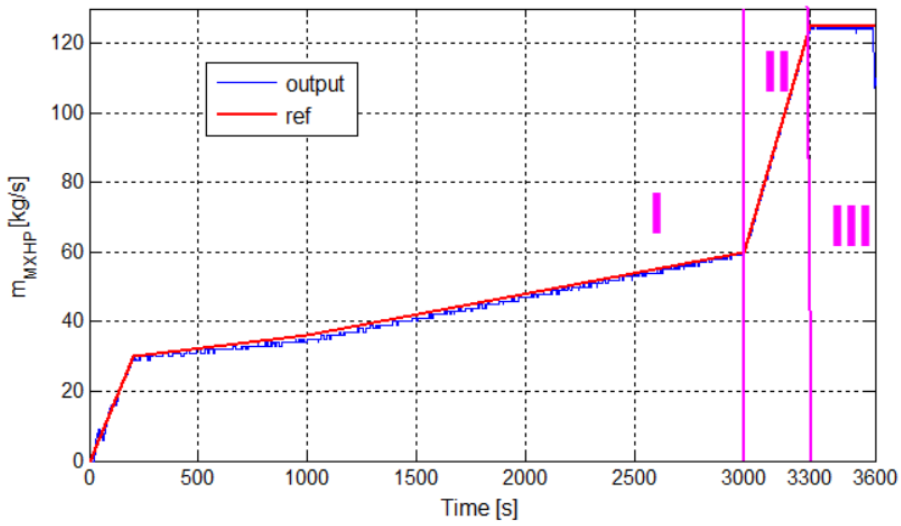

Figure 4.28: $\dot{m}_{MXHP}$ behavior comparison between reference value and obtained output.

Table 4.12: Mean relative errors between reference signals and controlled outputs in the simulation phases.

	Bypass Start-up	Turbine Run-up	Bypass Shut-down
P_{SH} (HIL)	$< 2\%$	$< 1.6\%$	$< 3\%$
P_{SH} (simulation)	$< 0.1\%$	$< 0.1\%$	$< 0.1\%$
T_{MXHP} (HIL)	$< 0.3\%$	$< 0.5\%$	$< 1.2\%$
T_{MXHP} (simulation)	$< 0.2\%$	$< 0.3\%$	$< 0.9\%$
$\dot{m}_{MXHP}$ (HIL)	$< 1.5\%$	$< 0.4\%$	$< 0.3\%$
$\dot{m}_{MXHP}$ (simulation)	$< 0.1\%$	$< 0.1\%$	$< 0.2\%$

Conclusions

In this thesis innovative techniques devoted to the development of efficient models, RT systems and HIL architectures for the testing of industrial components and systems are presented.

First of all, the state-of-the-art on the topic of Real Time and Hardware In the Loop architectures have been analyzed in order to understand the basic concepts and constraints typical of this kind of simulations. Consequently, both the RTOs working principles and the main features of HIL simulations have been explained, in particular describing the general architecture and the main elements present in HIL systems.

Subsequently, an innovative modelling approach, based on Bond-Graph techniques is presented to describe the dynamics of industrial systems characterized by the presence of compressible or incompressible fluids. The typical elements that build up industrial plants can be substantially divided in capacitive and resistive ones, according to the physical variables that each element has to evaluate, respectively through the momentum balance (continuity/mass conservation) and mass plus energy balances (enthalpy balances and more generally expressions derived from the first principle of thermodynamics) derived from the 1-D Navier-Stokes equations. Consequently, a network of these elements, characterized by a bidirectional data flow, can be developed, ensuring a high degree of customization and modularity. Also, the possibility to automatically extract the plant topology from P&ID schemes and to carry out virtual HazOp analyses is guaranteed. In addition, an efficient way to compute the circuit losses and the fluid properties (e.g thermal conductivity, density, specific heat) based on a polynomial approach are provided. To this aims, during the research activity, a full library of typical industrial plant components was developed in Matlab-Simulink.

The aim of the proposed modelling approach was to achieve the best trade-off between accuracy of results and execution efficiency. Therefore, it was applied in two distinct test-cases, related to the energy industry, for which the development of a RT control and HIL architecture were respectively needed.

The first test-case is presented in the third chapter. The aim of the activity described in this chapter consisted in developing a new model-based approach and an optimization strategy for the control auxiliary lubrication plants. According to the above-mentioned modeling strategy, a complete model of the auxiliary lubrication plant has been realized in Matlab-Simulink aiming at reaching a high accuracy degree in the simulation of the plant transient phases, with results comparable with complete 3D models and a higher numerical efficiency. Moreover, an innovative strategy for the PID control optimization based on a flexible simplex technique has been realized and applied to a regulator of a Pressure Control Valve. As a consequence, the model has been compiled and uploaded on MicroAutoBoxII, a commercial RT platform produced by dSpace®, which interacts with the real plant through an electrical interface. The comparison between the numerical results obtained through the completely simulated system and the acquired experimental data show a good agreement, also denoting the encouraging performances and reliability of the proposed control strategy. The model and the control strategy have been developed and validated in collaboration with *GE Nuovo Pignone S.p.a.*, which provided the experimental data acquired in the testing plant situated in Ptuj (Slovenia).

The last chapter of this thesis deals with the second test-case. In particular, a simplified dynamical model of a two-stages and oil-fired steam plant and the HIL testing of its control system are presented. With respect to the current state of the art, the proposed model is optimized to be implemented on a low cost DSP (the C2000 target produced by Texas Instruments®) and to be integrated on an industrial control system. In particular, the system is optimized for multitasking implementation and to be executed using a low order fixed step solver with relatively large integration steps. Using the proposed model, two different control strategies of the plant have been simulated. For both control strategies, simulated results are coherent respect to the data of a benchmark case study available in literature. This result is useful to verify the robustness of both model and controllers with respect to the multitask approach adopted for the RT implementation. The described test rig has been employed to execute open loop tests for the identification of the rig actuators dynamics. Moreover, the linearized transfer functions were found from the non-linear Simulink model.

Therefore, the control system tuning has been improved according to the results of the stability margin analysis for which the identified transfer functions were used. Finally, the model has been used to successfully control the complete HIL test rig which is still used for the testing of valves and positioners. The model and the control strategy have been developed and validated in collaboration with *Velan ABV S.p.a.*, which provided the experimental data acquired on the test rig developed and situated in Capannori (Lu, Italy).

Finally, the possible future developments will include:

- extension of the proposed appraoch to the modelling of bi-phase ore multi-phase systems;
- extension of the proposed approach to other similar plants (e.g. combined cycle plants) to verify the effectiveness of the modelling, RT and HIL techniques proposed in this thesis;
- RT control and HIL testing of different components (e.g. Temperature Control Valves, Main Pressure Control Valve Actuators, Extraction Control Valve Actuators, Current-to-Pressure Converters);
- employment of alternative control strategies, for instance robust or adaptive controllers and, for HIL applications, the adoption of MIMO (Multiple Input, Multiple Output) regulators that are able to control a complete plant, comprehending the turbines dynamics.

Appendices

Appendix A

Notations

Acronyms	
BVHP	High-pressure bypass valve
BVLP	Low-pressure bypass valve
C	Capacitive
CFD	Computational Fluid Dynamics
CND	Condenser
CPC	Current-to-Pressure Converter
ECO	Economizer
EV	Evaporator
FW	Feed-water
GAS	Gas from the gas turbine
HIL	Hardware In the Loop
HMI	Human Machine Interface
I	Electric current
Is	Isentropic
ME	Mixed Element
MXHP	High-pressure mixer
MXLP	Low-pressure mixer
ODE	Ordinary Differential Equation
PCV	Pressure Control Valve
PDE	Partial Differential Equation
PID	Proportional Integral Derivative
PWM	Pulse Width Modulation

R	Resistive
RH	Reheater
RI	Resistive-Inertial
RT	Real Time
SH	Superheater
TCV	Temperature Control Valve
THP	High-pressure turbine
TLP	Low-pressure turbine
TPJB	Tilting Pad Journal Bearing
TTH lib	Transient Thermal Hydraulic library
TCV	Temperature Control Valve
WVHP	High-pressure spray water valve
WVLP	Low-pressure spray water valve
W,EV	Evaporator water

Variables	
A	Section $[m^2]$
ar	Absolute roughness $[m]$
c	Pump displacement $[m^3]$
c_h	Specific heat coefficient $[kJ/\left(kg \cdot K\right)]$
c_p	Specific heat at constant pressure $[kJ/\left(kg \cdot K\right)]$
c_v	Specific heat at constant volume $[kJ/\left(kg \cdot K\right)]$
C_v	Valve flow coefficient $[-]$
D_h	Hydraulic diameter $[m]$
e_p	Pressure error $[Pa]$
e_y	Position error $[-]$
f	Friction factor $[-]$
f_x	Axial tangential effort $[kg/\left(m^2 \cdot s^2\right)]$
F	Open loop transfer function
$F_k\left(\gamma\right)$	Specific heats ratio factor $[-]$
F_p	Piping geometry factor $[-]$
g	Acceleration of gravity $[m/s^2]$
G_{act}	Transfer function of the PCV actuator
G_p	Transfer function of the plant
G_{pos}	Transfer function of the position controller
$\hat{G}_{PCV}$	Transfer function of the PCV

G_{PID}	Transfer function of the pressure controller
h	Specific enthalpy $[J/kg]$
h_c	Convection coefficient $[W/Km^2]$
IAE	Integral Absolute Error $[sbar]$
J_p	Piston inertia $[kgm^2]$
J_m	Motor inertia $[kgm^2]$
k	Gain of the identified transfer function $[-]$
k_p	Proportional gain $[1/bar]$
k_i	Integral gain $[1/(s \cdot bar)]$
k_d	Derivative gain $[s/bar]$
l	Length $[m]$
L	External work $[J]$
m	Fluid mass $[kg]$
$\dot{m}$	Mass flow rate $[kg/s]$
N	PID constant $[-]$
N_6	Numerical constant $[Pa]$
p	PCV downstream pressure $[Pa]$
p_{cr}	Critical pressure value $[Pa]$
p_{cr}^c	Critical pressure for compressible fluids $[Pa]$
p_{in}	PCV upstream pressure $[Pa]$
p_{prec}	Precharge pressure $[Pa]$
p_{ref}	Set-point pressure $[Pa]$
p_{opt}	Pressure behaviour with optimized PID $[Pa]$
p_{std}	Pressure behaviour with standard PID $[Pa]$
P_W	Power coefficient $[-]$
r_p	Piston run $[m]$
rr	Relative roughness $[-]$
R	Specific gas constant $[kJ/kg \cdot K]$
Re	Reynolds number $[-]$
s	Specific entropy $[kJ/(kg \cdot K)]$
SG	Specific Gravity $[-]$
t	Time $[s]$
T	Temperature $[K]$
$\dot{T}$	Temperature variations $[K/s]$
T_0	Time period $[s]$

$T_{a,\epsilon}$	Settling time $[s]$
T_{ref}	Reference temperature $[K]$
$Te(n)$	Speed-torque response $[Nm]$
T_{env}	Environment temperature $[K]$
T_f	Falling time $[s]$
T_r	Rising time $[s]$
T_{res}	Resistant torque $[Nm]$
Tm	Required mechanical torque $[Nm]$
TF	Plant transfer function
u_{PCV}	PCV internal command $[-]$
u_y	Position command $[-]$
v_s	Specific volume $[m^3/kg]$
$\dot{v}_s$	Specific volume variations $[m^3/\left(kg \cdot s\right)]$
v_x	Longitudinal velocity $[m/s]$
V	Volume $[m^3]$
$\dot{V}$	Volume variations $[m^3/s]$
W	Power $[kW]$
W_{sp}	Specific power $[kJ/kg]$
x	Longitudinal direction $[m]$
x_c	control signal $[-]$
x_t	Pressure drop ratio factor $[-]$
X	Ratio of pressure drop to upstream absolute static pressure $[-]$
y	Measured opening position $[-]$
y^{idf}	Identified opening position $[-]$

Greek symbols

ΔP_{rg}	Pressure drop of the spray water valve rings $[Pa]$
α	Inclination angle $[rad]$
β	Bulk modulus $[Pa]$
χ	Prevalence dimensionless coefficient $[-]$
δ	Average value of the protrusions $[m]$
η	Efficiency $[-]$
η_m	Mechanical efficiency $[-]$
η_v	Volumetric efficiency $[-]$
γ	Specific heats ratio $[W/\left(m \cdot K\right)]$
γ_{SW}	Specific weight $[-]$

λ_p	Thermal conductibility $[-]$
μ	Dynamic viscosity $[kg/\left(m \cdot s\right)]$
ϕ	Flow rate dimensionless coefficient $[-]$
ψ	Exponential coefficient of dynamic viscosity $[kg/m^3]$
ω	Angular speed $[rad/s]$
ρ	Fluid density $[kg/m^3]$
τ	Time constant of the identified transfer function $[s]$
θ	Inclination angle with respect to the ground $[rad]$
ζ	Total friction factor $[-]$

Subscripts	
$_{gas}$	Gas related variable
$_{in}$	Inlet variable
$_{out}$	Outlet variable
$_{nom}$	Nominal value of the corresponding variable

Superscripts	
*	Set-point variable

Appendix B

Design of the test rig

In this appendix the construction drawings used for the manufacturing of the rig for the HIL testing of a TBV controller described in chapter 4 are included. In particular, the appendix is organized considering the mechanical, pneumatic and electric design of the test rig.

B.1 Mechanical Design

The mechanical layout of the tested system is composed of a supporting structure on which are mounted the following components:

- two linear simple-effect actuators;
- the control panel with the electro-pneumatic components;
- the cabinet containing the controller;
- the two dissipative elements that simulate the presence of the two implemented valves.

Figure B.1 shows a view of the assembly from the side on which the positioners are mounted, while Figure B.2 shows a view of the assembly from the side of the control panel.

Figure B.1: View of the test rig: positioners side.

The linear actuator manufactured by the industrial partner is a pneumatic device used to control the opening and closing of valves in linear movement.

Figure B.2: View of the test rig: control panel side.

Figure B.3 illustrates a section in which the main components are visible.

It consists of a cylinder closed between two flanges fixed by means of tie rods, inside which a piston can sealingly slide.

The lower end of the piston is fixed to one rod connected to the movable element of the valve whose the opening and closing movement have to be controlled.

At the upper side the piston is in contact with the coil end of a suitably preloaded helical spring, housed inside the secondary chamber of the cylinder, since the upper end of the coil rests on an abutment which is constantly in contact with the upper flange of the cylinder.

Through an intake hole formed in the bottom flange of the pneumatic cylinder (not visible in the figure), pressurized air is introduced into the primary chamber (where the dead volume is represented in violet color), whose action causes the raising of the piston and, consequently, of the movable element of the controlled valve, which will be opened or closed in relation to the type of its trim.

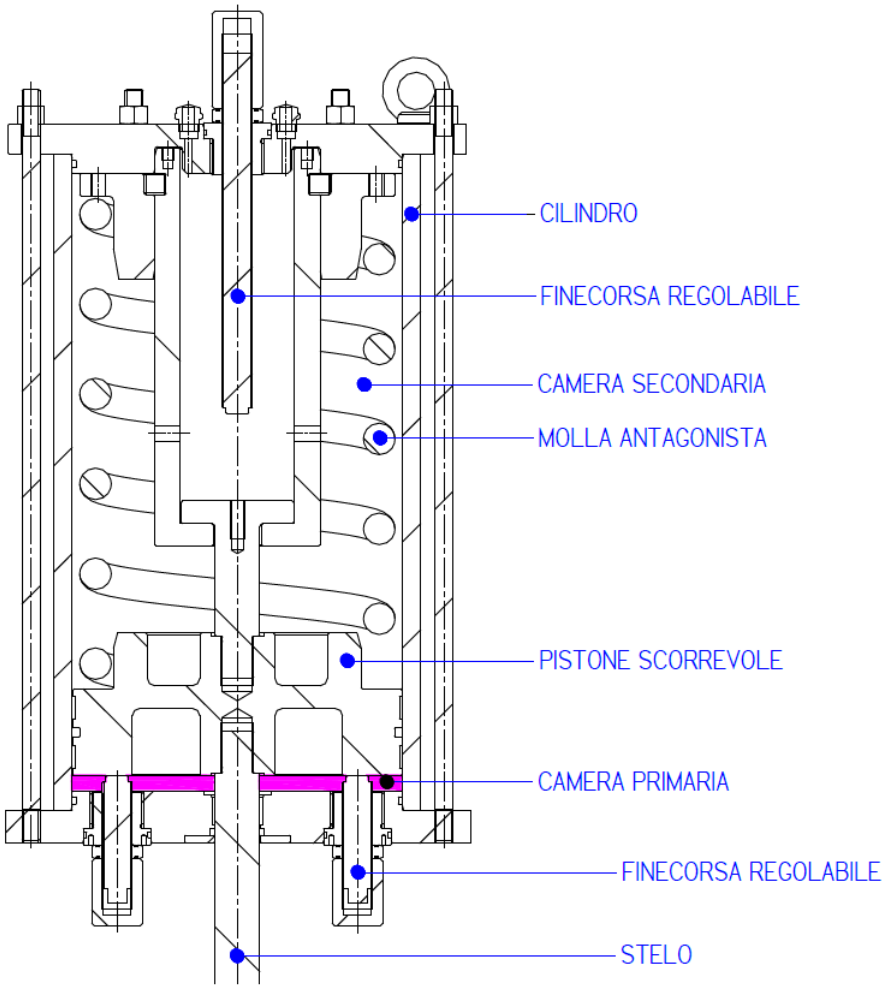

Figure B.3: Section of the linear actuator.

The raising of the piston compresses the counteracting spring that exerts an increasing reaction in proportion to its compression.

When the air introduction into the cylinder is removed, by releasing the primary chamber, the spring is released, causing the lowering of the piston and, therefore, of the movable element of the valve. The component that governs the valve control, which interacts with the controller working according to a precise and predetermined logic, is a pneumatic positioner. Figure B.4 shows one of the two positioners.

Figure B.5 shows the detail of the positioner connection with the linear actuator.

When pressurized air is given the supply circuit, the output shaft of the positioner rotates by an angle proportional to the linear run, which must fulfill the actuator rod.

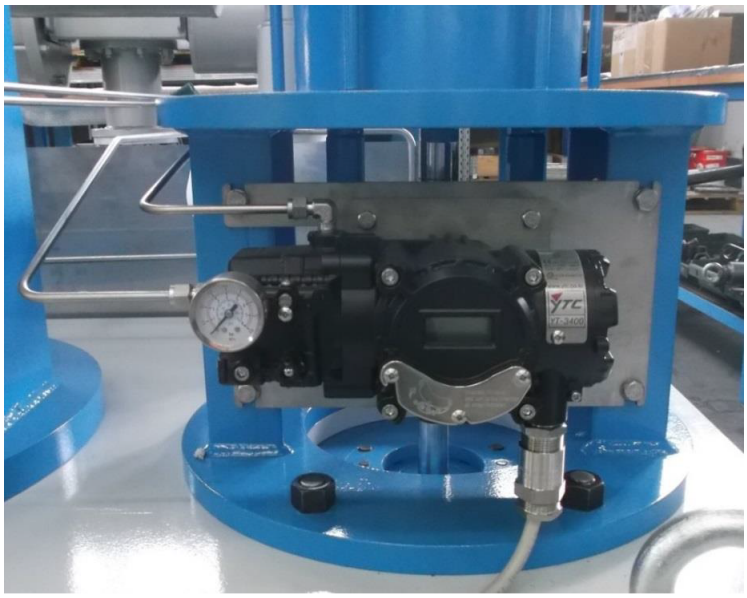

Figure B.4: View of the test rig positioner.

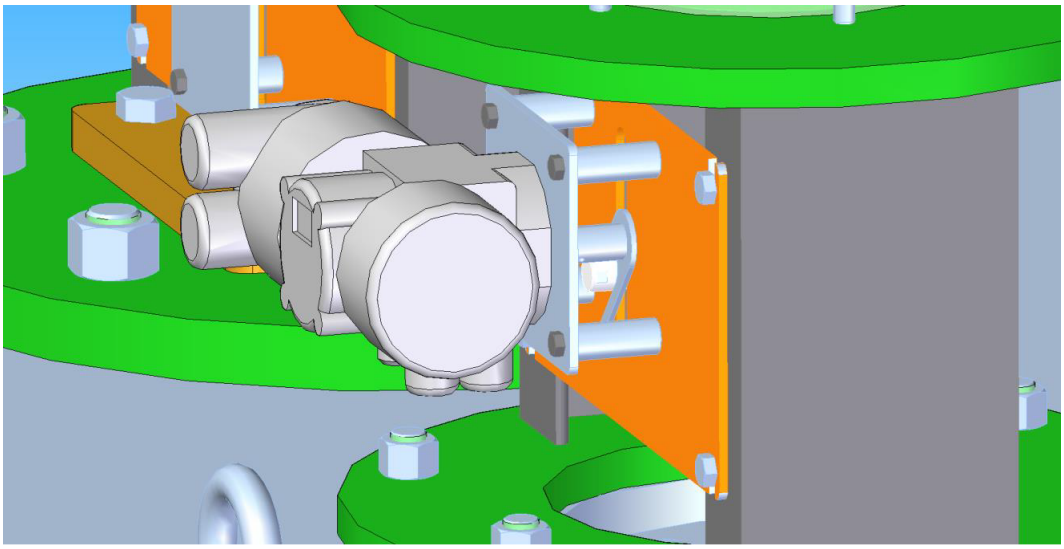

Figure B.5: View of the positioner connection with the linear actuator.

The rotation of the positioner shaft is converted into a linear movement of the rod by means of a fork keyed on the shaft itself, provided with a slot, inside which the integral guide pin to the rod flows.

The pin is integral with the stem and is guided within a suitably shaped groove provided on a fixed support of the actuator. In this way, the actuator rod cannot rotate around its own axis during the vertical translation movement.

Therefore, the shaft is not subject to potentially dangerous inflections. The details of the components described above are visible in Figure B.6 and Figure B.7.

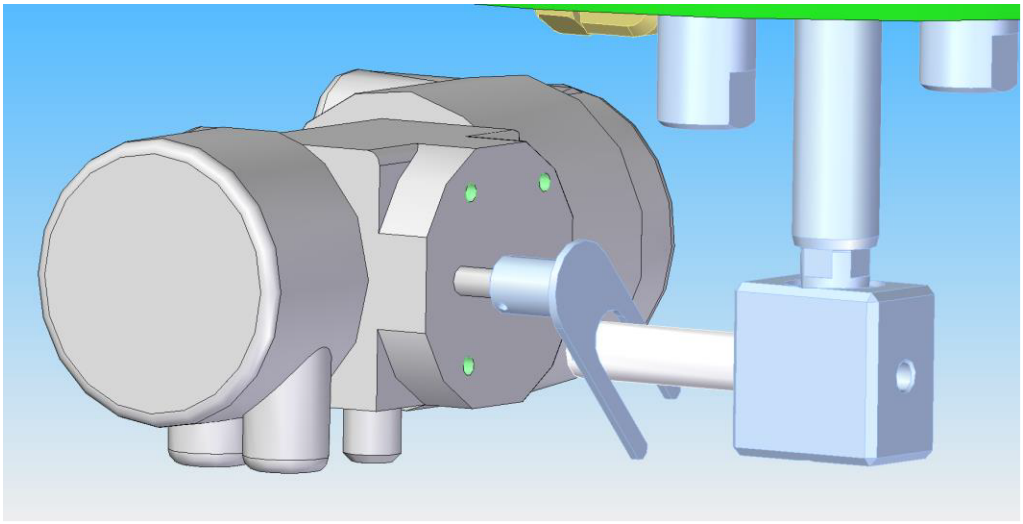

Figure B.6: Detail of the positioner shaft.

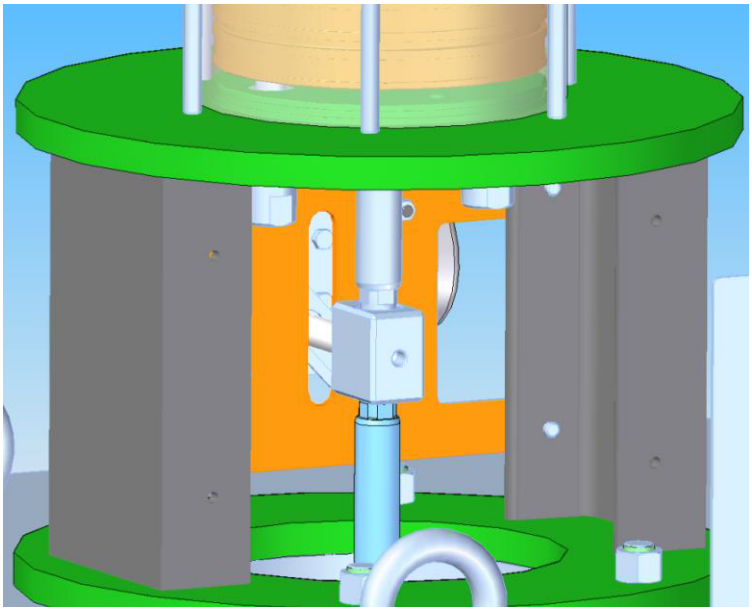

Figure B.7: Detail of the actuation system.

On the realized structure, in substitution of the valves, two dissipative elements have been provided. In particular, these elements consist of two pressurized pneumatic cylinders directly connected to a pneumatic control panel, so that a virtually constant resistance during the vertical movement of the valve stem is obtained.

Figure B.8 shows a view of the two elements, which are mounted between the two the two plates that constitute the crankcase.

Figure B.8: View of a dissipative element.

Figure B.9 shows the CAD assembly where the two dissipative elements are visible without the control panel and the electro-pneumatic connections.

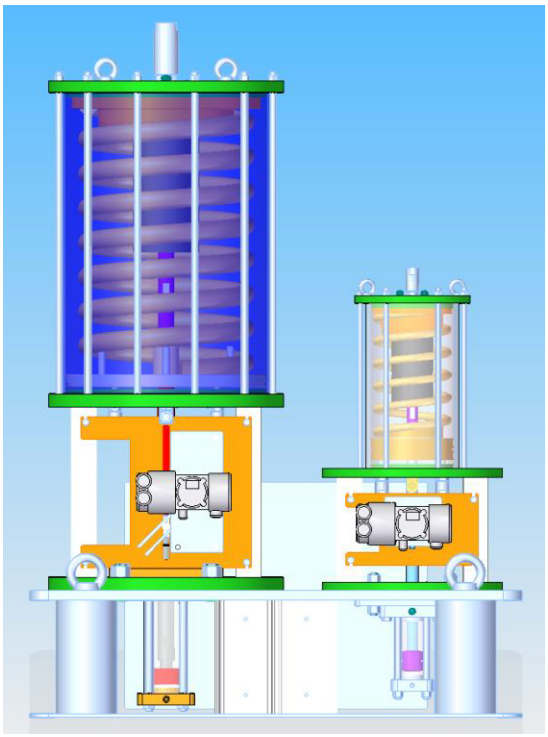

Figure B.9: View of the CAD assembly of the test rig.

B.2 Pneumatic Design

The pneumatic layout for the control of a TBV is schematically shown in Figure B.10. The control of each actuator is performed by the positioner with its volume booster, while the emergency line is managed by a 3/2 solenoid valve.

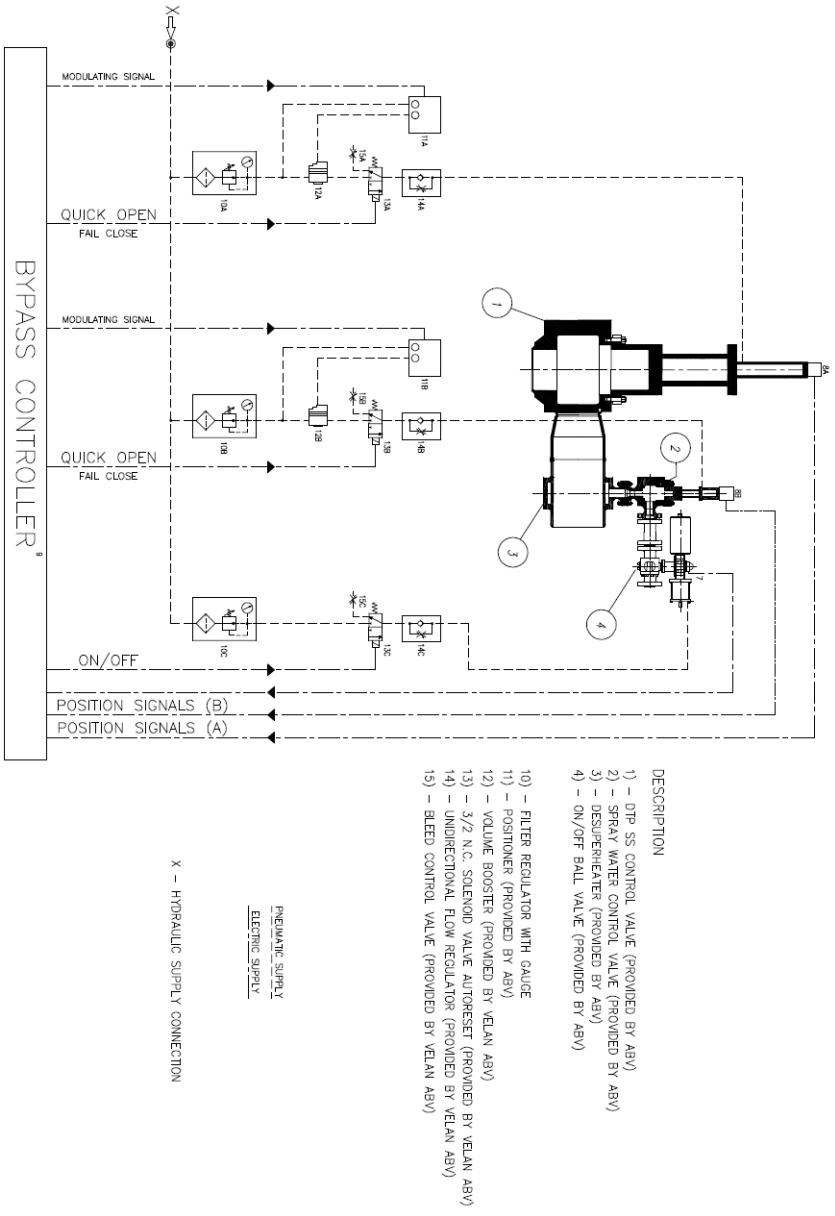

Figure B.10: Pneumatic layout and components of a TBV stage.

B.3 Electric Design

In Figure B.11 shows the construction scheme of the junction box ($380 \times 460 \times 180$ mm) where the various electrical elements and their connections are arranged.

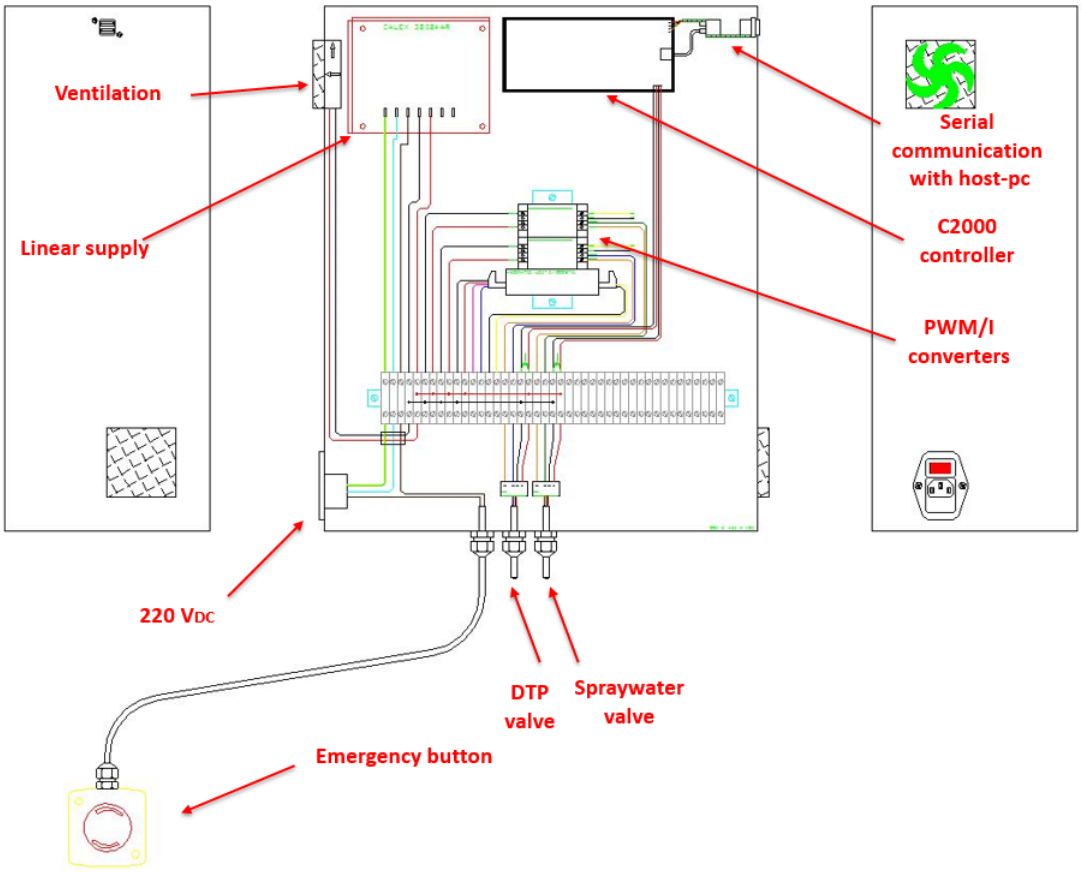

Figure B.11: Electric layout: CAD model.

The junction box is provided with a button that allows the connection between the power supply and the 220VDC electric network. A passage for the emergency push cable is housed on the casing to ensure a rapid shutdown when the operating conditions become dangerous for the user or the equipment itself. A simple ventilation apparatus for cooling the various electrical and electronic components is present and, moreover, a passage for the cables which allow the connection between the microcontroller and the host-PC and between the microcontroller and positioners of the two valves are provided.

The chosen power supply is a stabilized linear power supply (manufactured by Calex), which produces a power of 28.8 W and a voltage of 24VDC to power the various

electronic converters for the conditioning of the control signal.

In particular, the choice of this model takes into account the power required by the individual components to be supplied.

From the datasheet of the components, the current absorbed, and consequently, the power required by each component were observed, as described in Table B.1:

Table B.1: Currents and power absorbed by the electric components.

Component	Absorbed current $[mA]$	Absorbed power $[W]$
Plant type	Oil-fired generating unit	-
Axiomatic AX130201	30	0.72
Axiomatic AX130201	30	0.72
Axiomatic TD2014AX	30	0.72
Positioner YT-3400	20	0.48
Positioner YT-3400	20	0.48
Relay G6DS OMRON	7.5	0.18
Relay G6DS OMRON	7.5	0.18
24/5 V converter	8	0.192
Total	**145**	**3.672**

For this reason, the chosen model is the one with a lower power output (which however is sufficient with a wide margin for supplying the entire electrical panel), and especially at lower cost.

Then, the voltage is supplied to the various components (including the two PWM/I Axiomatic converters and the static converter from 24V to 5V) through the connections formed on the terminal block, which allows to interface the control hardware (C2000 microcontroller from Texas Instruments) and conversion components with the positioners and, consequently, the pneumatic actuators. Finally, two relays were added, controlled through the HMI, by two digital microcontroller pins, which, in case of emergency, instantly discharge the air present in the system to the atmosphere.

The electrical panel (shown in Figure B.12) is vertically connected directly to the side of the testing pneumatic cylinder relative to the test.

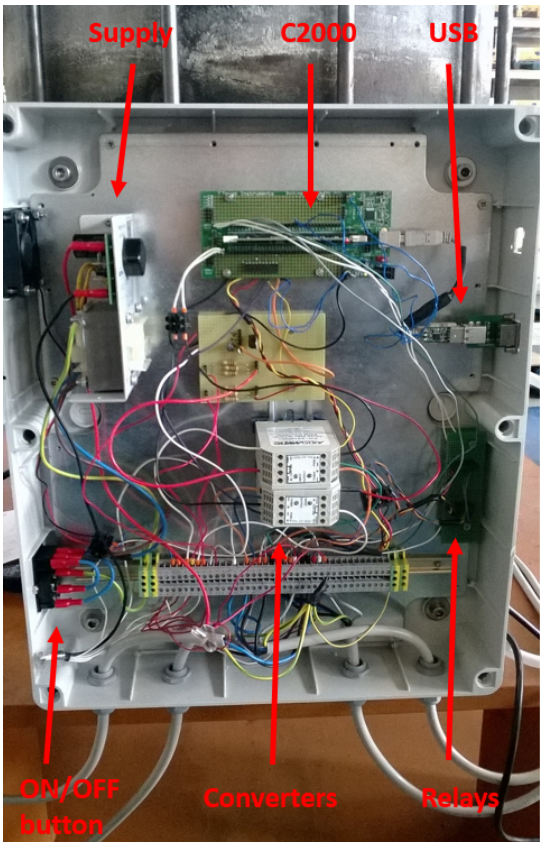

Figure B.12: Electric panel of the test rig

Appendix C

Publications

In this appendix the various publications arising from the research activity carried out during these years can be found. The publications are listed in chronological order:

1. E. Meli, A. Rindi, D. Nocciolini, L. Pugi, E. Galardi, R. Conti, A. Frilli, S. Rossin (2016). An efficient quasi-3D rotordynamic and fluid dynamic model of Tilting Pad Journal Bearing. TRIBOLOGY INTERNATIONAL. Vol. 103, pp 449-464, November 2016.

2. R. Conti, P. D'Adamio, E. Galardi, E. Meli, D. Nocciolini, L. Pugi, A. Rindi (2016). Control design, simulation and validation of a turbo-machinery auxiliary plant. In Proceedings of the Institution of Mechanical Engineers Part E Journal of Process Mechanical Engineering 1989-1996 vol. April 2016.

3. P. D'Adamio, J. Escalona, E.Galardi, L.Marini, E. Meli, L. Pugi, A. Rindi (2016). Development of a Novel Wheel-Rail Contact Model for Real-Time Applications. ISBN:978-1-905088-65-2. In CIVIL-COMP PROCEEDINGS.

4. P. D'Adamio, J. Escalona, E. Galardi, E. Meli, L. Pugi, A. Rindi (2016). Multicore Computing for the Multibody Simulation of Railway Vehicles. In Proceedings of the WCRR2016 congress.

5. P. D'Adamio, E. Galardi, E. Meli, L. Pugi, A. Rindi (2016). Real Time Modelling of a Railway Multibody Vehicle: Application and Validation on a Scaled Railway Vehicle. ISBN:978-1-905088-65-2. In CIVIL-COMP PROCEEDINGS.

6. E. Galardi, N. Lucchesi, G. Pallini, L. Paolucci, L. Pugi (2016). Design and testing of a pulley and cable actuator for large ball valves. DOI:10.1177/0959651816642093. pp.1-18. In PROCEEDINGS OF THE INSTITUTION OF MECHANICAL ENGINEERS. PART I, JOURNAL OF SYSTEMS AND CONTROL ENGINEERING - ISSN:0959-6518.

7. E. Galardi, L. Pugi, N. Lucchesi (2015). Application of a wire transmission to a Quarter Turn Actuator: design and testing procedure. DOI:10.1115/1.4032404. pp.1-13. In JOURNAL OF MECHANISMS AND ROBOTICS - ISSN:1942-4302.

8. E. Galardi, L. Pugi, N. Lucchesi, L. Paolucci (2015). Un banco prova per gli attuatori di un Turbine Bypass System. pp.1-8. In OLEODINAMICA PNEUMATICA - ISSN:2421-4388 vol. Dicembre 2015.

9. E. Galardi, D. Nocciolini, L. Pugi (2015). Hardware and Fluid in the Loop Testing: The Application to the Testing of Fluid Systems, Some Examples and Applications. pp.1-30. In Mechatronics : principles, technologies and applications - ISBN:978-1-63482-801-7. In MECHANICAL ENGINEERING THEORY AND APPLICATIONS.

10. L. Pugi, E. Galardi, C. Carcasci, N. Lucchesi (2015). Hardware-in-the-loop testing of bypass valve actuation system: Design and validation of a simplified real time model. DOI:10.1177/0954408915589513. pp.1-24. In PROCEEDINGS OF THE INSTITUTION OF MECHANICAL ENGINEERS. PART E, JOURNAL OF PROCESS MECHANICAL ENGINEERING - ISSN:0954-4089.

11. E. Galardi, E. Meli, D. Nocciolini, L. Pugi, A. Rindi (2015). Development of efficient models of Magnetic Braking Systems of railway vehicles. DOI:10.1080/23248378.2015.1015219. pp.97-118. In INTERNATIONAL JOURNAL OF RAIL TRANSPORTATION - ISSN:2324-8378 vol. 3.

12. E. Meli, A. Rindi, D. Nocciolini, L. Pugi, E. Galardi, R. Conti, A. Frilli, S. Rossin (2015). Efficient Models of 3D Tilting Pad Journal Bearings for the Study of the Interactions between Rotor and AND NONLINEAR DYNAMICS-ISSN:1555-1423.

13. E. Galardi, D. Nocciolini, L. Pugi (2015). Sperimentazione di Sistemi Idraulici: Esempi ed Applicazioni. pp.70-80. In TRASMISSIONI DI POTENZA OLEODINAMICA PNEUMATICA LUBRIFICAZIONE - ISSN:1122-5017 vol. 2.

14. L. Pugi, E. Galardi, N. Lucchesi, G. Pallini, L. Paolucci, A. Rindi (2015). Development of an innovative wire actuator for quarter turn valves. pp.180-189. In AIMETA 2015 MEMORIE ESTESE XII CONGRESSO DELL'ASSOCIAZIONE ITALIANA DI MECCANICA TEORICA E APPLICATA - ISBN:978-88-97752-55-4.

15. R. Conti, P. D'Adamio, E. Galardi, E. Meli, D. Nocciolini, L. Pugi, A. Rindi (2015). Control design, simulation and validation of a turbo-machinery auxiliary plant. pp.160-169. In AIMETA 2015 MEMORIE ESTESE XXII CONGRESSO DELL'ASSOCIAZIONE ITALIANA DI MECCANICA TEORICA E APPLICATA - ISBN:978-88-97752-55-4.

16. R. Conti, A. Frilli, E. Galardi, E. Meli, D. Nocciolini, L. Pugi, A. Rindi, S. Rossin (2015). A Tilting Pad Journal Bearing Model for Coupled Fluid Dynamical - Rotor Dynamical Analyses. Proceedings of the IDETC/CIE 2015 Congress. 02-05/08/2015 Boston, Massachusetts (USA).

17. R. Conti, A. Frilli, E. Galardi, E. Meli, D. Nocciolini, L. Pugi, A. Rindi, S. Rossin (2015). An Efficient quasi-3D Model of Tilting Pad Journal Bearing for Turbomachinery Applications. In JOURNAL OF VIBRATION AND ACOUSTICS - ISSN:1048-9002 vol. 137.

18. L. Pugi, R. Conti, D. Nocciolini, E. Galardi, E. Meli (2015). A Comprehensive Tool for the Optimization of Traction and Braking systems with respect to the Application of Energy Storage devices. DOI:10.4203/ijrt.4.1.4. pp.69-93. In INTERNATIONAL JOURNAL OF RAILWAY TECHNOLOGY - ISSN:2049-5358 vol. 4.

19. R. Conti, E. Galardi, E. Meli, D. Nocciolini, L. Pugi, A. Rindi (2015). Energy and wear optimisation of train longitudinal dynamics and of traction and braking systems. Vehicle System Dynamics, p. 1-22, ISSN: 0042-3114, doi: 10.1080/00423114.2014.990466.

20. L. Pugi, E. Galardi, C. Carcasci, A. Rindi, N. Lucchesi (2015). Preliminary design and validation of a Real Time model for hardware in the loop testing of bypass valve actuation system. ENERGY CONVERSION AND MANAGEMENT, vol. 92, p. 366-384, ISSN: 0196-8904, doi: 10.1016/j.enconman.2014.12.061.

21. R. Conti, E. Galardi, E. Meli, D. Nocciolini, L. Pugi, A. Rindi, S. Rossin, R. De Paolis (2014). System Control logic enhancements through Fluid-Mechanical valve dynamic transfer functions. In: Proceedings of the International CAE Conference. p. 1-10, International CAE Conference.

22. R. Conti, A. Frilli, E. Galardi, E. Meli, D. Nocciolini, L. Pugi, A. Rindi, S. Rossin (2014). Development and Preliminary Validation of Efficient 3D Models of Tilting Pad Journal Bearings. Proceedings of the IFToMM ICORD 2014 Congress. 22-25/09/2014 Milano.

23. L. Pugi, C. Carcasci, E. Galardi, A. Rindi, N. Lucchesi (2014). Real Time Simulation of a Turbine Bypass Controller. In: Mechatronics and Embedded Systems and Applications (MESA), 2014 IEEE/ASME International Conference on. p. 1-6, IEEE, Senigallia, 10-12 Settembre 2014.

24. E. Galardi, L.Pugi, N. Lucchesi, A Rindi (2014). Hardware In the Loop Testing of a Steam Turbine Bypass Regulator Using a TI C2000 Micro-Controller. In: EDERC 2014: European Embedded Design in Education and Research Conference. p. 1-6, IEEE, Milano, 11-12 settembre 2014.

25. L. Pugi, R. Conti, D. Nocciolini, E. Galardi, A. Rindi, S. Rossin (2014). A Tool for the Simulation of Turbo-Machine Auxiliary Lubrication Plants. INTERNATIONAL JOURNAL OF FLUID POWER, vol. 2-15, p. 87-100, ISSN: 1439-9776, doi: 10.1080/14399776.2014.931130.

26. C. Carcasci, E. Galardi, L. Pugi, A. Rindi, N. Lucchesi (2014). Preliminary Design and Validation of a Real Time Model for Hardware In the Loop Testing of Bypass Valve Actuation System, In: (a cura di): Leo J De Vin and Jorge Solis, Proceedings of the 14th Mechatronics Forum International Conference, Mechatronics 2014. p. 413-420, Carlstadt University, ISBN: 9789170635649, Carlstadt Svezua, 16-18 giugno 2014.

27. A. Biagini, R. Conti, E. Galardi, L. Pugi, E. Quartieri, A. Rindi, S. Rossin (2013). Development of RT models for Model Based Control-Diagnostic and Virtual HazOp Analysis, 12th IMEKO TC10 Workshop on Technical Diagnostics-New Perspectives in Measurements, Tools and Techniques for Industrial Applications -June 6-7, 2013, Florence, Italy.

Bibliography

[1] P. Patil, S. Bhosale, Review on Hardware-in-Loop Simulation used to Advance Design Efficiency and Test Competency, International Journal of Science and Research (IJSR) ISSN (Online) 4 (3) (2015) 2466 - 2468.

[2] C. Dufour, S. Cense, V. Jalili-Marandi, J. Bélanger, Review of state-of-the-art solver solutions for HIL simulation of power systems, power electronic and motor drives, in 2013 15th European Conference on Power Electronics and Applications (EPE) (2013) 1 - 12.

[3] A. Silberschatz, P. Galvin, G. Gagne, Sistemi Operativi: Concetti ed esempi, Pearson AddisonWesley, 8th ed. 2009.

[4] R. Mall, Real-Time Systems - Theory and Practice, Dorling Kindersley, Pearson Education, India, 2009.

[5] P. Tucci, Hardware/Software Design of Dynamic Real-Time Schedulers for Embedded Multiprocessor Systems, Ph.D thesis, Bologna, 2012.

[6] R. Boot, J. Richert, H. Schütte, A.Rükgauer, Automated Test of ECUs in a Hardware-in-the-Loop Simulation Environment, Proceedings of the 1999 IEEE International Symposium on Computer Aided Control System Design Kohala Coast-Island of Hawai, Hawaii, USA (22-27 August 1999) 587 - 594.

[7] S. Chuanxue, X. Feng, P. Silun, Implementation of Electric Vehicle Hardware-in-the-Loop Test Platform, International Journal of Multimedia and Ubiquitous Engineering 10 (11) (2016) 147 - 158.

[8] D. Bullock, B. Johnson, R. B. Wells, M. Kyte, Z. Li, Hardware-in-the-loop simulation, Transportation Research Part C 12 (2004) 73-89.

[9] H. Hanselmann, Hardware-in-the-Loop Simulation Testing and its Integration into a CACSD Toolset, Proceedings of the 1996 IEEE International Symposium on Computer-Aided Control System Design SM03 250 Dearborn, MI (15-18 September 1996) 152 - 156.

[10] M. Bacic, On hardware-in-the-loop simulation, Proceedings of the 44th IEEE Conference on Decision and Control, and the European Control Conference 2005, Seville, Spain (12-15 December 2005) 3194 - 3198.

[11] K. Hong, H. Sohn, J.K. Hedrick, Modified Skyhook Control of Semi-Active Suspensions: A New Model, Gain Scheduling, and Hardware-in-the-Loop Tuning, Transactions of the ASME, JOURNAL OF DYNAMIC SYSTEMS, MEASUREMENT, AND CONTROL 124 (1) (2002) 158 - 167.

[12] S.B. Choi, Y.T. Choi, D.W. Park, A Sliding Mode Control of a Full-Car Electrorheological Suspension System Via Hardware in-the-Loop Simulation, Transactions of the ASME, Journal of Dynamic Systems, Measurement, and Control 119 (2000).

[13] Georg F. Lauss, M. Omar Faruque, Karl Schoder, Christian Dufour, James Langston, Alexander Viehweider, Characteristics and Design of Power Hardware-in-the-Loop Simulations for Electrical Power Systems, IEEE TRANSACTIONS ON INDUSTRIAL ELECTRONICS 63 (1) (2016) 406 - 417.

[14] R. Razzaghi, F. Colas, X. Guillaud, M. Paolone, F. Rachidi, Hardware-in-the-Loop Validation of an FPGA Based Real-Time Simulator for Power Electronics Applications, in: 11th International Conference of Power Systems Transients (IPST), Croatie (June 2015).

[15] H. Zhang, J. Sun, FPGA-Based Simulation of Power Electronics Using Iterative Methods, 2014 International Power Electronics Conference (IPEC-Hiroshima 2014 - ECCE-ASIA) (18-21 May 2014) 2202 - 2207.

[16] X. Wu, S. Lentijo, A. Monti, A Novel Interface for Power-Hardware-In-the-Loop Simulation, 2004 IEEE Workshop on Computers in Power Electronics, 2004, Proceedings, (15-18 August 2004) 178 - 182.

[17] C. Seitl, J. Kathan, G. Lauss, F.Lehfub, Selection and Implementation of a Generic Battery Model for PHIL Applications, Industrial Electronics Society, IECON 2013 - 39th Annual Conference of the IEEE (2013) 5412 - 5417.

[18] B. Lu, X. Wu, H. Figueroa, A. Monti, A Low-Cost Real-Time Hardware-in-the-Loop Testing Approach of Power Electronics Controls, IEEE TRANSACTIONS ON INDUSTRIAL ELECTRONICS 54 (2) (2007) 919 - 931.

[19] T. Letrouvé, A. Bouscayrol, W. Lhomme, J. Pouget, Signal HIL Simulation of a Hybrid locomotive using Energetic Macroscopic Representation, Vehicle Power and Propulsion Conference, VPPC'15 - Montreal, Canada (2015).

[20] P. Terwiesch, T. Keller, E. Scheiben, Rail Vehicle Control System Integration Testing Using Digital Hardware-in-the-Loop Simulation, IEEE TRANSACTIONS ON CONTROL SYSTEMS TECHNOLOGY 7 (3) (1999) 352 - 362.

[21] B. Allotta, R. Conti, M. Malvezzi, E. Meli, L. Pugi A. Ridolfi, A Full-Scale Roller Test Rig for the HIL Testing of Traction and Braking On Board Subsystems, Vehicle System Dynamics 0 (0) (2012) 1 - 38.

[22] S.E. Slagowski, J.E. Vican, P.S. Kenney, A Hardware-In-The-Loop Simulator for Software Development for a Mars Airplane, AIAA meeting papers on disc, (2007-6477), American Institute of Aeronautics and Astronautics, Reston, Va. (2007) 1 - 11.

[23] J.S. Cole, A.C. Jolly, Hardware-in-the-loop simulation at the US Army Missile Command, in Technologies For Synthetic Environments: Hardware-In-The-Loop Testing, Proceedings OfThe Society OfPhoto-Optical Instrumentation Engineers (Spie) 2741 (1996) 14 - 19.

[24] M.E. Sisle, E.D. McCarthy, Hardware-In-The-Loop Simulation For An Active Missile, Simulation 39 (1982) 159 - 167.

[25] M. Gehlen, V. Kurtcuoglu, M. S. Daners, Patient Specific Hardware-in-the-Loop Testing of Cerebrospinal Fluid Shunt Systems, IEEE TRANSACTIONS ON BIOMEDICAL ENGINEERING 63 (2) (2016) 348 - 358.

[26] G. Cai, B.M. Chen, T.H. Lee, M. Dong, Design and implementation of a hardware-in-the-loop simulation system for small-scale UAV helicopters, Mechatronics 19 (2009) 1057 - 1066.

[27] J.A. Ferreira, A.F. Quintã, C. M. Cabral, Hardware-in-the-loop simulation experiments with a hydraulic manipulator model, Australian Journal of Mechanical Engineering 2 (2) (2005) 125 - 132.

[28] H. Temeltas, M. Gokasan, S. Bogosyan, A. Kilic, Hardware in the Loop Simulation of Robot Manipulators through Internet in Mechatronics Education, Proceedings of the 28th Annual Conference of the IEEE Industrial Electronics Society, Sevilla, Spain (5-8 November 2002) 4 2617 - 22.

[29] H.K. Fathy, Z.S. Filipi, J. Hagena J.L. Stein, Review of Hardware-in-the-Loop Simulation and Its Prospects in the Automotive Area, Proc. of SPIE 6228 (0 - 1) (2006) 1 - 20.

[30] A.C. Oldani, Metodi e strumenti per simulazioni multi-body finalizzate ad applicazioni HIL, Ph.D thesis, Bergamo, 2010.

[31] H. Li, M. Steurer, K.L. Shi, S. Woodruff, D. Zhang, Development of a Unified Design, Test, and Research Platform for Wind Energy Systems Based on Hardware-in-the-Loop Real-Time Simulation, IEEE TRANSACTIONS ON INDUSTRIAL ELECTRONICS 53 (4) (2006) 1144 - 1151.

[32] M. Iacob, G. Andreescu, Real-time hardware-in-the-loop test platform for thermal power plant control systems, in: IEEE 9th International symposium on intelligent systems and informatics (SISY), Subotica, Serbia (8-10 September 2011) 495 - 500.

[33] E. de Jong, R. de Graaff, P. Vaessen P, European white book on real-time powerhardware-in-the-loop testing. European Distributed Energy Resources Laboratories, DERlab Report No. R-005.0 (2012) 1 - 50.

[34] E. Zaev E, A. Tuneski, D. Babunski, Hydro power plant governor testing using hardware-in-the-loop simulation, in: Mediterranean conference on embedded computing (MECO), Podgorica Montenegro (19-21 June 2012) 271 - 274.

[35] R. Guofeng, T. Feng, Y. Lin, The research of thermal design for vehicle controller based on simulation, Appl. Therm. Eng. 58 (2013) 420 - 429.

[36] K. Thramboulidis, Model-Integrated Mechatronics-Toward a New Paradigm in the Development of Manufacturing Systems, IEEE TRANSACTIONS ON INDUSTRIAL INFORMATICS 1 (1) (2005) 54 - 61.

[37] R.H. Bishop, The Mechatronics Handbook, CRC Press LCC, The University of Texas at Austin, 2002.

[38] T.R. Anderson, P.Y. Li, Mathematical Modeling of a Two Spool Flow Control Servovalve Using a Pressure Control Pilot, Journal of Dynamic Systems, Measurement, and Control 124 (3) (2002) 420 - 427.

[39] D. Brugier M.T. Pasal, Influence of elastic deformations of turbo-generator tilting pad bearings on the static behavior and on the dynamic coefficients in different designs, ASME J. Tribol. 111 (2) (1989) 364 - 371.

[40] J. Bouyer M. Fillon, On the Significance of Thermal and Deformation Effects on a Plain Journal Bearing Subjected to Severe Operating Conditions, ASME J. Tribol. 126 (4) (2004) 819 - 822.

[41] Q. Chang, P. Yang, Y. Meng, S. Wen, Thermoelastohydrodynamic analysis of the static performance of tilting-pad journal bearings with the Newton-Raphson method, Tribol. Int. 35 (4) (2002) 225 - 234.

[42] S. Piffeteau, D. Souchet D. Bonneau, Influence of Thermal and Elastic Deformations on Connecting-Rod End Bearing Lubrication Under Dynamic Loading. ASME J. Tribol. 122 (1) (2000) 181 - 191.

[43] Z. Mazur, G. Urquiza, R. Campos B. McMahon, Improvement of the turbine main stop valves with flow simulation in erosion by solid particle impact CFD, Int J Rotat Mach 10 (1) (2004) 65 - 73.

[44] K.J. Astrom, R.D. Bell, Drum-boiler dynamics, Automatica 36 (1) (2000) 363 - 378.

[45] R. Kehlhofer, F. Hannemann, F. Stirnimann, Combined-cycle gas & steam turbine power plants, Tulsa, OK: PennWell Corporation (2009) 1 - 170.

[46] Y.L. Wang, Z.S. Liu, W.J. Kang, J.J. Yan, Approximate analytical model for fluid film force of finite length plain journal bearing, Proc. IMechE, J. Mechanical Engineering Science 226 (C) (2011) 1 - 11.

[47] G. Genta, Vibration of Structures and Machines - Practical Aspects, Second Edition, Springer-Verlag NY, 1999.

[48] G. Genta, Dynamics of Rotating Systems. Springer NY, 2005.

[49] N.F. Rieger J.F. Crofoot, Vibrations of Rotating Machinery, Part I: Rotor-Bearing Dynamics The Vibration Institute, Clarendon Hills, Illinois, 1977.

[50] H. Paynter, Analysis and Design of Engineering Systems, MIT Press, Cambridge, MA, 1961.

[51] H.E. Merrit Hydraulic Control Systems, Jonh Wiley and Sons Inc., New York, 1967.

[52] N.D. Manring Hydraulic Control Systems, Jonh Wiley and Sons Inc., New York, 2005.

[53] B.T. Kulakowski, J.F. Gardner, J.L. Shearer, Dynamic Modelling and Control of Engineering Systems, 3rd Edition, Cambridge: Cambridge University Press, 2007.

[54] D.C. Karnopp, R.C. Rosenberg, System dynamics, a unified approach, J. Wiley, New York, 1975.

[55] B.O. Bouamama, Bondgraph approach as analysis tool in thermofluid model library conception, Journal of the Franklin Institute 340 (1) (2003) 1 - 23.

[56] D. Karnopp, R.C. Rosenberg, A.S. Perelson, System dynamics, a unified approach, IEEE Trans. Syst. Man. Cybern SMC-6 (1976) 1 - 476.

[57] A. Malik, A. Khurshid, Bond Graph Modelling and Simulation of Mechatronic Systems, Proceedings IEEE INMIC (2003).

[58] L. Yu, X. Qi, Bond-Graph Modelling in System Engineering, International Conference on Systems and Informatics (2012).

[59] F. Casella, F. Pretolani, Fast start-up of a combined cycle power plant: A simulation study with modelica, in: 5th International modelica conference, Vienna, Austria (4-6 September 2006) 3 - 10.

[60] C. Y. Zhang, P. Zhang, Z. Yang, L. Song, Safety Assessment Modelling for Thermal Power Plants Using Hierarchical SDG-HAZOP Method, Proceedings IEEE (2009).

[61] F. Crawley, M. Preston, B. Tyler, HAZOP Guide To Best Practice, IChemE (2008).

[62] M. Glossop, A. Loannides, J. Gould, Review Of Hazard Identification Techniques, Health and Safety Laboratory (2000).

[63] W.F. Hughes, J.A. Brighton, Fluidodinamica, Schaum ETAS libri, Milano, 1982.

[64] F.M. White, Fluid Mechanics, McGraw-Hill, 1999.

[65] B.R. Munson, D.F. Young, T.H. Okiisshi, Fundamentals of Fluid Mechanics, John Wiley and Sons Inc., 1998.

[66] B.J. Hamrock, Fundamentals of Fluid Film Lubrication, Mc-Graw-Hill-International Editions, USA, 1994.

[67] A. Cameron, Principles of Lubrication. Longmans Green and Co. Ltd., London, 1966.

[68] B.C. Ahna and J.W. Mitchellb, Optimal control development for chilled water plants using a quadratic representation, Energy and Buildings 33 (4) (2001) 371 - 378.

[69] D. Sfyris, A. Chasalevris, An exact analytical solution of the Reynolds equation for the finite journal bearing lubrication, Tribology International 55 (2012) 46 - 58 .

[70] T. Waumans, P. Vleugels, J. Peirs, F. Al-Bender, D. Reynaerts, Rotordynamic behaviour of a micro-turbine rotor on air bearings: modelling techniques and experimental verification, PROCEEDINGS OF ISMA2006 0(0) (2006) 181-198.

[71] J.A. Nelder, R. Mead, A Simplex Method for Function Minimization, Computer Journal 7 (1965) 308 - 313.

[72] Z. Wei-hong, G. Hong-wei, Simplex Method Based Optimal Design of PID Parameters, Journal of Anhui Vocational College of Electronics & Information Technology 0 (3) (2006).

[73] W. Wei, Y. Jun-qi, Design of Optimal PID Controller Based on Simplex Method, Equipment Manufacturing Technology 0 (0) (2009).

[74] O. Nelles, Nonlinear System Identification, Springer, 2001.

[75] Nuovo Pignone General Electric SpA, Lube oil console data, Internal report of GE, 2014.

[76] Dresser Masoneilan, Pressure Control Valve specification, Internal report of Masoneilan, 2014.

[77] Nuovo Pignone General Electric SpA, Masoneilan valves and instrumentation, Internal report of GE, 2014.

[78] The Mathworks - MATLAB. Informations available at the Mathworks official website: http://it.mathworks.com/products/sysid/ (last accessed on 24 July 2015).

[79] Tech. doc. of Mathworks, www.mathworks.it/, 26/02/2014.

[80] C. Lubich, Linearly implicit extrapolation methods for differential-algebraic systems, Numer Math (1989) 55 197 - 211.

[81] P. Deuflhard , E. Hairer, J. Zugck, One-step and extrapolation methods for differential-algebraic systems, Numer Math 51 (1987) 501 - 516.

[82] A. Logar, T. Depolt, E. Gobrecht, Advanced steam turbine bypass design for flexible power plants, in: Proceedings of the 2002 international joint power generation conference, Scottsdale, Arizona, USA (IJPG2002), (24-26 June 2002) 43 - 49.

[83] P.S. Varbanov, J.J. Klemeš, Integration and management of renewables into Total Sites with variable supply and demand. Comput. Chem. Eng. 35 (2011) 1815 - 1826.

[84] F. Casella, M. Farina, F. Righetti, An optimization procedure of the start-up of Combined Cycle Power Plants, in: The 18th IFAC world congress, Milano, Italy (2011) 7043 - 7048.

[85] R.S. Amano, G.R. Draxler, High-pressure steam flow in turbine bypass valve system, Part 1: valve flow. J Propuls Power 18 (2002) 555 - 560.

[86] K. Krüger, M. Rode, R. Franke, Optimal control for fast boiler start-up based on a nonlinear model and considering the thermal stress on thick-walled components, in: Proceedings of the 2001 IEEE international conference on control applications, Mexico City, Mexico, (5-7 September 2001) 570 - 576.

[87] Velan ABV Spa, tech documentation available at http://www.abvvalves.com/ (last accessed on 3 June 2015).

[88] W.C. Kwon, G.R. Kim, S.C. Park, Design of a tortuous path trim for a high-pressure turbine bypass valve. Proc IMechE, Part E: J Process Mechanical Engineering 224 (2010) 149 - 153.

[89] Technical documentation of CCI/SULZER valves control available at http:/www.tj88.cn/down/down/CCI/512.pdf (last accessed on 7 May 2015).

[90] CCI/SULZER Valves, Turbine-bypass systems for greater plant performance, Tech. Bulletin available at https://www.sulzer.com/ (last accessed on 16 April 2015).

[91] S.H. Byun, J.H. Lee, I.H. Lim, Development of a high pressure turbine bypass system pressure control model for power plant simulator, J Korea Soc Simul 20 (2011) 49 - 58.

[92] C.W. Tsai, C. Shih, J.R. Wang, On study of steam bypass and pressure control system for Lungmen nuclear power plant, Procedia Eng 15 (2011) 5328 - 5332.

[93] L. Pugi, M. Malvezzi, A. Tarasconi, HIL simulation of WSP systems on MI-6 test rig, Veh. Syst. Dyn. 44 (2006) 843 - 852.

[94] C. Carcasci, B. Facchini, A numerical method for power plant simulation, Trans ASME J. Energy Resour. Technol. 118 (1996) 36 - 43.

[95] C. Carcasci, B. Facchini, S. Harvey, Modular approach to analysis of chemically recuperated gas turbine cycles, Energy conversion & management, Oxford: Pergamon Elsevier Science Ltd. (1998) 1693 - 1703.

[96] C. Carcasci, S. Harvey, Design Issues for the methane-steam reformer of a chemically recuperated gas turbine cycle, in: ASME International gas turbine and aeroengine congress & exhibition, ASME Paper 98-GT-35, Stockolm, Svezia (1998).

[97] P. Sindareh-Esfahani, A. Ghaffari P. Ahmadi, Thermodynamic modeling based optimization for thermal systems in heat recovery steam generator during cold start-up operation, Appl. Therm. Eng. 69 (2014) 286 - 296.

[98] P. Sindareh-Esfahani, E. Habibi-Siyahposh, M. Saffar-Avval, Cold start-up condition model for heat recovery steam generators, Appl Therm Eng 65 (2014) 502 - 512.

[99] F. Fang, L. Wei, Backstepping-based nonlinear adaptive control for coal-fired utility boiler-turbine units, Appl. Energy 88 (2011) 814 - 824.

[100] Q.B. Chou, S.G. Chow, C.R. Stevens, Design and dynamic performance of a steam turbine bypass control system for a large fossil-fired power generating unit, IEEE Trans Power Apparatus SystPAS-98 (1979) 738 - 747.

[101] W. Wagner, J.R. Cooper, A. Dittmann, The IAPWS Industrial Formulation 1997 for the thermodynamic properties of water and steam, ASME J Eng Gas Turbines Power 122 (2000) 150 - 182.

[102] Emerson Process Management, Control valve handbook, Marshalltown, IA: Fisher Controls International LLC, 1 - 283, 2005.

[103] Stodola A, Steam and gas turbine, Gloucester, MA: Peter Smith, 1 - 2, 1945.

[104] A. Chaibakhsh, A. Ghaffari, Steam turbine model, Simul. Model Pract. Theory 16 (2008) 1145 - 1162.

[105] Y. Qi, W. Bao, Bumpless switching scheme design for continuous-time controller switched systems, in: Proceedings of the 30th Chinese control conference (2011) 1702 - 1706.

[106] M. Pasamontes, J.D. Alvarez, J.L. Guzmań, Bumpless switching in control - A comparative study, in: IEEE Conference on emerging technologies and factory automation (ETFA) (2010) 1 - 8.

[107] Texas Instruments official site with tec. Doc. www.ti.com/product/tms320f28335 (last accessed on 28 November 2015).

[108] K.N.N. Kumar, C.P. Kurian, Model based control using C2000 microcontroller, in: 2014 International conference on advances in energy conversion technologies (ICAECT), MANIPAL, India, (23-25 Januany 2014) 13 - 20.

[109] L.V. Oppenheim, R.W. Schafer, Discrete-Time Signal Processing, Pearson Higher Education, 3rd edition, Harlow, UK, 1 - 1115, 2014.